Title
Brake System Analysis, Reliability Testing And Control Using Bench Experiments

Permalink
https://escholarship.org/uc/item/9vd8d401

Authors
Xu, Z.
Yang, B.

Publication Date
1997

This paper has been mechanically scanned. Some errors may have been inadvertently introduced.

Brake System Analysis, Reliability Testing and Control Using Bench Experiments

Z. Xu

B. Yang

Brake System Analysis, Reliability Testing and Control using Bench Experiments

Z. xu
Center for Advanced Transportation Technologies
University of Southern California

B. Yang
Department of Mechanical Engineering
University of Southern California

Final Report on Project MOU 140

Brake System Analysis, Reliability Testing and Control using Bench Experiments

Z. X u and B. Yang

Summary of Completed Project

Implementation of intelligent vehicle/highway systems (IVHS) calls for good understanding of dynamics and reliability of automated brake systems. In this project we investigate the dynamics and reliability of a brake control system using a test bench, which is a Lincoln Town Car brake system specifically designed by Ford Motor Company. The objectives of this project are:

(a) To experimentally characterize the brake system;

(b) To obtain good nonlinear models of the brake system;

(c) To perform reliability analysis of the brake control system;

(d) To develop algorithms for brake malfunction detection and brake reliability enhancement.

By using the brake test bench, the dynamic characteristics of the brake-actuator system are studied experimentally. Based on the experimental results, two models are obtained for the first time - one for the whole brake-actuator system, the other for the hydraulic actuator. Efficient controllers are then designed to cancel the nonlinearities in the brake system. Through extensive experiments, algorithms for malfunction detection have been developed. Also, the feasibility of the brake control system to AVCS applications has been investigated.

Contents

List **of Figures**

List of Tables

1 Test Bench

The brake test bench, which is the main facility for this project, consists of a full-scale brake used in Ford/Lincoln Town Car, and an auxiliary hydraulic module (AHM) actuator. The actuator is specifically designed by Ford Motor Company for automatic braking. **A** schematic of the test bench is shown in Figure **1.** The brake system consists of a brake pedal, a master cylinder, a booster, a hydraulic cylinder, a control valve unit, a pump, an electronic control board, a computer, and some pressure sensors. The hydraulic cylinder, control valve, pump, electronic control board, and computer along with pressure sensors are the devices used to carry on actuation in automatic brake control. In braking mode, the pump keeps running, and pumps hydraulic fluid to the valve. When the control valve is open, the hydraulic fluid is returned to a reservoir tank. When the valve is closed, the fluid goes into the cylinder where the hydraulic pressure is being built up. The pressure will move the piston of the cylinder so **as** to push the operation rod of the booster. **As** a result, brake is applied. The longer the valve is closed, the higher the hydraulic pressure in the actuator and the braking pressure. If after a while, the control valve is reopened, the pressure in the cylinder will be reduced. Pulled by springs (not shown in the figure), the piston and operation rod will move back; the braking pressure will be reduced. The hydraulic cylinder is connected to the pedal bar in such a way that manual brake control is always possible without any effect on the actuator.
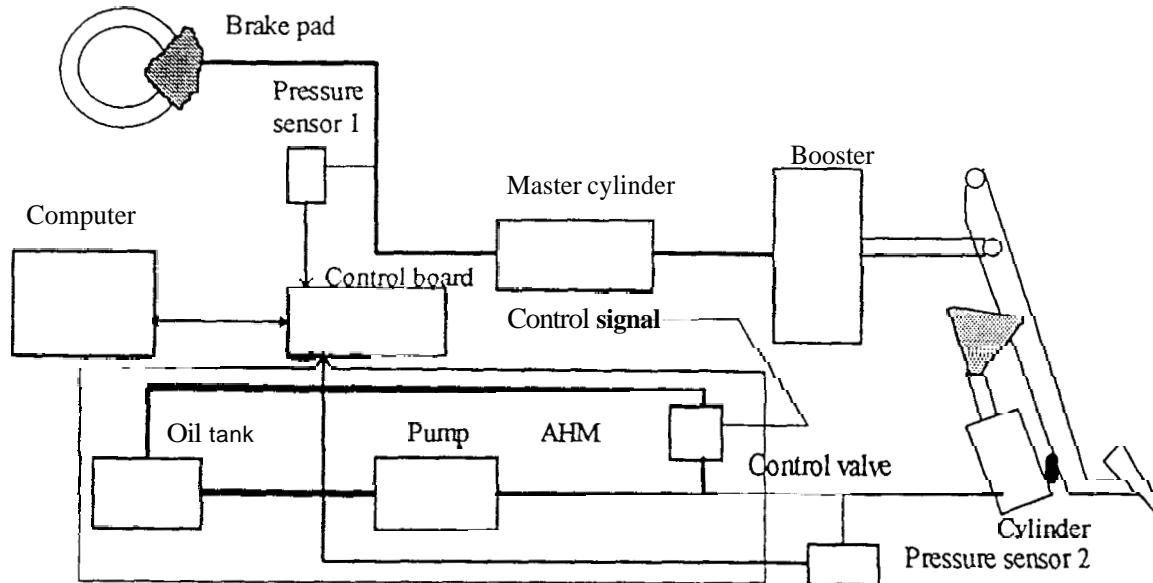

Figure 1: Schematic of the brake test bench.

1

According to the above description, the braking pressure can be controlled by opening and closing the control valve. Thus in the automatic control mode, the control input of the brake-actuator system is the opening/closing command to the valve; the output of the brake-actuator system is the brake-line pressure. The controller (the computer and the electronic control board) generates control signals (opening and closing commands) which are square waves with fixed frequency and magnitude and adjustable wave width, and are called pulse width modulated (PWM) signals. When the control signal is high, the valve is closed, and when the control signal is low or zero, the valve is open. The percentage of the wave width in a wave period is called duty cycle. The controller will control the braking pressure by changing the duty cycle of square waves.

2 Developments and Results

The main results obtained from this project are summarized in the following five subsections.

2.1 Modeling and Dynamic Analysis

2.1.1 The Input-Output Relation of the Whole Brake-Actuator System

The brake subsystem is one of the most significant part of a vehicle with respect to safety. The design of a computer controlled brake system has the capability of acting faster than the human driver during emergencies, and therefore has the potential of improving safety. In this study a nonlinear model for describing the input output behavior of the brake system is proposed. The brake model is developed based on a series of experiments conducted on the test bench described in Section **1.**

The developed model has the form of a first-order nonlinear system, where the system nonlinearities are lumped in the model coefficients. The unknown model parameters are identified by using curve fitting techniques on the experimental data. The major characteristics of the system input output curves such as time delay, effect of static friction, transient and steady state parts, have been identified in terms of model parameters. While it was done using staircase inputs, the parameter identification was shown to be valid for various continuous inputs. The hysteresis phenomenon was modeled by isolating the two operating modes (building mode and bleeding mode), and identifying separate sets of parameters for each mode. The modeling error in the worst case was found to be less than 5% within range of interest of the system.

For details on the model development, see the technical report [1].

2.1.2 Modeling of the Auxiliary Hydraulic Module (Actuator)

While the experimental model described in Section **2.1.1** provides a good description of the input-output dynamic behavior of the whole brake system, controller design and reliability

studies also request good understanding of the dynamics of some key components in the brake control system. Specifically, the **AHM** actuator is a main electro-hydraulic servo unit in the brake control system whose dynamic behavior is decisive to the transient response of the whole brake control system. Thus, accurate dynamic characterization of the actuator is essential to controller design and reliability studies for the brake control system.

A model of the control valve unit in the auxiliary hydraulic module is developed based on a series **of** experiments conducted on the test bench. The model is governed by a set of first-order nonlinear differential equations whose parameters are adjustable by lookup tables, according to different operating states of the control valve unit. The values of parameters in those lookup tables are determined from the experimental data by the standard curve fitting method.

It is noticed that for a step input (duty cycle) the pressure transients of the hydraulic cylinder fluid exhibit a "pseudo steady state" in a short period of time, which happens when the pressure increases from a low value and reaches a threshold. Physically, the pseudo steady state is mainly due to the time needed to build up the momentum of the fluid in the hydraulic cylinder so as to overcome the friction forces in the cylinder and other mechanical components. It is observed that the pseudo steady state has significant influence to the system transience. The conditions for the pseudo steady state to occur are determined based on the experimental data and by the theory of fluid dynamics.

The model developed has also been used to predict the dynamic response of the actuator under other types of inputs. The numerical simulations using the developed model are in good agreement with the experiments in the parameter range of interest. Details on the modeling can be seen in the technical report [2].

2.2 Brake Controller Design

The strict spacing requirement of automated highway system **(AHS)** demands a brake controller that can provide good tracking of braking commands with minimum possible overshoot. On the other hand during emergency maneuvers the required braking force should be achieved with minimum possible delay. These conflicting control strategies are standard in control practice and are usually handled by introducing appropriate trade offs in the control design.

The objectives of brake controller **design** are to cancel the nonlinearities **of** the system, and to make the brake system behave **as** uniformly **as** possible throughout the operating range of the system. The main advantage of this linearization is that the vehicle following controllers can be designed without considering the details of nonlinearities of a particular brake system. The brake controller design proposed here, makes use of standard feedback linearization technique **[6]** applied to the nonlinear brake model developed earlier *(see Section 2.1.1).

3

A **PI** compensator with some modifications is introduced in the closed loop to meet the performance specifications. The required swiftness of response, without significant sacrifice of performance requirements, is achieved by introducing a modification in **PI** compensator design. This modification allows **us** to obtain the fastest possible response, restricted by the physical constraints of the system, with no overshoot. While the logic is developed for the specific brake system under consideration, it can be easily adopted for different systems having saturation limits in the control authority.

The simulation results show that the proposed controller guarantees no overshoot and zero steady state error for step inputs. The controller is tested on the brake test bench, results indicate that the required performance is achieved. See the technical report **[3]** for details.

2.3   Malfunction Detection

Potential failure modes associated with complete or partial loss of braking capability of a computer controlled brake system are identified by fault tree analysis. In the analysis deductive reasoning is applied to find basic events leading to complete or partial brake failure. The results are useful for building cause and effect relationship for the potential failures, which is required for a comprehensive fault diagnosis scheme [5].

Three different fault detection schemes are proposed based on the residual error detection theory [7]. The residual error is obtained by comparing the output of brake system with that of the validated brake model obtained in the earlier part of the study. These schemes differ on the basis of underlying assumptions and hence the applicability and detection accuracy. The concept of closed loop system detection is introduced to increase the robustness of detection against parameter shifts and modeling inaccuracies.

The basic events, for potential failure modes, identified by fault tree analysis are used to test the accuracy of the proposed fault detection schemes. Finally, the successful implementation of the detection algorithm on the brake system test bench proves the effectiveness of the proposed scheme.

The above-mentioned malfunction detection schemes are presented in the technical report [4].

2.4   Feasibility Study

The feasibility of the brake actuator to **AVCS** applications is investigated based on its dynamics characterized from the test bench. Different operating scenarios in vehicle following involving two vehicles are studied; the minimum safe headway in each case is calculated under the assumption that the brake actuator is used in an automatically controlled vehicle.

The detail of the analysis is given in the Appendix **A.** For the convenience of discussion, the following parameters are defined:

J_{lm}, a_{lm}: maximum jerk and deceleration of leading vehicle that is manually driven

J_{fm}, a_{fm}: maximum jerk and deceleration of trailing vehicle that is manually driven

J_{fc}: maximum jerk of the trailing vehicle in automatic driving mode

V_{lm}, V_{fm}: speeds of leading and trailing vehicles, respectively

t_{fa}: detection time delay plus actuator time delay.

Case 1(a): The leading vehicle is manually driven, the trailing vehicle is under automatic control, and there is no driver intervention. The leading vehicle has a maximum deceleration of 0.8 g and the maximum jerk of **32, as** measured from the test bench. The minimum safe time headway is about **4.33** sec. in this operating scenario.

Case 1(b): The leading vehicle is manually driven, the trailing vehicle is under automatic control, and there is driver intervention. Based on the different driver reaction times, the minimum safe headways are calculated, and shown in Table 1. In the table, the values of t_{fa}, J_{fc} and J_{lm} are measured from the test bench, and the values of J_{fm}, a_{lm}, a_{fm} are assumed based on a conservative estimation. For the comparison purposes, the minimum safe headways in manual driving situation are also listed in the table.

Case 2(a): Both the leading and trailing vehicles are under automatic control, and there is no vehicle-to-vehicle communication and driver intervention. With the same parameters as given in Table 1, the minimum safe time headway is found to be **0.946** sec., which is slightly shorter than that in manual driving.

Case 2(b): Both the leading and trailing vehicles are under automatic control; there is driver intervention, but no vehicle-to-vehicle communication. In this case the minimum safe headway is the same as that in **case** 1(a).

Case 2(c): Both the leading and trailing vehicles are under automatic control; there is vehicle-to-vehicle communication, but no driver intervention. **In** this operating situation, the minimum safe headway is about **0.5456** sec.

Case 2(d): Both the leading and trailing vehicles are under automatic control; there is vehicle-to-vehicle communication and driver intervention. The minimum safe headways for different driver reaction times are listed in Table **2,** where the parameters are the same as in Table 1. The detail of the above study is given in the Appendix A of this report.

$V_l(0) = 60mph,\ V_f(0) = 63mph,\ a_{lm} = 0.8g\ a_{fm} = 0.6g$ $J_{lm} = 32m/s^3,\ J_{fc} = 3.92m/s^3,\ J_{fm} = 24m/s^3,\ t_{fa} = 0.4$				
	automatic		manual	
Reaction time t_{fc} (s)	minimum headway (m)	minimum t-headway (s)	minimum headway (m)	minimum t-headway (s)
0.4	32.66	1.17	32.66	1.17
0.6	37.02	1.32	38.26	1.36
0.8	40.73	1.45	43.86	1.57
1.0	43.79	1.56	49.46	1.77
1.2	46.86	1.67	55.06	1.97
1.4	49.94	1.78	60.66	2.17
1.6	52.96	1.89	66.26	2.37
1.8	55.92	2.00	71.86	2.57
2.0	58.83	2.10	77.46	2.77

Table 1: Minimum safe headway in Case 1(b)

$V_l(0) = 60mph,\ V_f(0) = 63mph,\ a_{lm} = 0.8g\ a_{fm} = 0.6g$ $J_{lm} = 32m/s^3,\ J_{fc} = 3.92m/s^3,\ J_{fm} = 24m/s^3,\ t_{fa} = 0.4$				
	automatic		manual	
Reaction time t_{fc} (s)	minimum headway (m)	minimum t-headway (s)	minimum headway (m)	minimum t-headway (s)
0.4	22.26	0.791	32.66	1.17
0.6	22.39	0.795	38.26	1.36
0.8	22.25	0.790	43.86	1.37
1.0	21.85	0.776	49.46	1.77
1.2	21.46	0.762	55.06	1.97
1.4	21.09	0.749	60.66	2.17
1.6	20.73	0.736	66.26	2.37
1.8	20.38	0.724	71.86	2.57
2.0	20.05	0.712	77.46	2.77

Table 2: Minimum safe headway in Case 2(d)

6

This brake actuator can apply soft brake. If the automated vehicles equipped with this brake actuator are mixed with the manually driven vehicle in one lane, then driver interventaion is necessary. Otherwise, the desired headway will be too large. If the automated vehicles equipped with this brake actuator are on a designated auto-lane, then driver intervention are not recommended without vehicle to vehicle communication. If vehicle to vehicle communication is used, the minimum time headway will be always not larger than that required for manual driving. In some case, the minimum safe time headway can be as small as 0.55 seconds with this brake actuator.

2.5 Reliability Study

The brake system of a vehicle is used tens of thousand times during its whole life. Any failure in the brake system may lead to catastrophic consequences, which is specially true in automated brake systems. It is therefore important to foresee a failure in the brake control system before it happens. Although reliability tests have been conducted on standard parts of brakes on manually driven vehicles, comprehensive reliability study of the whole brake control system has not been addressed.

Repeated brake operations are conducted on the test bench over a long period of time period. The purpose is to check the stability of the system characteristic parameters (such as brake line and auxiliary hydraulic module pressures to certain inputs), and hence to conclude the reliability of the brake system. As shown in Fig. 1 pressure sensors 1 and 2 measure the cylinder hydraulic pressure and the brake line pressure, respectively; a temperature sensor monitors the temperature at the surface of the pump motor, which is the hottest spot on the whole test bench, and is susceptible to failure due to overheating in case of long continuous operation. A brake operation on the test bench, as a simulation of real braking situation, takes three steps: (i) start the pump and apply the brake by building up pressure in the actuator; (ii) release the brake by settling the actuator to idle position; and (iii) stop the pump. This operation is automatically controlled by a computer. In the test, brake is applied four time per minute for 40 hours; i.e., total **9,600** times of braking. This number can be translated into the brake usage for a driving distance of **3,200** to 4,800 miles, assuming that the brake is applied 2 to **3** times per mile of normal driving.

The brake line pressure and cylinder pressure remain stable and the pump motor temperature is within a reasonable range, showing that the brake system under consideration can be operated reliably for extended period of time without serious deterioration of system characteristics.

3 Concluding Remarks

Based on experiments on the test bench which is a real brake system in a Lincoln Town Car, we have obtained nonlinear models of the brake-actuator system and an auxiliary hydraulic

module. It has been shown that the predictions by the models are in good agreement with the experimental data. By using these models, reliability and malfunction detection for the brake control system have been investigated. To make the brake system behave as uniformly as possible throughout its operating range, control algorithms that cancel the nonlinearities of the brake-actuator system have been designed. The results obtained from this project will be useful for the future studies on robustness and safety of automatic brake control, and for other IVHS projects.

4 Publications Resulting from this Project

1. Brake Modeling **for** AVCS Application, Raza, **H.,** Xu, Z., Ioannou, **P.,** Yang, B., USG CATT Report #94-

2. Experimental Model of Control Valve Unit in the Auxiliary Hydraulic Module of a Vehicle Brake System, Du, **L.,** Xu, Z., Yang, **B.,** USGCATT Report #95-06-01

3. Modeling and Control Design for a Computer Controlled Brake System, Raza, H., Xu, Z., Ioannou, P., Yang, B., USC-CATT Report #95-06-02

4. Failure Detection of a Computer Controlled Brake System, Raza, **H.,** Xu, Z., Ioannou, P., Yang, B., USC-CATT Report #95-06-03

Appendix A: Feasibility Study of the Brake Actuator

The brake actuator has been tested on the bench **for** its characteristics like bandwidth, rise time, maximum pressure, etc. Based on the experiment results, we now analyze the feasibility of brake actuator to IVHS in terms of the capability of avoiding collision in emergency situation if the trailing vehicle is equipped with this brake actuator.

We analyze the minimum safe headway under different operation situations. In each o p eration situation we consider the general stopping scenario for vehicle following: the leading vehicle commences a stopping maneuver at the time the trailing vehicle has a faster speed than the leading vehicle. Some researchers use the worst case scenario where leading vehicle commences a stopping maneuver when the trailing vehicle is at maximum acceleration. However, when the trailing vehicle's speed is faster than that of leading vehicle, it is reasonable to assume that the trailing vehicle is about to decelerate (at least the acceleration is zero). This is true under manual driving and when the relative space is small. This is more likely under automatic control. In addition, the acceleration is normally small, the effect of positive acceleration is not significant based on our calculation. Thus, in our analysis, we assume that both vehicle has zero acceleration in the beginning of the stopping maneuver. Of course, if necessary, we can change the initial relative speed to counteract the effect of initial acceleration.

Case 1. The leading vehicle is driven manually and the trailing vehicle is under automatic control.

In the emergency stopping scenario in this case the leading vehicle behavior is described as follows:

At time $t = 0$, the leading vehicle brake with maximum jerk (J_{lm}) until it reaches its maximum deceleration $(-a_{lm})$. Then it keeps this deceleration until a full stop. The acceleration profile of the leading vehicle is shown in Figure **2** where the t_l, is the time at which the vehicle reaches the maximum deceleration and t_{ls} is the time at which the vehicle reaches full stop. Let $X_l(0)$ and V_0 indicate the initial position and speed respectively. Then based on this acceleration profile, we have that

$$t_{ls} = \frac{V_l(0) - J_{lm} \, t_{la}^2/2}{a_{lm}} + t_{la}, \tag{1}$$

$$t_{la} = \frac{a_{lm}}{J_{lm}} \tag{2}$$

and

$$X_l(t_{ls}) = X_l(0) + V_l(0)t_{ls} - \frac{J_{lm}}{6}t_{la}^3 - \frac{J_{lm}}{2}t_{la}^2(t_{ls} - t_{la}) - \frac{a_{lm}}{2}(t_{ls} - t_{la})^2 \tag{3}$$

Now let us consider the trailing vehicle's behavior. There are two situations: (a) no driver intervention, (b) having driver intervention in emergency. We consider them sepa-
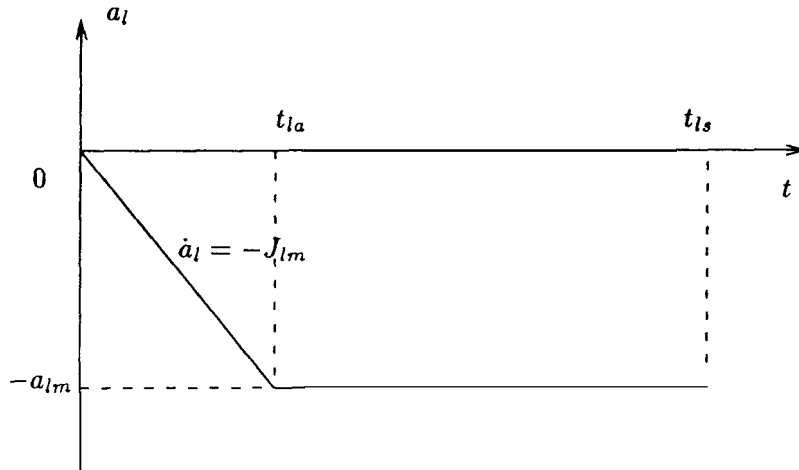
Figure **2:** Acceleration profile for the leading vehicle in emergency stopping

rately.

(a) No driver intervention.

In this case the trailing vehicle behavior is described as follows:

At $t = 0$ the trailing vehicle is at constant speed. After certain time delay (t_{fa}) due to the data processing and actuating delay, the trailing vehicle starts to brake with certain jerk $(-J_{fc})$ until it reaches the deceleration limit (a_{fa}) applied by the software at $t = t_{fb}$. Then it keeps this deceleration until full stop at $t = t_{fs}$. the profile of acceleration of the trailing vehicle in this case is shown Figure **3.**

Based on the bench test and road test results we find that manual braking may have the jerk of $-32\ m/s^3$, that is $J_{lm} = 32\ m/s^3$. From the bench test we also find that the current brake actuator can only achieve **260** psi brake line pressure which is approximately corresponding to $0.25g$ deceleration for Lincoln Towncar, the jerk is about $J_{fc} = 3.92m/s^3$, and actuator time delay is about **0.2** seconds. Assume that $V_l(0) = V_f(0) = 60$ mph, $a_{lm} = 0.8g = 0.784m/s^2$ which is achievable by many vehicles, the detection time delay is **0.2** second (which implies $t_{fa} = 0.4s$). Then based on Figures **2** and **3** and using the software developed in [8], we find that the minimum initial safe headway is **115.39** meters, or equivalently the minimum initial safe time headway is **4.33** seconds. This time headway is too large and this operation scenario should be prevented.

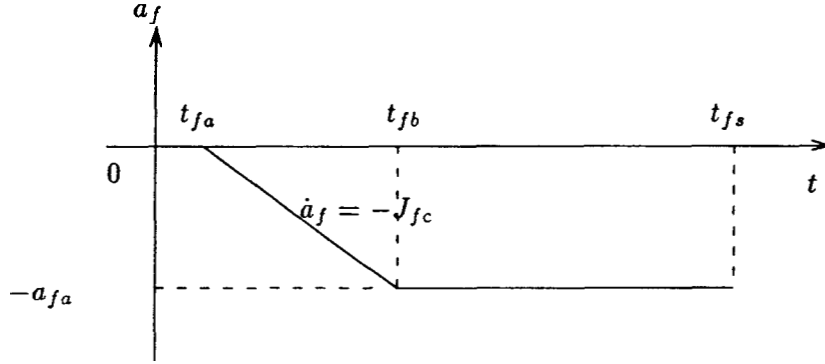(b) Having driver intervention.

Figure **3:** Acceleration profile for the trailing vehicle in emergency stopping, no driver intervention

In this case the trailing vehicle has the same acceleration profile **as** that in Figure **3** in the beginning. However, after certain time t_{fc} the driver takes over the brake and applies the brake with maximum jerk (J_{fm}) until the deceleration reaches the maximum value $-a_{fm}$. Then the vehicle keeps this deceleration until full stop. The time t_{fc} is the driver reaction time. **As** in situation (a),we take $t_{fa} = \mathbf{0.4}$ seconds, $a_{fa} = 0.25$ **g**, $\boldsymbol{J_{fc} = 3.92m/s^3}$, $J_{lm} = 32m/s^3$, $a_{lm} = 0.8g$, and $V_l(0) = 60mph$. For conservative caculation, we assume that $V_f(0) = 63mph$ (because the trailing vehicle is under automatic longitudinal control, **3** mph speed difference is suitable,) $J_{fm} = 24m/s^3$, and $a_{fm} = 0.6g$. Then Figures 2 and **4** and using the software offered in [8], we can find the minimum safe headway for each given diver rsaction time **as** shown in Table **3.**

For comparison, we also list the corresponding minimum safe headway and time headway under manual driving, that is the brake is applied at t_{fc} with J_{fm} and a_{fm}. It is seen from this table that with this brake actuator, the minimum safe time headway has slight improvement over the manual driving if the driver reaction time is less than 1 second, and have significant improvement over the manual driving if the driver reaction time is large. This improvement is due to the reduction in reaction time by the automatic controller.

Case 2. The leading vehicle and trailing vehicle are both under automatic control.

In this case there are several situations: (a) no vehicle to vehicle communication and no driver intervention, (b) no vehicle to vehicle communication but with driver intervention, (c) with vehicle to vehicle communication but **no** driver intervention, **(d)** with vehicle to vehicle communication and with driver intervention. We now discuss them separately.

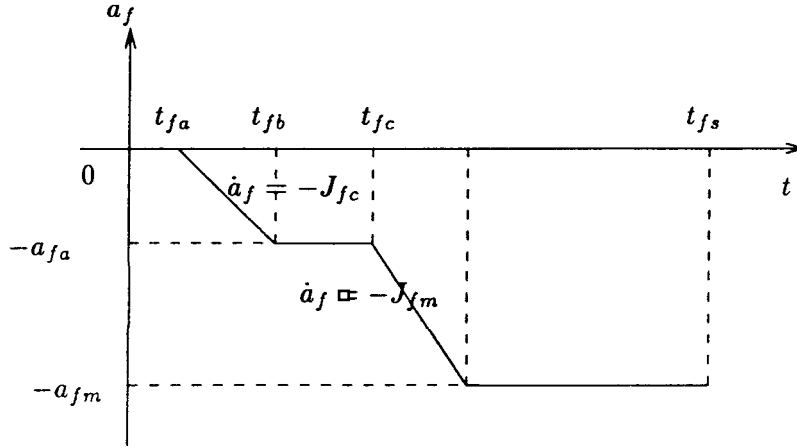(a) No vehicle to vehicle communication and no driver intervention.

11

Figure 4: Acceleration profile for the trailing vehicle in emergency stopping, having driver intervention

$V_l(0) = 60mph$, $V_f(0) = 63mph$, $a_{lm} = 0.89$ $a_{fm} = 0.6g$ $J_{lm} = 32m/s^3$, $J_{fc} = 3.92m/s^3$, $J_{fm} = 24m/s^3$, $t_{fa} = 0.4$				
	automatic		manual	
Reaction time t_{fc} (s)	minimum headway (m)	minimum t-headway (s)	minimum headway (m)	minimum t-headway (s)
0.4	32.66	1.17	32.66	1.17
0.6	37.02	1.32	38.26	1.36
0.8	40.73	1.45	43.86	1.57
1.0	43.79	1.56	49.46	1.77
1.2	46.86	1.67	55.06	1.97
1.4	49.94	1.78	60.66	2.17
1.6	52.96	1.89	66.26	2.37
1.8	55.92	**2.00**	71.86	2.57
2.0	58.83	2.10	77.46	2.77

Table 3: Minimum safe headway in Case 1(b)

In this situation the leading vehicle's behavior during stopping maneuver is similar to that in situation (a) in Case **1** with the J_{lm} and a_{lm} substituted by J_{lc} and a_{la} respectively. We assume that the leading vehicle and the trailing vehicle are equipped with the same brake actuators, which implies that $J_{lc} = J_{fc}$ and $a_{la} = a_{fa}$.

The acceleration profile of the trailing vehicle is exactly same as shown in Figure **3.** Assume that $V_l(0) = \mathbf{60}$ **mph,** $V_f(0) = 63mph$, and detection time delay is **0.2** seconds. **Based** on Figure **3** and Figure **2,** where the J_{lm} and a_{lm} are replaced by $J_{lc} = J_{fc}$ and $a_{la} = a_{fa}$ respectively, and using the previous number for J_{fc}, a_{fc}, and actuator time delay, and the software in [8], we can find that the minimum initial safe headway is **26.48** meters, and the minimum initial time headway is 0.946 seconds. This time headway requirement is slightly smaller than that in manual driving.

(b) No vehicle to vehicle communication but with driver intervention.

Because the driver can intervene during the emergency, the acceleration profile of the leading vehicle during emergency stopping may be exactly the same as in case **1** (manually driven case). Thus, the minimum time headway requirement is the same as in situation (b) of case **1.**

(c) With vehicle to vehicle communication but no driver intervention.

In this situation we assume that the leading vehicle will communicate the message to the trailing vehicle as soon as it detects a emergency situation. Because the communication delay is normally very small (one sampling period) the brake in the trailing vehicle will be applied almost at the time as in the leading vehicle during emergency. Since the actuator time delays are same in both leading and trailing vehicles, these actuator time delays can be ignored, leading to the same acceleration profiles for both leading and trailing vehicles as shown in Figure **3** with $t_{fa} = 0$. Assume that $V_l(0) = \mathbf{60}mph$, $V_f(0) = 63mph$, $J_{lc} = J_{fc} = 3.92m/s^3$, $a_{la} = a_{fa} = 0.25g$. Then based on Figure **3** with $t_{fa} = 0$ and using the software in [8], we have that the minimum safe headway and time headway at $t = 0$ are respectively **15.28** meters and **0.5456** seconds. This time headway is much less than that required for manual driving.

(d) With vehicle to vehicle communication and with driver intervention.

Suppose at the time $t = 0$, an emergency happens before the leading vehicle. The behaviors of the leading vehicle and trailing vehicle are described as follows:

Leading vehicle: At $t = 0$, the acceleration of the leading vehicle is zero (assumption). At $t = t_{la}$ the controller detects the emergency] applies the brake, and communicates

the information to the trailing vehicle. At $t = t_{lb} = t_{la} +$ actuator delay, the acceleration decreases with slope J_{lc}. Normally, t_{lb} is less than the driver reaction time. At $t = t_{lc}$ (driver reaction time), the driver intervenes and the acceleration decreases with slope J_{lm}. At $t = t_{ld}$, the deceleration reaches the maximum value a_{lm}. Starting from $t = t_{ld}$, the vehicle keeps this deceleration until full stop at $t = t_{fs}$. The acceleration profiles of the leading vehicle is shown in Figure **5.**
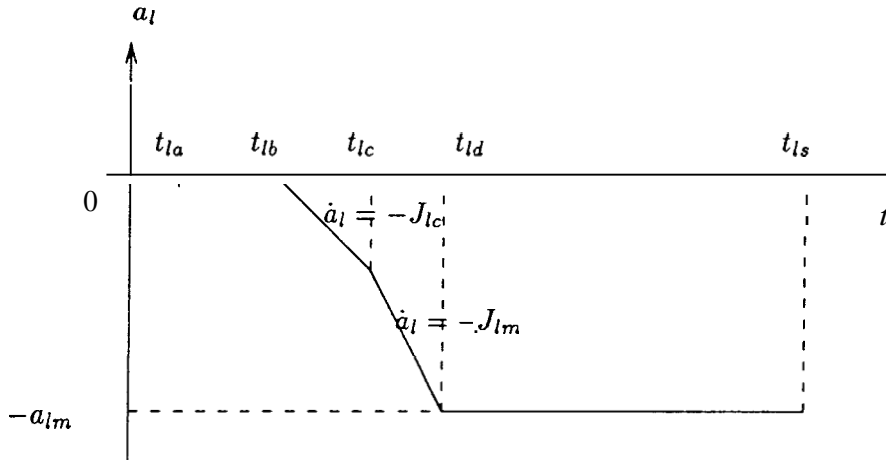
Figure **5***:* Acceleration profile of leading vehicle during emergency stopping, with communication and driver intervention

Trailing vehicle: If we ignore the communication time delay, the trailing vehicle will apply brake automatically at $t = t_{la}$. At $t = t_{fb} = t_{la} +$ actuator delay, the acceleration decreases with slope J_{fc}. At $t = t_{fc}$ (driver reaction time), the driver intervenes and the acceleration decreases with slope J_{fm}. At $t = t_{fd}$, the deceleration reaches the maximum value a_{fm}. Starting from $t = t_{fd}$, the vehicle keeps this deceleration until full stop at $t = t_{fs}$. The acceleration profiles of the trailing vehicle is shown in Figure **6.**

Assume the brake actuator under consideration is used in both the leading and trailing vehicles, leading to $t_{fb} = t_{lb}$ and $J_{fc} = J_{lc}$. Based on our bench test we have that actuator time delay is **0.2** seconds, $J_{lm} = 32 m/s^3$ $J_{fc} = J_{lc} = 3.92 m/s^3$. We also assume $a_{fa} = a_{la} = $ **0.25g**, and the detection time $t_{la} = $ **0.2** seconds. For a conservative estimate, we assume that $J_{fm} = 24 m/s^3$, $a_{lm} = 0.8g$, $a_{fm} = 0.69$, $V_l(0) = 60mph$ and $V_f(0) = 63mph$. We further assume that both drivers have the same reaction time. Using Figure 5 and Figure **6** and these numbers, we have the results on minimum safe headwaw **as** shown in Table **4.**

Remarks

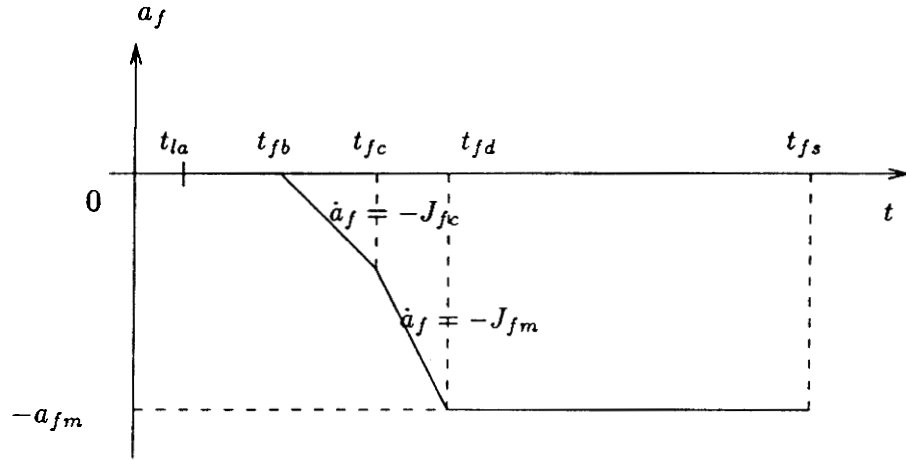- From Table **4** we can **see** that the safe minimum time headway only changes slightly

14

Figure 6: Acceleration profile of trailing vehicle during emergency stopping, with communication and driver intervention

$V_l(0) = 60mph$, $V_f(0) = 63mph$, $a_{lm} = 0.8g$ $a_{fm} = 0.6g$				
$J_{lm} = 32m/s^3$, $J_{fc} = 3.92m/s^3$, $J_{fm} = 24m/s^3$, $t_{fa} = 0.4$				
	automatic		manual	
Reaction time t_{fc} (s)	minimum headway (m)	minimum t-headway (s)	minimum headway (m)	minimum t-headway (s)
0.4	**22.26**	0.791	*32.66*	1.17
0.6	22.39	0.795	*38.26*	**1.36**
0.8	22.25	0.790	43.86	1.57
1.0	21.85	0.776	49.46	**1.77**
1.2	21.46	0.762	**55.06**	1.97
1.4	21.09	0.749	60.66	2.17
1.6	**20.73**	0.736	66.26	2.37
1.8	**20.38**	0.724	71.86	2.57
2.0	20.05	0.712	77.46	2.77

Table 4: Minimum **safe** headway in Case 2(d)

15

with respect to driver reaction time in this operation sicenario. This is because we assume the same driver reaction time in the leading vehicle and the trailing vehicles.

o In this operation sicenario, the time headway shows a significant reduction over that in manually driving case.

o Although it is possible that the trailing vehicle may be more than **3** mph faster than the leading vehicle, the time headways requirement shown in Table **4** are reliable since we have taken conservative assumption in the maximum jerk and maximum deceleration for the trailing vehicle.

Feasibility Conclusion

This brake actuator can apply soft brake. If the automated vehicles equipped with this brake actuator are mixed with the manually driven vehicle in one lane, then driver interventaion is necessary. Otherwise, the desired headway will be too large. If the automated vehicles equipped with this brake actuator are on a designated auto-lane, then driver intervention are not recommended without vehicle to vehicle communication. If vehicle to vehicle communication is used, the minimum time headway will be always not larger than that required for manual driving. In some case, the minimum safe time headway can be as small as 0.55 seconds with this brake actuator.

Appendix B: Brake Modeling for AVCS Application

(See the attached technical report.)

Brake Modeling **for** AVCS Application

by

H. Raza, Z. Xu, P. Ioannou and B. Yang

Brake Modeling for AVCS Application *

H. Raza, Z. Xu and P. Ioannou

Dept. of Electrical Engineering-Systems

University of Southern California

Los Angeles, CA 90089-2563

B. Yang

Dept. of Mechanical Engineering

University of Southern California

Los Angeles, CA 90089-1453

Abstract. In this paper we consider the problem of dynamic modeling of the brake system for AVCS application. The brake model is developed **based** on a series of experiments conduted on a test bench which contains the actual conventional brake components and the actuator designed specifically for AVCS by Ford Motor Company. The proposed nonlinear model is simplified to match the general form of a first order linear system with the system nonlinearities lumped in the model coefficients. This approach results in a model which can be easily adopted for controller design. The unknown model parameters are identified using standard curve fitting techniques. The major characteristics of the input output curves, time delay, effect of static friction, transient and steady state parts have been dealt separately.

1 Introduction

With an ever-increasing number of vehicles on the limited highways, it has become urgent to develop sophisticated technical solutions to today's surface transportation problems. It has been shown that Intelligent Vehicle/Highway Systems (IVHS) are promising solutions [1]-[5]. An Important part of IVHS is the Automated Vehicle Control Systems (AVCS), which has three essential parts: throttle control, steering control, and brake control. From safety point of view, brake control is more important than the throttle and steering control. To reduce the risk of human life, an extremely reliable brake system and its controller must be used. In order to design a reliable and fault tolerant brake controller the brake system should be precisely modeled.

During past few years, a sufficient interest has developed among different research groups to develop the models of the brake system for AVCS application. One of the significant contribution is the work of Gerdes et al [6]. A bondgraph method for modeling the components

of manual brake system is considered in the paper by Khan, Kulkarni and Yocef-Toumi [7]. In these studies more emphasis is given to identify the dynamics associated with each component. What clearly lacking is a comprehensive dynamic model of brake system to identify the mapping from input to output. ***The main purpose of this* paper *is to develop a model that can be used to design a controller* for *brake* system *in AVCS application.***

The brake model is developed based on experiments with the brake test bench provided by the Ford Motor Company. The block diagram of the complete brake system is shown in figure (1). The test bench has all the conventional brake components: brake pedal, vaccum booster, master cylinder and brake lines. In addition, the test bench contains an auxiliary hydraulic module (AHM) which consists of a hydraulic pump, control valves and an actuator and is designed by Ford specifically for automatic brake application.

The **AHM** takes control input in the form of a pulse width modulated **(PWM)** signal and generates a pressure to be applied to the brake pedal through an actuator. The output pressure of the actuator and hence the brake line pressure can be controlled by changing the duty cycle of PWM signal. The AHM is designed specifically for **AVCS** applications and has not been considered in the previously developed models. In this paper we will develop the model for the brake system which includes the **AHM.**

The approach followed here is to propose a model motivated by the experimental results. A series of experiments were conducted on the brake test bench. The curve fitting techniques are then applied to data obtained from these experiments to identify the unknown model parameters. The resulting model is nonlinear but easy for control design.

The following section describes the structure of the brake system components. Only brief introduction of the main components of brake system is given here. For a detailed discussion of the subject, suggested readings are [8], [6]. The proposed model and the motivation for this selection is discussed in section three. In section four we consider the problem of identification of unknown model parameters. This is followed by simulation results and model validation. Section six covers some of the limitations of the proposed model. Key points are discussed again in conclusion section.

2 Brake System Components

The main components of the brake system shown in figure (1) are discussed below.

2.1 Auxiliary Hydraulic Module

The function of **AHM** is to provide an input force to vaccum booster through an actuator and brake pedal. The force applied to brake pedal is a function of the input **(PWM)** signal, which is in the form of a square wave of fixed frequency but varying duty cycle.
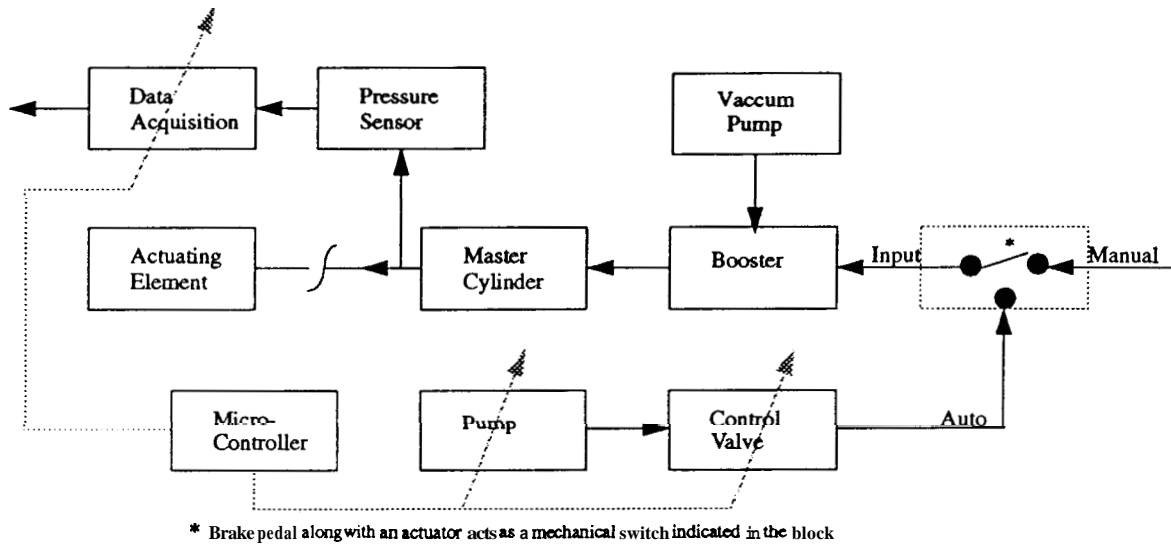
* Brake pedal along with an actuator acts as a mechanical switch indicated in the block

Figure 1: **Block Diagram** of **the Brake** System
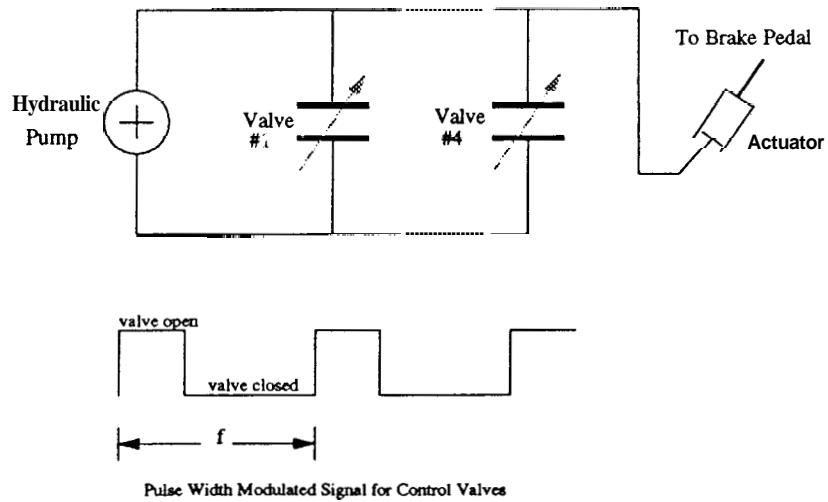

Pulse Width Modulated Signal for Control Valves

Figure 2: Block Diagram of **Auxiliary Hydraulic Circuit**

As shown in figure (2) **AHM** consists of a hydraulic pump, an arrangement of valves and an actuator. **As** a constant amount of fluid is pumped through the valves by the hydraulic pump, no pressure is developed inside the cylinder of the actuator if the valves are open. Whereas a sudden rise of pressure is obtained if the valves are closed completely. Hence an average amount of pressure can be maintained inside the cylinder of the actuator by switching the valves at high frequency (typically 100 Hz) with changeable duty cycle (percentage of valve open time in one switching period). This pressure will push the piston of the actuator and apply a force to the brake pedal.

When the duty cycle is changed, the pressure inside the cylinder of the actuator changes too. Hence the force applied to the brake pedal can be controlled by varying the duty cycle of the PWM signal. It should be noted that the maximum value of duty cycle corresponds to valves being open for most of the time and hence no force is applied to the brake pedal, which results in minimum brake line pressure at the output of master cylinder. From the overall system point of view any permissible pressure value at the output of master cylinder can be obtained by some particular value of duty cycle. *The purpose of this* `paper` *is to identify this mapping from duty cycle to the line pressure.*
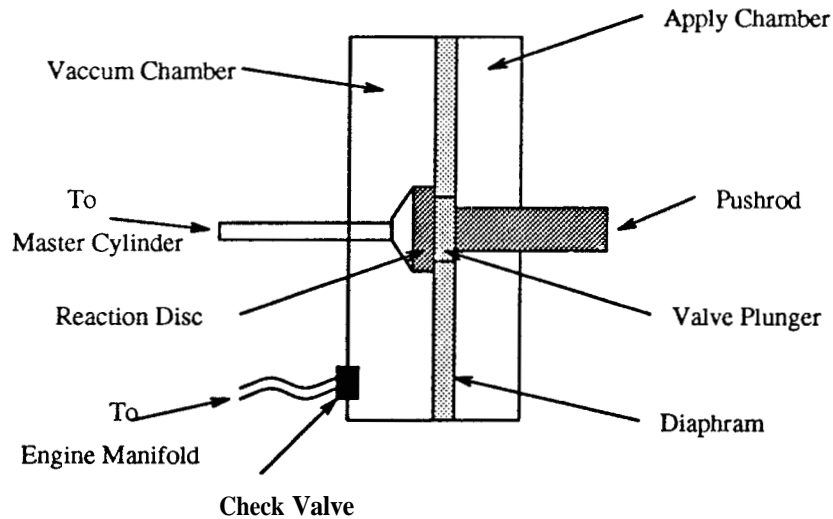
2.2 Vaccum Booster

Figure **3:** Block Diagram of Vaccum Booster

The simplified construction of vaccum booster is shown **in** figure **(3).** The force amplification is caused by a pressure differential between the apply and vacuum chambers. Ideally, the amplification ratio between input and output force should be constant over the recommended range of operation. However, due to booster dynamics this ratio is not constant.
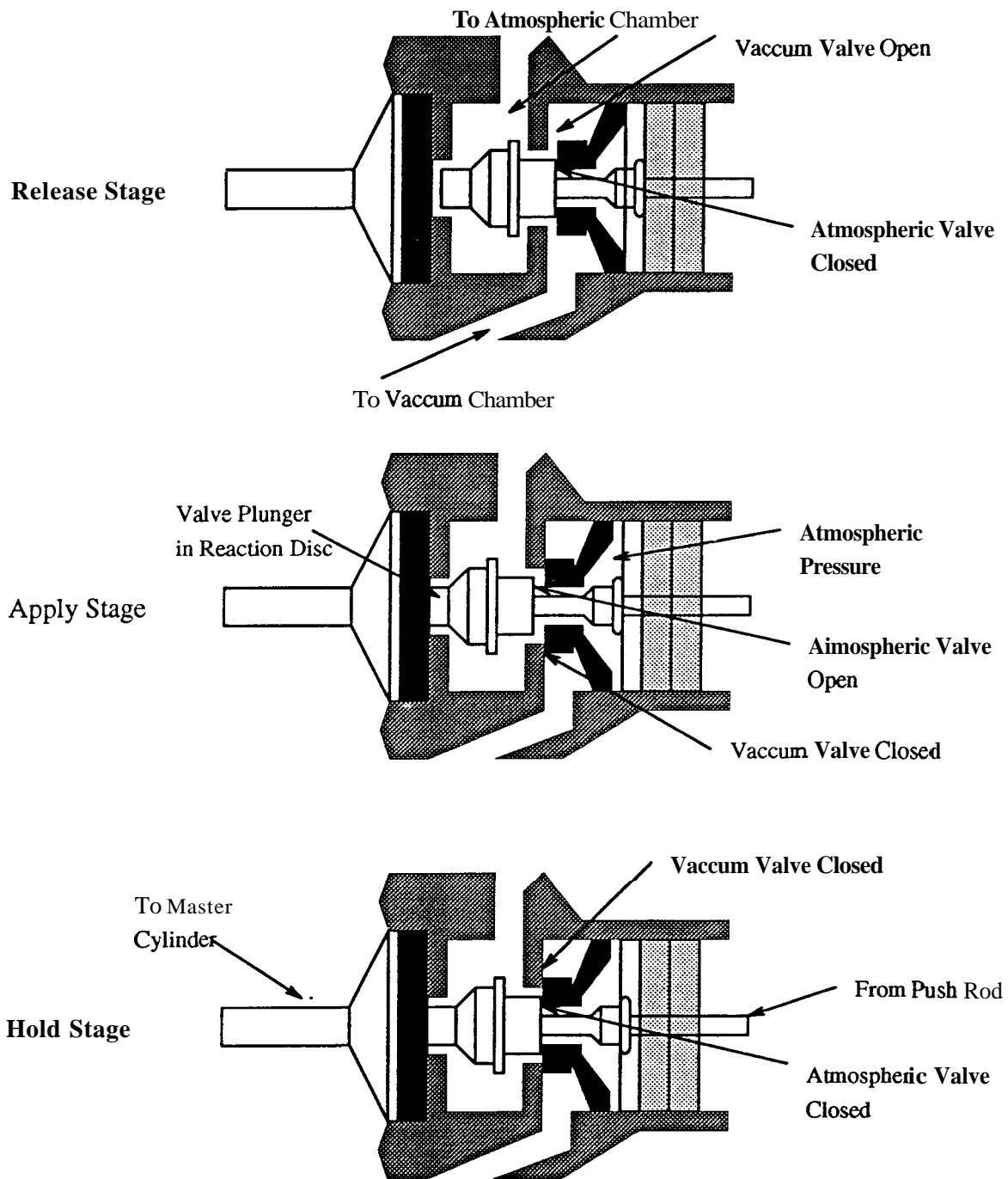
Release Stage

To Atmospheric Chamber

Vaccum Valve Open

Atmospheric Valve Closed

To Vaccum Chamber

Apply Stage

Valve Plunger in Reaction Disc

Atmospheric Pressure

Aimospheric Valve Open

Vaccum Valve Closed

Hold Stage

To Master Cylinder

Vaccum Valve Closed

From Push Rod

Atmospheric Valve Closed

Figure 4: Vaccum Booster Operation

According to operation of booster each brake application operation can be broken down into three basic stages: **1.** apply stage 2. hold or lap stage **3.** release stage. These steps are shown in figure **(4).**

o In the apply stage control valve moves forward, atmospheric valve is opened and vaccum valve is closed, hence a pressure differential is created, cuasing the diaphragm to move forward.
o When the diaphragm travels further, valve housing catches up with the control valve. This movement also closes atmospheric valve. The diaphragm and valve body are now in hold position.
o When the brake pedal is released, the control valve moves back due to spring force, apply and vaccum chambers are connected and the pressure differential is reduced to zero.

Since the inertia of pushrod and diaphragm is quite significant, the associated dynamics can not be neglected. Furthermore, the changes of pressure in apply and vaccum chambers also give rise to thermodynamics. For more detailed discussion of these effects, see [6].
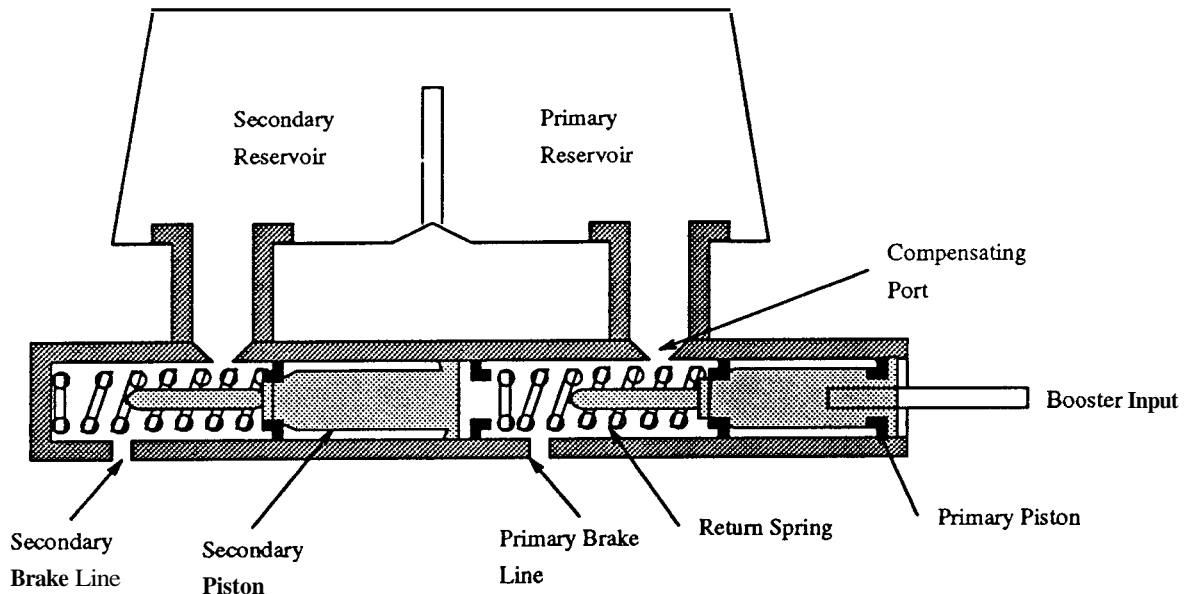
2.3 Master Cylinder

Figure 5: Block Diagram of Master Cylinder

The block diagram of a tandem master cylinder is shown in figure (5). Input force, after being amplified by the vaccum booster, is applied through a push rod to the primary piston. The secondary piston, however, is pushed by hydraulic force built up by the primary piston.

Each portion of the master cylinder has its own separate reservoir, compensating port and outlet port. When an input force is large enough to move the primary piston to close the compensating port, pressure begins to build up between the primary and secondary piston. When the secondary compensating port is closed, pressure buildup occurs in the secondary portion too. At the same time hydraulic pressure developed during this operation is transferred through primary and secondary brake lines to brake pads.

As discussed in [6], since the masses of the pistons are negligible, the dynamics associated with them can be neglected.

3 Proposed Brake Model

Plot of brake line pressure for different inputs
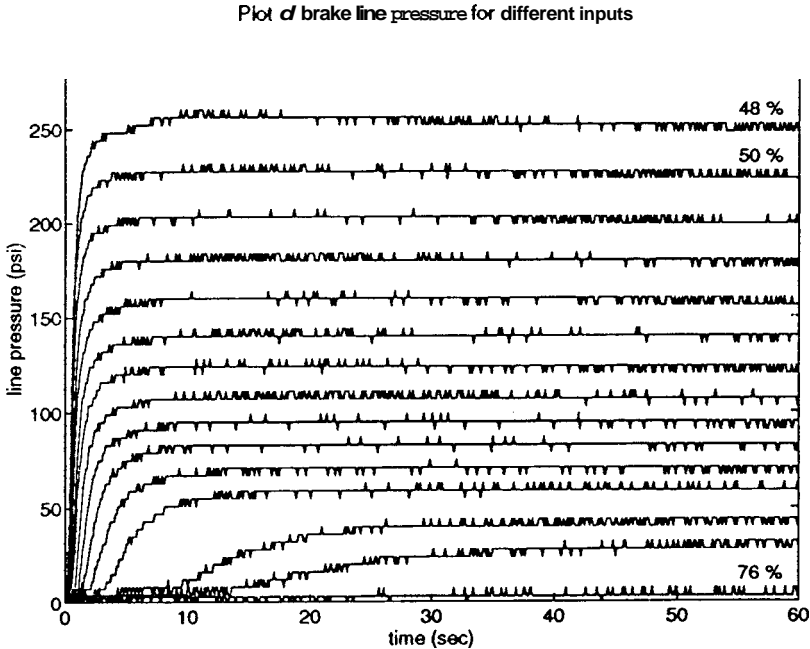
Figure **6:** Brake line pressure for building mode. Inputs range from 76 to 48 %

A series of experiments were conducted on the test bench of brake system. Some results of the experiments with step inputs of different magnitudes (corresponding to inputs of different duty cycle) are shown in figures (6) and (7). These figures portray two basic modes of operation of the system: building and bleeding pressure modes.

These results suggest the presence of the dominant first order dynamics. Further analysis, to be explained later, exhibits nonlinear behaviour of the system and motivates the
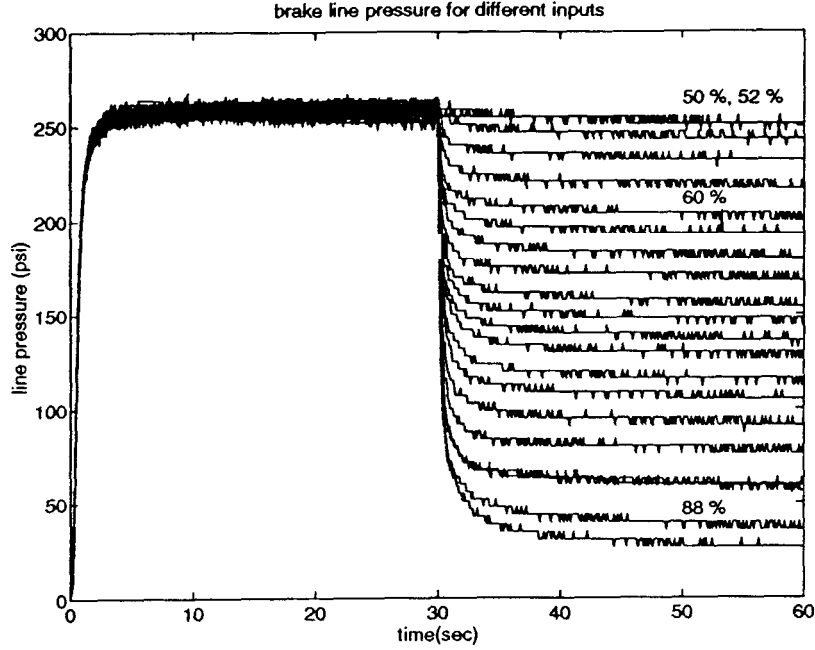
7

Figure 7: Brake line pressure for bleeding mode. Input is 48 % for $0 \leq t < 30sec$ and is changed at $t = 30sec$ to different values ranging from 50 to 90%.

following nonlinear dynamic model:

$$\dot{x}(t) = f(x, u, u(t - \tau)) \tag{1}$$

In case of brake system the variables in (1) are:

  x : system state (brake line pressure)

  u : system input (duty cycle of the pwm signal)

  f : unknown function to be identified

where $x, u \in \mathcal{R}^1$ and $u(t - \tau)$ denotes the previous input, τ is some small number (normally equal to the sampling period). It should be noted that at this moment, we assume that the input if of staircase type. This assumption is necessary for the identification of the parameters. However, this assumption would be relaxed later. It would be shown that the concept of previous input **also** helps to identify one of the two modes of operation of system.

Furthermore, the shape of response for each fixed input, shown in figures **(6)** and (7), can be approximated by a first order system given **as:**

$$\dot{x}(t) = -bx + ba \tag{2}$$

8

where $a, b \in \mathcal{R}^+$. Parameters a and b in (2) characterize the steady state value and the speed of transient response respectively. These parameters have similar meaning in linear systems, but have nonlinear relationship in this case. Analysis of experimental data suggests a functional form for the parameters a and b, which are given as:

$$a = g(u, u(t - \tau)) \tag{3}$$
$$b = h(x, u, u(t - \tau)) \tag{4}$$

where g and h are unknown functions to be identified. Equations (3) and (4) dictated by experimental results, with staircase inputs, indicate that steady state value of pressure, a, depends not only on the current input but also on the previous input. Similarly the transient response quantified by the parameter b in addition is sensitive to current state of the system.

4 Parameter Identification

The step response curves shown in figures (6) and (7) for each fixed input u can be approximated as a solution to the first order linear differential equation:

$$x(t) = a_o e^{-b(t-t_o-t_d)} + a(1 - e^{-b(t-t_o-t_d)}) \tag{5}$$
$$\tag{6}$$

where

a : steady state value

$1/b$: time constant

t_d : time delay

a_o : initial condition

t_o : time at which input is applied

This simplification helps us to identify the parameters a and b for each input separately by using standard least squares curve fitting techniques. It should be noted that the exponential function approximation given in (5) does not hold true for inputs with duty cycle greater than 68 %. However, for actual braking purposes, line pressures below 70 psi, corresponding to the aforementioned inputs, have little or no significance. Hence this approximation has no effect on model accuracy within range of interest of equipment.

Furthermore, the two modes of operation shown in figures (6) and (7) have different steady state values and slopes for the same inputs. The reason is the hystresis produced due to friction, pre-loaded spring inside the vaccum booster and dead zone associated with

9

the master cylinder. Hence separate mappings for the two modes are required. The experimental results in figure (6) suggest that for building case both a and b depend only on the current input, i.e.,

$$a = g(u) \; ; \; b = h(u) \qquad \text{(building)} \qquad (7)$$

On the other hand for bleeding mode a is a function of current input whereas b depends also on the current state x, i.e.,

$$a = g^*(u) \; ; \; b = h^*(u, x) \qquad \text{(bleeding)} \qquad (8)$$

These mappings g, h, g^* and h^* are given in tables 1 and 2 respectively. From table 1, it is obvious that due to hystresis, $g^*(u) \geq g(u)$. From the experiments it was found that if a change in input causes the system state to be switched from building to bleeding mode with $g^*(u) > g(u(t - \tau))$ then a $= x$, and the line pressure, x, would maintain its previous value. Hence for bleeding state a in (8) can be rewritten as:

$$a = min(x, g^*(u)) \qquad (9)$$

Time delay t_d is an important factor in calculation of safety distance for normal vehicle following. A large time delay of the order of 0.2 second is observed for relaxed system, i.e., when line pressure is zero. This time delay become negligibly small ($\approx 0.05 sec$) for any line pressure other than zero. Hence this leads to the following relation:

$$t_d = \begin{cases} 0.2 & \text{if } x = 0 \\ 0.05 & \text{else} \end{cases} \qquad (10)$$

The system response in figure (9) shows different time delays for the two cases discussed above.

Another series of experiments were conducted with inputs changing from one value to the different values and these changes were made to occure at different line pressures. Results show that the values of a calculated in these cases are consistant with those given by table 1. Whereas the values of b vary significantly and was found to be a function of the current pressure, x, at which input was changed. The change in value of b as a function of current pressure for two different Au is shown in figure (8). Guided by the experimental results, the following simplification was introduced to model this change:

$$b = h(u) \left(\frac{5}{4} - \frac{x}{2g(u(t - \tau))} \right) \quad \text{when } x \geq \frac{g(u(t-\tau))}{2} \qquad (11)$$

Summarizing the results given above, (12), (13), (14) and (15) describe the parameter values a and b for the two modes.

u (%)	$a = g(u)$ (psi)	$b = h(u)$	$a = g^*(u)$ (psi)
48	253	1.8	253
50	226	1.7	253
52	202	1.6	252
54	181	1.4	251
56	159	1.2	245
58	140	1.0	233
60	124	0.9	219
62	108	0.75	194
64	94	0.65	182
66	83	0.50	170
68	70	0.35	157
70	60	0.20	148
72	48	0.10	138
74	30	0.07	129
76	5	0.02	116
78	0	0	107
80	0	0	94
82	0	0	79
84	0	0	65
86	0	0	57
88	0	0	40
90	**0**	**0**	**29**

Table 1: Least square fit values of functions g, h and g^* for the curves in figures (6) and (7)

u \ x	0	30	60	80	95	105	125	145	160	180	200	225	253
48	X	X	X	X	X	X	X	X	X	X	X	X	1.8
50	X	X	X	X	X	X	X	X	X	X	X	1.7	1.8
52	X	X	X	X	X	X	X	X	X	X	1.6	1.7	1.8
54	X	X	X	X	X	X	X	X	X	1.4	1.6	1.7	1.9
56	X	X	X	X	X	X	X	X	1.2	1.4	1.6	1.8	1.9
58	X	X	X	X	X	X	X	1.0	1.2	1.4	1.7	1.8	2.0
60	X	X	X	X	X	X	0.9	1.0	1.2	1.5	1.7	1.9	2.1
62	X	X	X	X	X	0.75	0.9	1.0	1.3	1.5	1.8	1.9	2.2
64	X	X	X	X	0.65	0.75	0.9	1.1	1.3	1.6	1.8	2.0	2.3
66	X	X	X	0.5	0.65	0.75	1.0	1.1	1.4	1.6	1.9	2.0	2.4
68	X	X	X	0.5	0.65	0.8	1.0	1.2	1.4	1.7	1.9	2.1	2.5
70	X	X	0.2	0.5	0.7	0.8	1.0	1.2	1.5	1.8	2.0	2.2	2.6
72	X	X	0.2	0.5	0.7	0.8	1.1	1.3	1.5	1.8	2.0	2.3	2.6
74	X	0.07	0.2	0.6	0.7	0.9	1.1	1.3	1.6	1.9	2.1	2.4	2.7
76	X	0.07	0.2	0.6	0.7	0.9	1.1	1.4	1.6	1.9	2.2	2.5	2.7
78	0	0.07	0.3	0.6	0.7	0.9	1.2	1.4	1.7	2.0	2.3	2.5	2.8
80	0	0.07	0.3	0.6	0.7	0.9	1.2	1.5	1.7	2.0	2.3	2.6	2.8
82	0	0.07	0.3	0.7	0.7	1.0	1.2	1.5	1.8	2.1	2.4	2.6	2.9
84	0	0.07	0.4	0.7	0.8	1.0	1.3	1.5	1.8	2.1	2.4	2.7	2.9
86	0	0.07	0.4	0.7	0.8	1.0	1.3	1.6	1.9	2.2	2.5	2.7	3.0
88	0	0.07	0.4	0.7	0.8	1.0	1.3	1.6	1.9	2.2	2.5	2.7	3.0
90	0	0.07	0.4	0.7	0.8	1.0	1.3	1.6	1.9	2.2	2.5	2.7	3.0

Table 2: Least square fit values of $b = h^*(u, x)$ for the curves in figure (7). An X as a table entry indicates an invalid state for bleeding mode.

building:

$$a = g(u) \tag{12}$$

$$b = \begin{cases} h(u) & \text{if } x < \frac{g(u(t-\tau))}{2} \\ h(u)\left(\frac{5}{4} - \frac{x}{2g(u(t-\tau))}\right) & \text{if } x \geq \frac{g(u(t-\tau))}{2} \\ b(t-\tau) & \text{if } \Delta u = 0 \end{cases} \tag{13}$$

bleeding:

$$a = min(x, g^*(u)) \tag{14}$$

$$b = h^*(u, z) \tag{15}$$

The condition to determine the current mode of operation is:

$$x < g(u) \Rightarrow \text{pressure is building} \tag{16}$$

This means that if current pressure is strictly less than the steady state value for the current input, then the system is in building mode and vice versa. Hence by using the condition **(16)** the results given in (12), **(13)**, **(14)** and **(15)** can be combined to give the final form for *a* and *b* as:

$$a = \begin{cases} g(u) & \text{if } x < g(u) \\ min(x, g^*(u)) & \text{if } x \geq g(u) \\ a(t-\tau) & \text{if } \Delta u = 0 \end{cases} \tag{17}$$

$$b = \begin{cases} h(u) & \text{if } x < \frac{g(u(t-\tau))}{2} \\ h(u)\left(\frac{5}{4} - \frac{x}{2g(u(t-\tau))}\right) & \text{if } x \geq \frac{g(u(t-\tau))}{2} \\ h^*(u, x) & \text{if } x \geq g(u) \\ b(t-\tau) & \text{if } \Delta u = 0 \end{cases} \tag{18}$$

It should be noted that in **(17)** and **(18)** a situation Au = 0 is added, **as** the experimental results indicate that the change in *a* or *b* occurs only if the input changes. Hence checking Au is required to conform to the actual situation. In **(17)** and **(18)** *a(t − τ)* and *b(t − τ)* are the values of the parameters *a* and *b* before a change in input occurs.

5   Model Validation

The model described by (2), **(17)** and (18) was simulated for different inputs, results are shown in figures **(10)** and **(11). From** figure (11), we *see* that the actual system and model output differ for low pressure values ($\leq$ 60 psi). However, **as** discussed before, due to less

significance of these pressure values for actual braking purposes, this error is not severe.

It can also be seen form figure **(11)** that for pressure values greater than **60** psi the error is within ± 8 psi. This error figure is not too bad considering the fact that the pressure sensor used in the actual system has resolution of **4** psi. Furthermore, from figure **(11)**it is obvious that the model output for staircase approximation of continuous signal is same **as** that **of** the original signal. Hence it can be ascertained that the initial assumption of input signal being a staircase function can be relaxed. The estimates of parameters a and b which were calculated **as** though the input signal is made up of finite steps hold even when the step width τ is reduced to zero, i.e.,

$$u(t_-) = u(t) = u(t_+)$$

6 Limitations

1. Model accuracy, for the represetation given above, depends mainly on the accuracy of identification of parameters a and b.
2. The modification for b given by **(11)** holds only if $x < g(u(t - \tau))$, i.e., steady state is not attained. When steady state actually is achieved, then the value of b shows a further decrease **as** time increses. In other words, the longer the system stays at one steady state value, the harder it is for system to change the state. It was found by experiments that for a fixed input the steady state is not attained for a step width of less than 5 seconds, hence in this case the approximation given by **(11)** holds true. This is not a severe limitation considering the fact that actual braking commands do fall into this category.

7 Conclusion

A nonlinear model for describing the input ouput behaviour of the brake system was proposed. The model was simplified to make it resemble the first order linear system but with nonlinear coefficients and time delays. The unknown parameters were identified using the least squares curve fitting technique on the data obtained by conducting experiments on the test bench with real brake system of Lincoln Town Car and actuator for automatic brake control. Although the parameter identification was done using staircase inputs but was shown to be valid for continuous inputs. The worst case modeling error was found to be less than **5%** within range **of** interest of the system.

For the first time a variable time delay was introduced in the model of brake system. Similarly the hystresis phenomenan **was** modeleld by islolating the two operating modes and identifying seperate **sets** of parameters for each case. Although the model was develop from the analysis of input-output data, not from the physical analysis of each component, it is convenient for controller design and simulation due to the first order dynamics associated

with the proposed model. The model presented above is also fairly general and can be applied to a wide class of brake systems with some modifications in parameter set.

References

[1] Shaldoven, S., E., "Longitudinal Control of Automotive Vehicles in Close-Formation Platoons", **ASME** Journal on Dynamic Systems, Measurement and Control, vol. 113, 1991, pp. 231-241.

[2] Shaldoven, S., E., Desor, C., A., Hedrick, J., K., Tomizuka, M., Warland, J., Zhang, W., B., McMohan, D., Peng, H., Sheikholselam, S., McKeown, N., "Automatic Vehicle Control Developments in PATH Program, IEEE Trans. on Vehicular Technology", vol. 40, 1991, pp. 114-130.

[3] Sheikhulsalam, S., Desoer, C., A., "A System Level Study of the Longitudinal Control of a Platoon of Vehicles", ASME Journal of Dynamic Systems, Measurement, and Control, 1991.

[4] Varaiya, P., "Smart Cars on Smart Roads: Problems of Control", PATH Technical Memorandum, 91-S, December 1991.

[5] Chien, C., C., Ioannou, P., "Automatic Vehicle Following", Proc. American Control Conference, Chicago, Il., June 1992.

[6] Gerdes, J., C., Maciuca, D., B., Devlin, P., E., Hedrick, J., K., "Brake Modeling for IVHS Longitudinal Control", ASME 1993.

[7] Khan, Y., Kulkarni, P., and Youcef-Toumi, K., "Modeling, Experimentation and Simulation of a Brake Apply System", Proceedings of the 1992 American Control Conference, pp. 226-230.

[8] Nunney, M., J., "Light and Heavy Vehicle Technology", 2nd Edition, Newnes, Oxford OX2 8DP, 1992, pp 516-552.

Figure 8: Change in b for change in input from 56% to **50%** $(\Delta u = 6)$ and from 68% to 64% $(\Delta u = 4)$
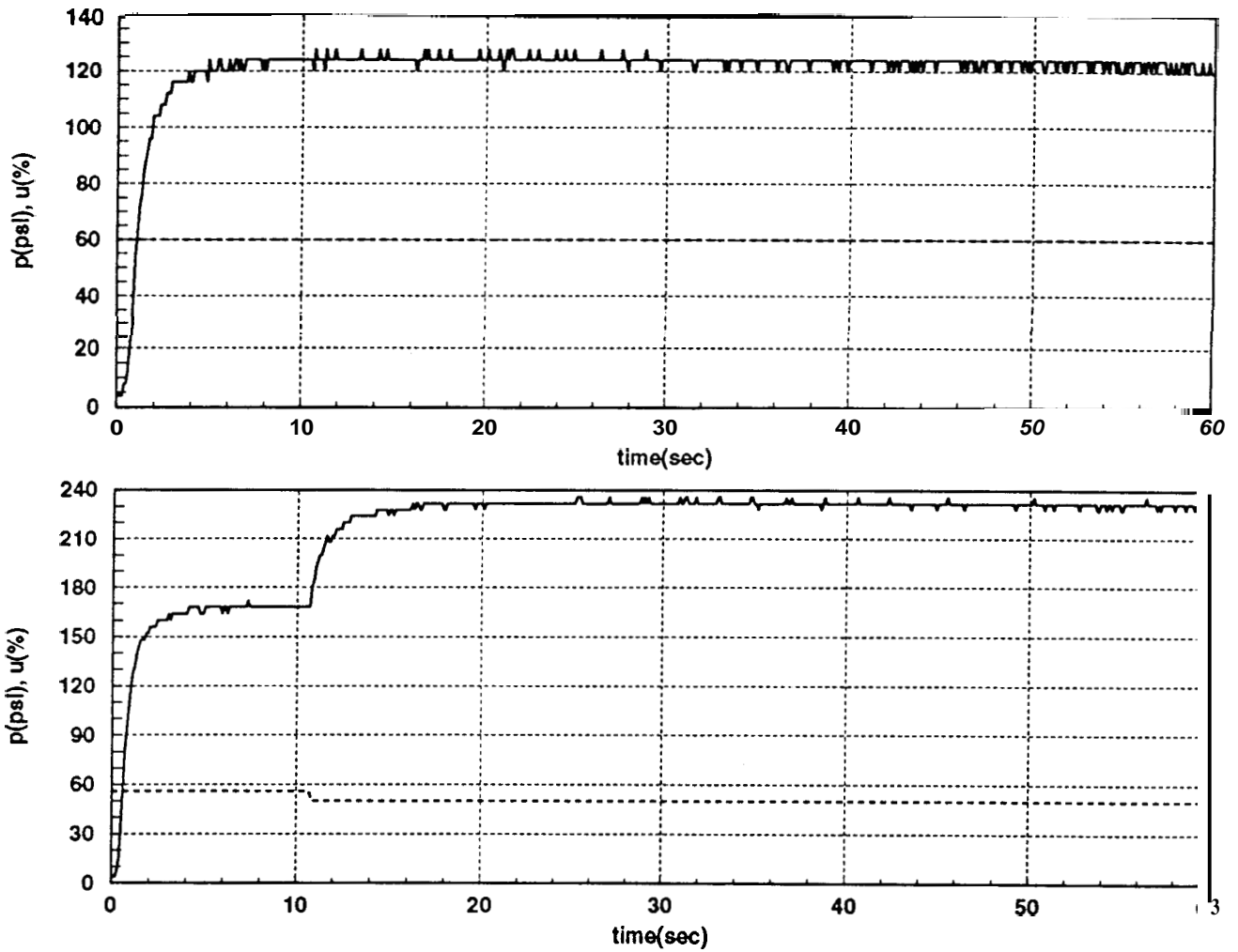
Figure 9: Top portion of the figure shows that for relaxed system a large time delay, **0.2** sec, is observed. However, for any subsequent change in input(bottom portion), time delay is very small (≈ 0.05 sec).
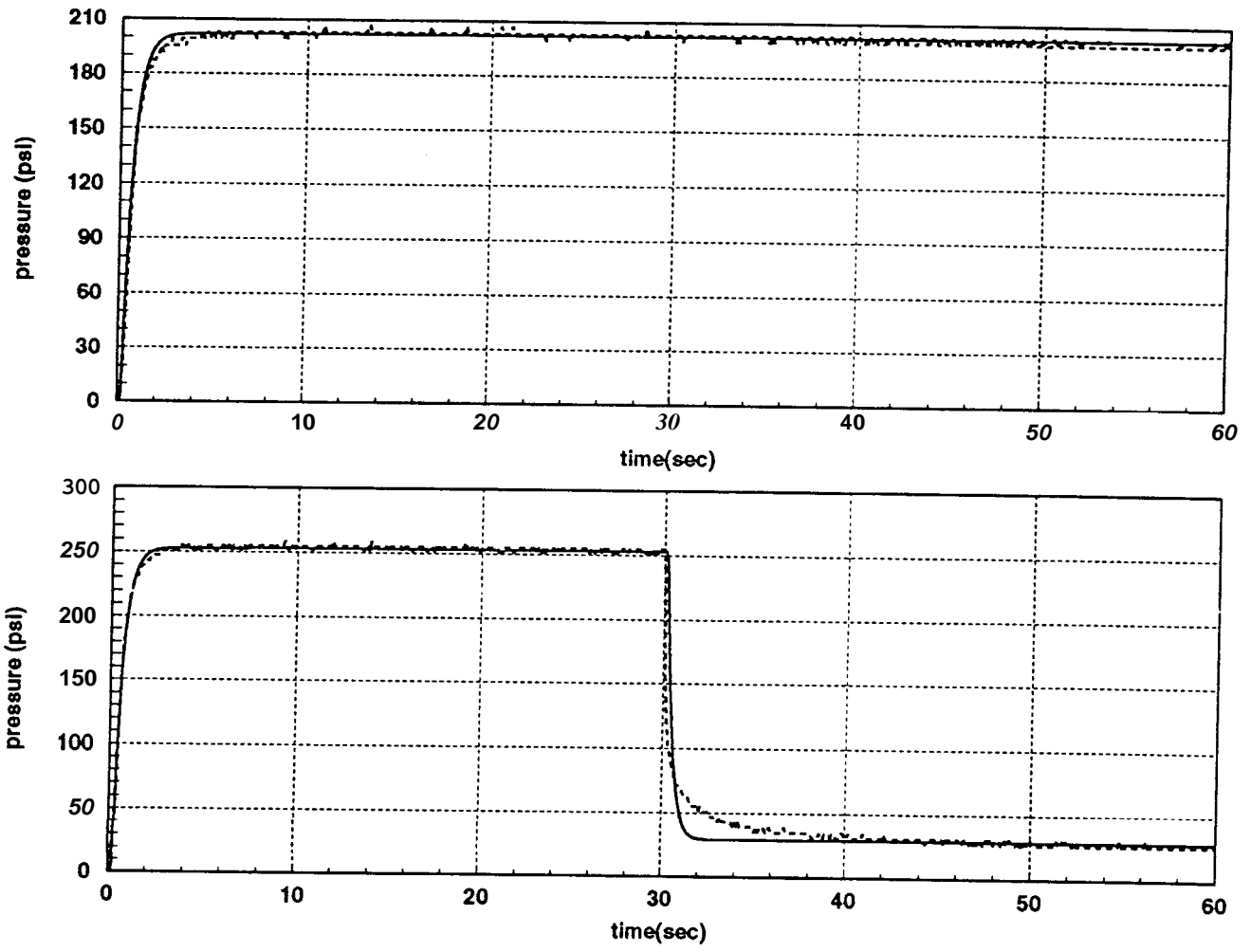
Figure 10: A comparison of the actual and model output for a step input of 52% is shown in the top portion of the figure. Whereas in the bottom one input changes from 48% to 90% at t=30 sec.

18
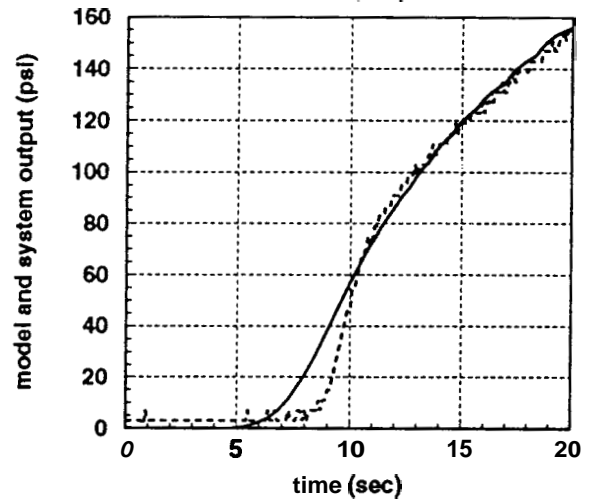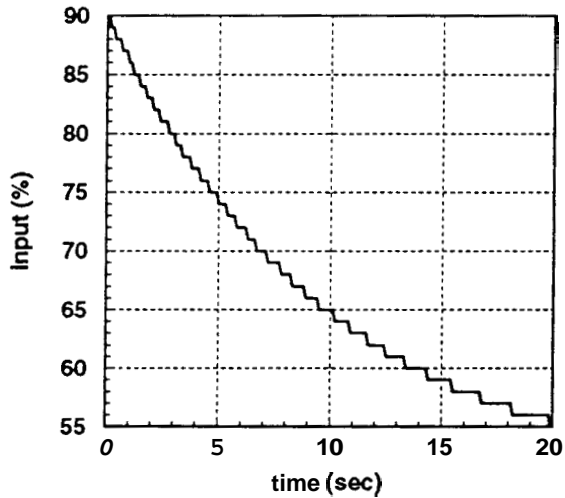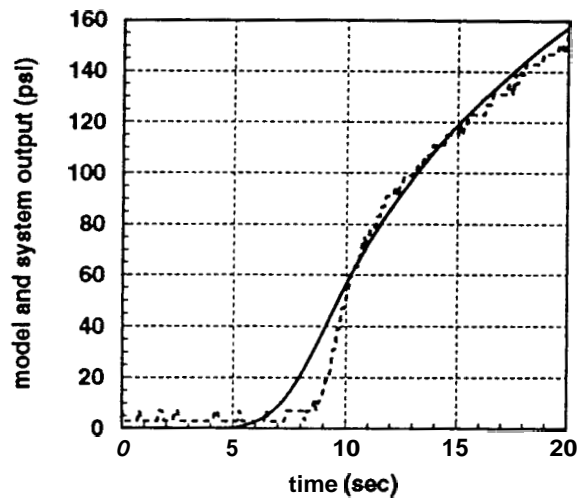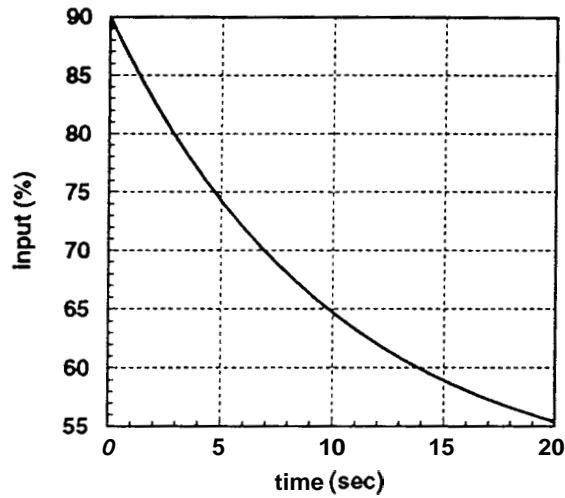
Figure 11: The top left portion of the figure shows the input signal being applied to actual system and brake model for comparison. The system and model outputs are shown in top right position for given input signal. A staircase approximation of the same input signal is shown in bottom left graph. The comparison of outputs is shown in bottom right graph.

Appendix C: Experimental Model of Control Valve Unit in the Auxiliary Hydraulic Module of a Vehicle Brake System

(See the attached technical report.)

Experimental Model of Control Valve Unit

In the Auxiliary Hydraulic Module

Of a Vehicle Brake System

by

D. Li, B. Yang and Z. Xu

Report 95-06-01   June 1995

Experimental Model of Control Valve Unit
In the Auxiliary Hydraulic Module of a Vehicle Brake System'

D. Li and B. Yang
Dept. **of** Mechanical Engineering
University of Southern California
Los Angeles, CA 90089-1453

Z. Xu
Dept. of Electrical Engineering-Systems
University of Southern California
Los Angeles, **CA** 90089-2563

Abstract
In this paper we develop a dynamic model **for** a control valve unit in an auxiliary hydraulic module(AHM) of **a** real vehicle brake system provided by the Ford Motor Company on the **basis** of experiments conducted on the system. The parameters **of** the model are identified by applying **standard** curve fitting method to the experiment data. **A** "pseudo-steady state" phenomenon in the transient process, which is **caused** mainly by the energy-accumulation as well as frictional factors in the hydraulic and mechanical subsystems, and its significant influence to the system transience are discussed. Some switching conditions on the "pseudo-steady state" *are* determined by **using** the experiment **data** and common fluid dynamic theory. Model simulation results with several **types** of input are presented. With this model the dynamic behavior of control valve unit *can* be well predicted.

1. Introduction

As an important element of the national program to develop intelligent vehicle/highway systems (IVHS), PATH has launched several advanced vehicle control systems (AVCS)-related research projects. Brake System Analysis, Reliability Testing and Control Using Bench Experiments is one of these projects. The objectives of this project are to develop the brake model, study the reliability and feasibility of a brake actuator developed by Ford Motor Company. All these researches are conducted based on the expenments on a test bench which is also donated by Ford. The test bench consists on the standard brake components (brake rotor, pads, master cylinder, booster etc.) and an auxiliary hydraulic module (AHM) which performs as the actuator.

In the past a few months, an experimental model describing relationship of the input (input to AHM) and output (brake line pressure) has been proposed [1]. Although this model is useful for brake controller design, it is still desired to develop the model for the AHM because it is a new subsystem adopted by the Ford Company. The **AHM** model will also help to characterize the performance of the brake-actuator system, and help in malfunction detection..

In this paper we will offer a model for the *AHM*. The method used in developing this model was experimental method. We did a lot of experiments on the test bench, collected input, state data, then used the interpolation technique to identify the system parameters. The arrangement of this paper is as follows: Section **2** briefly describes the brake test bench and the AHM. Section **3** gives the format of AHM model based on experiment

results. Section **4** identifies the system parameters based on the test data. Section 5 compares the simulation and experimental results.

2. Brief description of brake system and AHM

Figure 1a is a block diagram of the brake system which consists of several components. Detailed discussion of these components can be seen in [1].
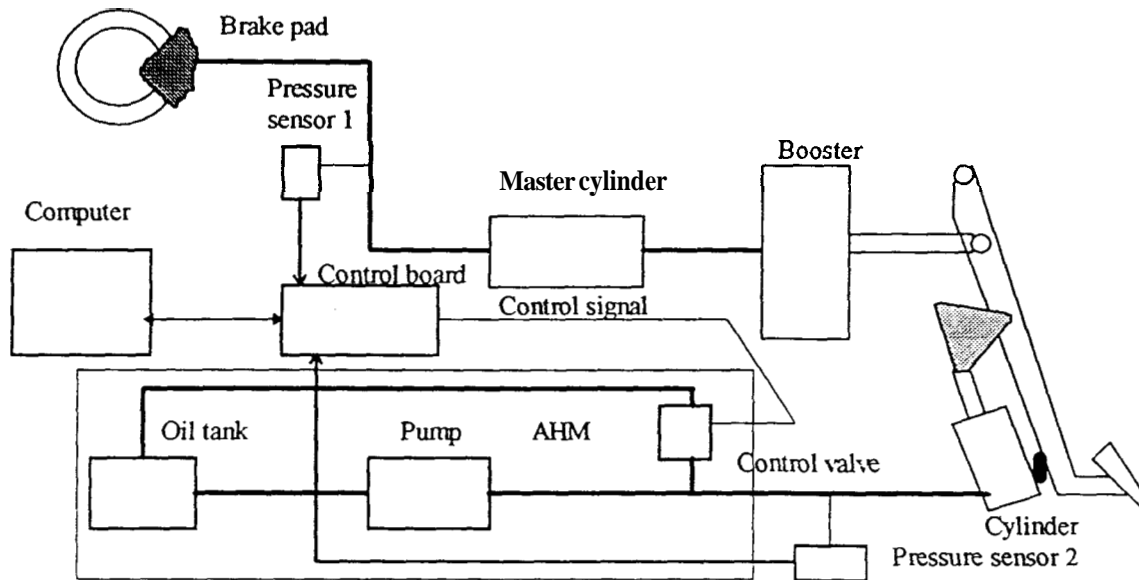

Fig. 1a Block diagram of the brake system

Among all the components, the above-mentioned *AHM* (shown in Fig.1b) is the main electro-hydraulic servo unit for the brake control system. In the automatic control status the hydraulic pump and valve supply the cylinder with pressured fluid and the cylinder applies initial braking force to the booster. Other components are the standard brake parts.

The AHM consists of a hydraulic pump, a control valve assembly and a cylinder. In this hydraulic Module the pump supplies fluid with constant flowing rate to the valve. The valve provides control of fluid power by a variable-area opening. When the valve is open, the fluid returns to a reservoir tank and the pressure in the hydraulic Module is low; while the valve is closed, most fluid goes to the cylinder and the hydraulic pressure is built up. By varying the openness or opening time of the valve, the control of flow and pressure of the fluid between the pump and the cylinder can be accomplished. Under the pressure of the fluid the cylinder piston will move so **as** to push the operation rod of the booster, and as a result the braking is applied. The longer the valve is closed, the higher the hydraulic pressure in the cylinder and the braking pressure in the master cylinder. If the closing time of control valve is reduced after a while, the cylinder pressure will decrease and the braking pressure will be released consequently.
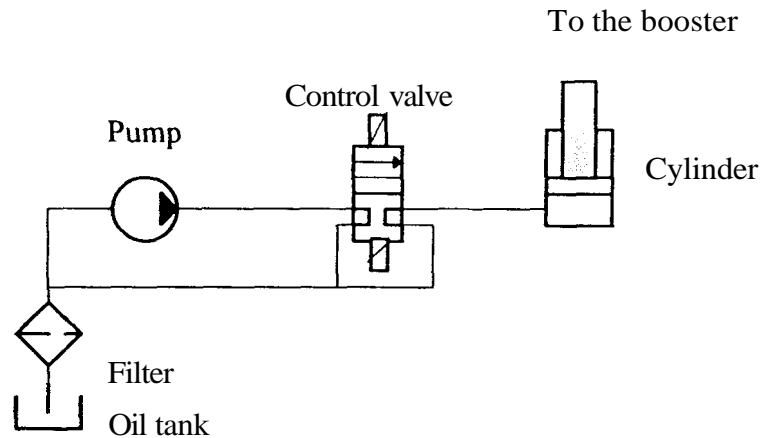
2

Fig.1b Schematic of the Auxiliary Hydraulic Module

It is seen from above description that the cylinder pressure and the braking pressure can be controlled by varying the closing time of the control valve. Thus in the automatic control mode, the control input of the AHM as well as the whole brake system is the opening/closing time command to the valve; the output of the AHM or the control valve unit is the hydraulic pressure. The controller (not shown in Fig.1b) generates control signals (opening and closing commands) which are pulse width modulated (PWM) signals with fixed frequency and magnitude. When the control signal is of high value, the valve is open; while the signal remains low, the valve is closed. The percentage of the wave width with high signal in a wave period is called "duty cycle", that is the opening time in a wave period. Smaller duty cycle means longer closing time and higher pressure and vice versa. By changing duty cycle i.e., the closing time, the hydraulic pressure in cylinder is conveniently controlled.

The dynamic behavior of the AHM especially that of the control valve unit is decisive to whole system because the transients of the *AHM* is the principal factor of the transient response of the whole brake system, therefore a well-developed model for this control valve unit is useful to the controller analysis and design and is necessary to the reliability studies of the control system.

It is generally assumed **[4]** that the pressure-flow characteristics of valves at any instant follow closely their steady-state characteristics during transient operation. However, this assumption may lead to errors in predicting transient flow conditions under certain circumstances. The control valve in the above mentioned hydraulic system **opens** and closes at a frequency of 100Hz. Its transient process can not be described by a commonly used steady-state model. Although techniques for transient flow analyses in piping systems are available, they are not directly applicable to the current hydraulic system due to the lack of knowledge of the transient behavior of the components. To our knowledge, there is no theoretical dynamic model for the control valve or the combination of control

valve and other hydraulic components as that used in our hydraulic Module. Thus developing an experimental model for this hydraulic sub-system becomes necessary and practicable. The proposed model in following sections is also useful to the theoretical analyses on the similar hydraulic systems.

3. Proposed Valve Unit Model

In order to get actual valve-cylinder fluid pressure data, a series of experiments was carried out. A pressure sensor is connected to the pipe line between the valve and cylinder in the **AHM** to measure the fluid pressure of valve-cylinder unit. **As** mentioned in previous section the input of the AHM is the PWM signal called "duty cycle"; smaller duty cycle means higher steady state fluid pressure value and larger duty cycle leads to lower pressure in both the brake line and cylinder. In the experiments duty cycle is changed such that a family of pressure curves are obtained. In these tests the sampling rate for acquiring cylinder pressure is 1000Hz that is 10 times of PWM signal frequency(100Hz).

A typical step input response curve is shown in Fig.2. The step input is first decreased from 90% to 54% then increased to 90%, which is denoted as "duty cycle curve" in the figure. The transient section where the pressure is increasing is called pressure building section and the transient section where the pressure is decreasing is called pressure releasing section. In this figure the duty cycle is scaled with 100 denoting 100% and the same scaling for duty cycle is also used in the rest of the figures.

From Fig.2 a high frequency oscillation in the pressure is noticed. This is caused by the quick opening and closing of the valve since it is controlled by the PWM signal. The pressure oscillation is ignored in modeling because of its little affection to the brake line pressure and the main tendency of cylinder pressure curve.

The most important phenomenon in this response curve is its "stair-shape" or "temporary steady state" stage which is marked by the number "2" on the figure. The mechanism of this phenomenon may be related to the hydraulic sub-system's pressure-flow status, energy loss and mechanical sub-system's fictional status as well as their combination. Among these factors, the mechanical sub-system's friction plays a main role. In the mechanical sub-system of the whole brake system there exists friction between those moving components and the resistant force applied to the cylinder rod can be considered as the resultant force of these frictional resistance.

When duty cycle is below a critical value, the cylinder pressure reaches a threshold value such that hydraulic force is large enough to overcome the static resistant force acting on the cylinder rod, the cylinder piston will move forward and leave a space for the hydraulic fluid to fill up. Since the flow rate of the pump is constant and finite, there is an energy or fluid accumulation process for filling up this "hydraulic gap" while the pressure average value remains almost unchanged. This fluid/energy accumulation procedure results in the "pseudo steady status" on pressure curves. After the completion of this process, the pressure will resume rising. Although the mechanism of the phenomenon is quite hard to

obtain analytically, this "time delay" can be characterized by using experimental data and standard fluid dynamic theory as explained in next section.
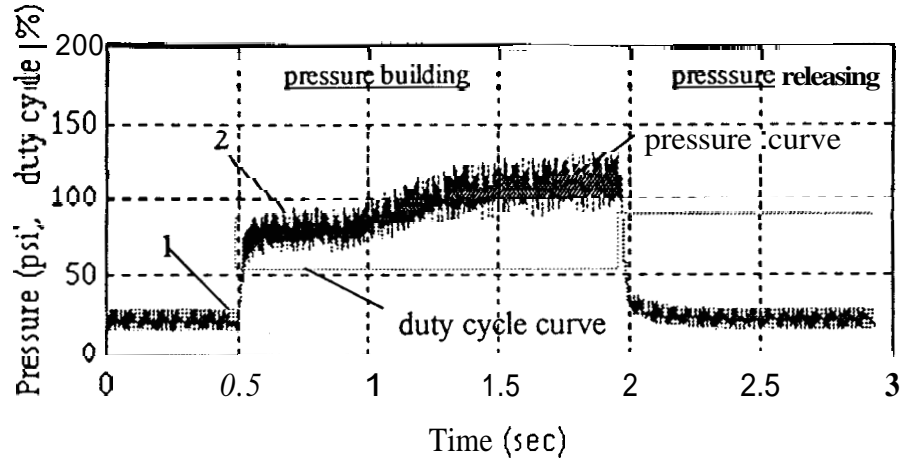

Fig.2 Step input response curve of pressure building and releasing.

After thoroughly scanning the step response curves, it is also noticed that at the very beginning of each step input response curve with duty cycle less than 85%, there is also a very short time delay marked by the number "1" in Fig.2 which may be explained and determined in the same way as for portion "2". Thus there should be two more state variables for these two "pseudo steady status" besides state variable pressure in the system model. They may be defined as "energy-accumulation" states.

Based on previous analysis, a general dynamic model is proposed as follows:

$$
\begin{cases}
\dot{p}(t) = f_1(p, u, x_1, x_2, t) \\
\dot{x}_1(t) = f_2(p, u, x_1, x_2, t) \\
\dot{x}_2(t) = f_3(p, u, x_1, x_2, t)
\end{cases}
\tag{1}
$$

where

t: time

$\dot{p}$:derivative of p with respect to time

p : pressure output from the valve

u: system input (duty cycle of PWM signal), $u = u(t)$

f_i: unknown function to be determined, $i = 1, 2, 3$

x_1 : energy-accumulation state variable for the first pseudo steady stage

x_2 : energy- accumulation state variable for the second pseudo steady stage

4. Parameter Identification

Step input response and standard curve fitting method are used to determine the parameters in the proposed model. Responses to other inputs such as ramp, sinusoidal and arbitrary inputs are used to verify the accuracy of the model.

In the parameter identification, the pressure building section of the typical response pressure curve is considered as a combination of four parts: two "pseudo steady state" stages denoted **by** "1" and "2" in **Fig.2,** the curve between them and the curve after the portion "2". The pressure releasing status will be treated separately.

For the portion "2", since the pressure **is** in a "temporary steady state" status if the smaller pressure oscillation discussed in section 2 is neglected, the pressure at this stage can be considered as constant value. That means the derivative **p is** zero. However, we need to determine the conditions or the effective period of time of this stage.

By Bernoulli's equation on an orifice, we have a relationship between pressure and flow rate of the fluid through the orifice which is the openness of the valve in our case. Further derivation **can** show that the flow rate through the valve openness is a linear function of duty cycle u. Thus the state variable x_2 is given by:

$$\mathbf{x,} = c, -u \qquad x_2 < c_4 \quad \& \quad u < u_2$$

Similarly for portion "1" which has the same pressure character as in portion "2", the state variable is of the form

$$\mathbf{x,} = c_1 - u \qquad \mathbf{x,} < c_3 \quad \& \quad u < 11,$$

For the clarity purpose, the above two equations are

$$\dot{\mathbf{x}}, = c_1 - u \qquad \mathbf{x,} < c_3 \quad \& \quad u < u_1$$
$$\dot{x}_2 = c_2 - u \qquad x_2 < c_4 \quad \& \quad u < u_2 \tag{2}$$

where c_i (i= 1,2,3,4) and u_i (i= 1,2) are the parameters to be determined.

The parameters in equation (2) are identified as

$$c, = 96, \quad c_3 = 0.88, \quad u_1 = 85$$
and $$c_2 = 66, \quad c, = \mathbf{4.8}, \quad u_2 = 66$$

Hence a model for *the* two "pseudo steady states" is in the order:

$$p = 0 \qquad\qquad x_1 \leq 0.88 \,\&\, u < 85\% \,\&\, p \leq p_f(u)$$

$$\textit{or } x_2 \leq 4 \,\&\, p \leq p_f(u) \,\&\, p \geq 79 \,\&\, x_1 \geq 0.88 \tag{3}$$

$$\textbf{x,} = 96 - u \qquad \textbf{x,} < 0.88 \;\&\; u < 85$$

$$\dot{x_2} = 66 - u \qquad x_2 < 4.8 \;\&\; u < 66$$

For the other two portions of pressure curve in Fig. 2 it is found that the dominant dynamics can be characterized as of **a** first-order system, and that the integral factors **x,** and x_2 do not change in these status. Thus the governing equation for these **two parts** of curve is generally in the following form:

$$p = -b\left(p - p_f\right)$$

$$\textbf{x,} = 0 \tag{4}$$

$$\textbf{x,} = 0$$

where b is a coefficient to be determined and p_f is a nonlinear function of u corresponding to the steady state value of the pressure:

$$p_f = p_f(u) \tag{5}$$

By conducting a series of step input experiments with a duty cycle increment of two, the average final steady state pressurepy can be obtained. Table 1 is the look-up table of duty cycle and the corresponding final steady state pressure for the Ford brake test bench.

Table 1. Look-up table for duty cycle u and steady state pressure p_f

u (%)	90	80	78	76	74	72	70	68	66	64	62	60	58	56	54	52	50	48	46	44
P_f (psi)	21	39	45	49	53	56	61	65	71	77	82	88	96	102	111	119	128	140	154	168

To determine the parameter b, we need to determine the starting condition for the second "pseudo steady state" because it is also related to the condition under which the first exponential curve finished.

From the same experiments it can be seen that when the mean value of the pressure reaches 79 psi which corresponds to **63%** of duty cycle the second "pseudo steady state" begins. That means under 79 psi the pressure curve experiences its first exponential portion.

By standard curve fitting the parameter b for the first exponential part is determined as:

$$b=17.7 \qquad\qquad p<79 \ \& \ x_1 \geq 0.88 \qquad \& \ x_2<4.8 \qquad\qquad (6)$$

At this stage the first "pseudo steady state" has been passed and second one has not come yet.

The parameter b for the second exponential part is:

$$b=3.7 \qquad\qquad p\geq 79 \ \& \ x_1 \geq 0.88 \ \& \ x_2 \geq 4.8 \qquad\qquad\qquad (7)$$

The previous description **is** based on the situation that the pressure is in the building mode. By the "pressure building mode" we mean the pressure is increasing. It is obvious that in this mode:

$$p \leq p_f.$$

For the pressure releasing portion of the curve in Fig. 2, fitst-order dynamics are its obvious character. Because the pressure is decreasing, we call this mode as pressure bleeding mode. In this mode, we have:

$$p > p_f$$

and the coefficient b is determined as

$$b=17.4 \qquad\qquad\qquad\qquad\qquad\qquad\qquad\qquad\qquad (8)$$

Figure 3 shows another pressure building situation where the final steady state pressure value is less than *79* psi, In these cases the parameter b is the same as given in equation (6).

Generalizing the above results, a complete model of the value is as follows

$$\dot{p}=\begin{cases} 0 & x_1 \leq 0.88 \ \& \ u < 85\% \ \& \ p \leq p_f(u) \\ & or \ x_2 \leq 4 \ \& \ p \leq p_f(u) \ \& \ p \geq 79 \ \& \ x_1 \geq 0.88 \\ -b_1[p-p_f(u)] & p \leq p_f(u) \ \& \ p < 79 \ \& \ x_1 > 0.88 \ \& \ x_2 < 4 \\ -b_2[p-p_f(u)] & p \leq p_f(u) \ \& \ p \geq 79 \ \& \ x_1 > 0.88 \ \& \ x_2 \ 2 \ 4 \\ -b_3[p-p_f(u)] & P > p_f(u) \end{cases} \qquad (9)$$

where $b_1 = \mathit{17.7} \qquad b_2 = 3.7 \qquad b_3 = 17.4$
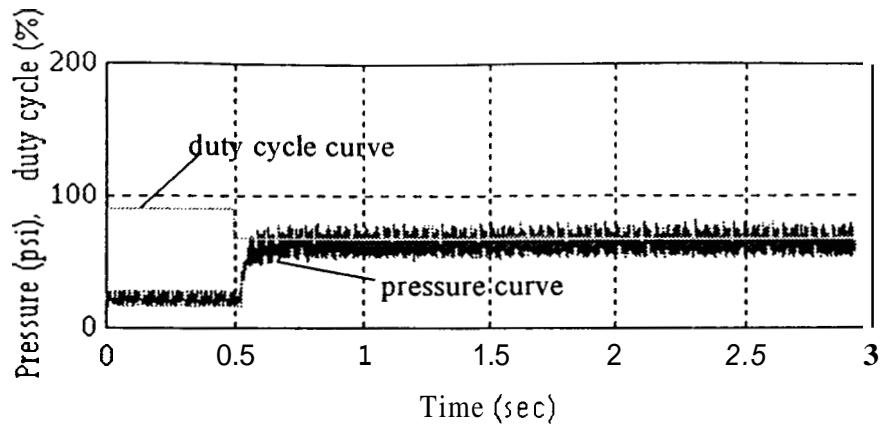
Fig.3 Step input response curve: duty cycle decrease from 90% to 68%

5. Verification of the proposed model

With this model some simulations for different step inputs were carried out. The results corresponding to Fig.2 and **3** are shown in Fig.4 and 5 respectively. In these figures a solid line lying in the shadowed area is the pressure response predicted by the proposed model, and the other solid line **is** the duty cycle curve with a scale 100 being 100% of duty cycle.
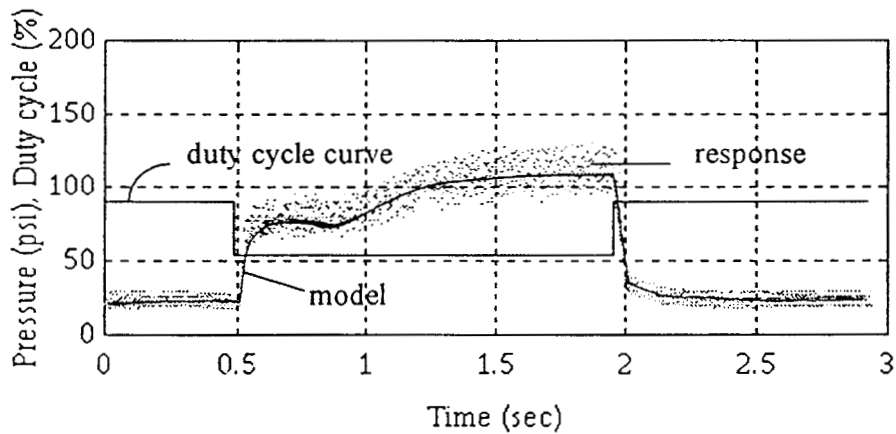
Fig.4 Model curve vs experimental curve: duty cycle decrease and increase

From these two figures we can see that model predicted outputs match the actual outputs very well for the step inputs.
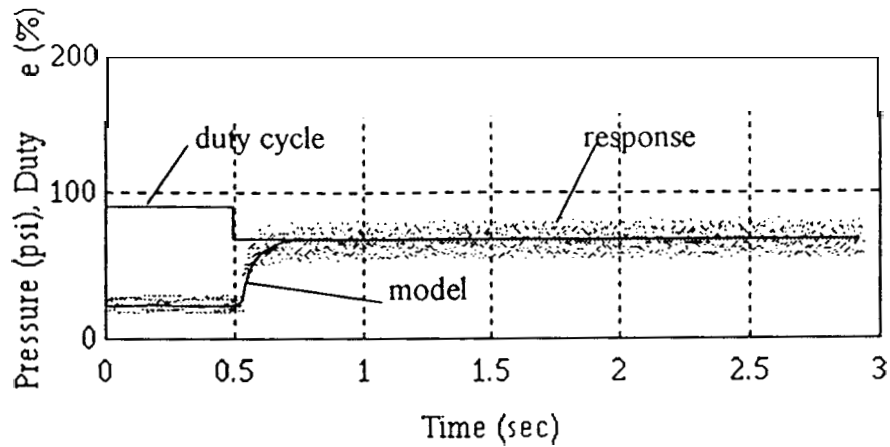
Fig.5 Model curve Vs experimental curve: duty cycle decrease from 90% to 68%

In Fig.5 the model curve and duty cycle curve partially overlapped.

To further verify the model's accuracy several experiments with different types of inputs other than step input were carried out. Fig.6 to **9** show the simulation results compared with the experimental data. The predictions by the modal are still in good agreement with the measured data.
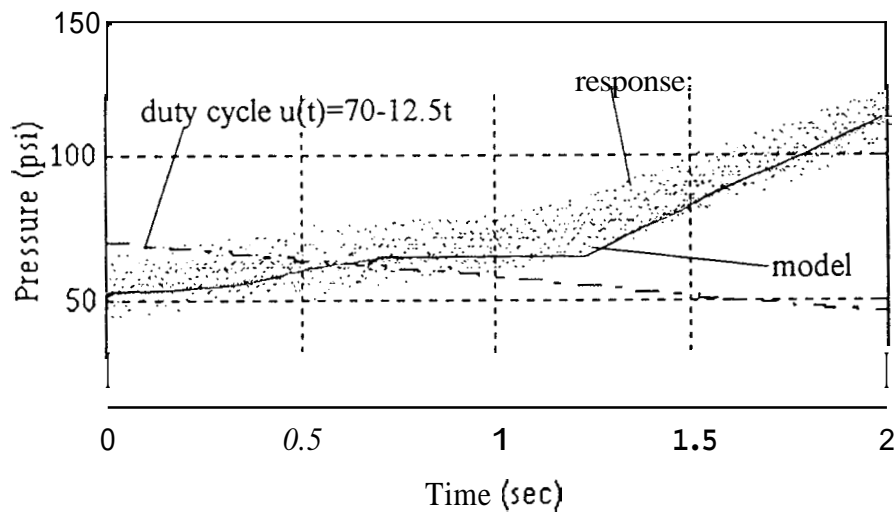
Fig.6 Model simulation result with ramp input $u(t)=70 - 12.5t$.
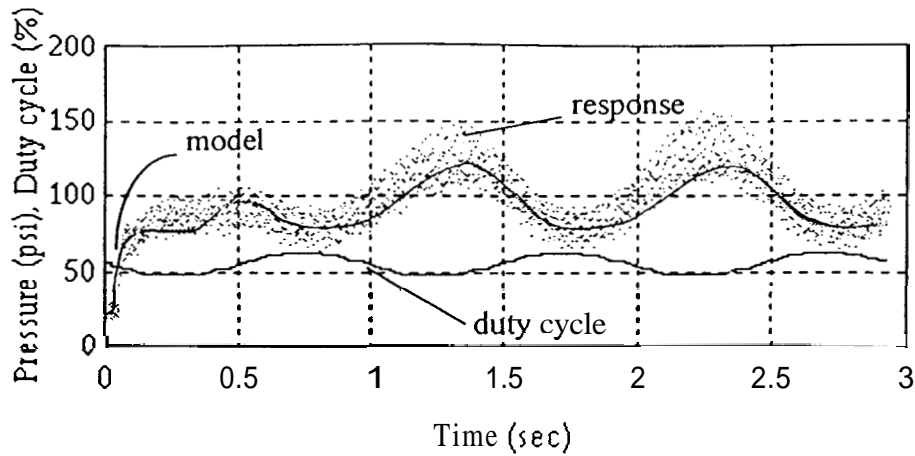
Fig.7 Model simulation result with sinusoidal input $u(t)= 56 - 8\sin2\pi t$.

For the sinusoidal duty cycle input it was noticed that if the input frequency is higher than 1 Hz, model error becomes larger. This is mainly due to the nonlinearities of the system. It was also observed that when the input frequency is higher than 1 Hz, the pressure change in the brake line is no longer sinusoidal; see Fig.8. In the figure it can be seen that when duty cycle and cylinder pressure change in sinusoidal way, there is little pressure drop in brake line. That means the higher duty cycle frequency has little effect on to the brake line pressure. Figure 9 shows the pressure response with 0.5 *Hz* duty cycle frequency. It can be seen that the brake line pressure varies in sinusoidal way.
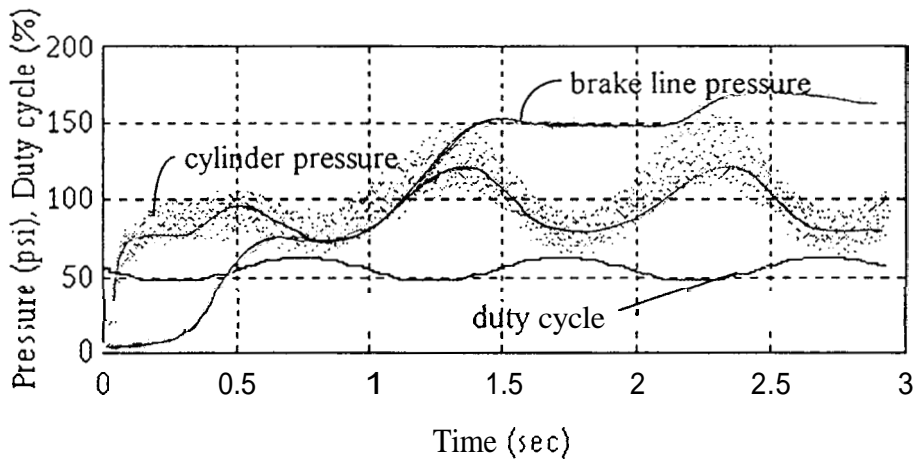
Fig.8 Pressure curves corresponding to $u(t)= 56 - 8\sin2\pi t$.
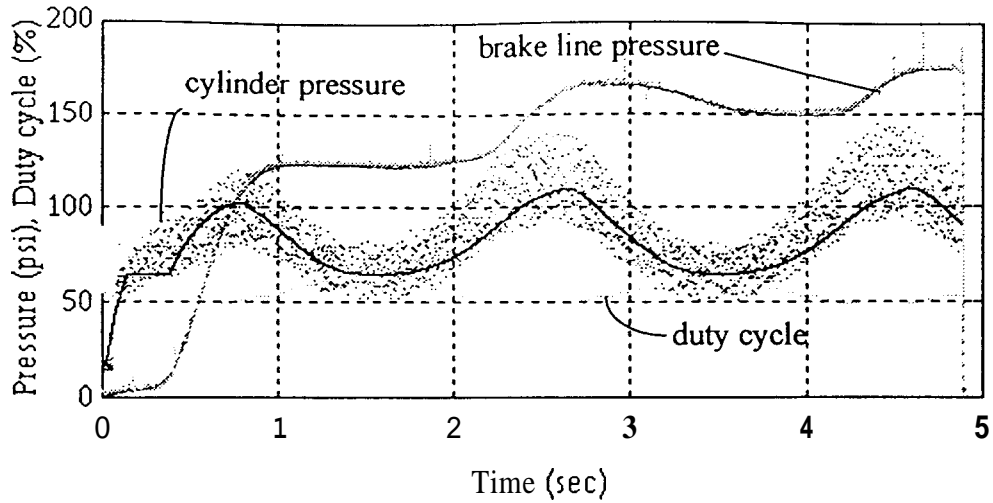
Fig.9 Pressure curves corresponding to $u(t)$= 56 − 8sinπt.
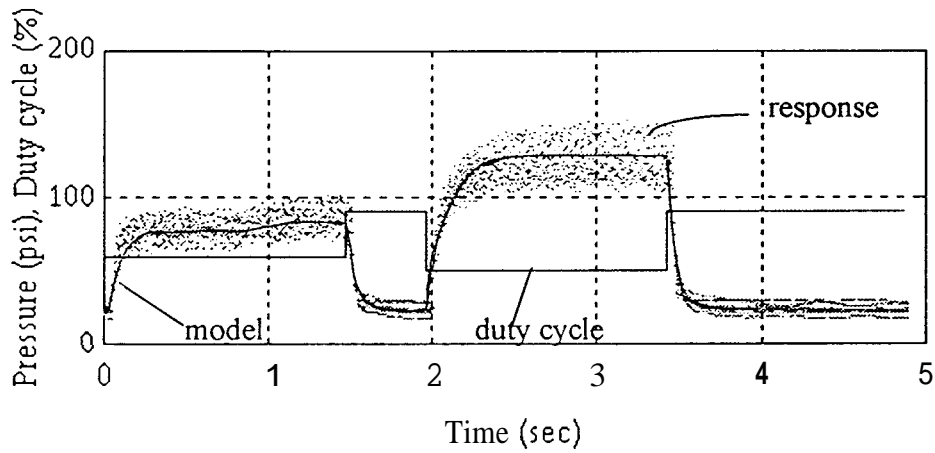
Fig.10 Model simulation result with successive step input u=90--60--90--50%.
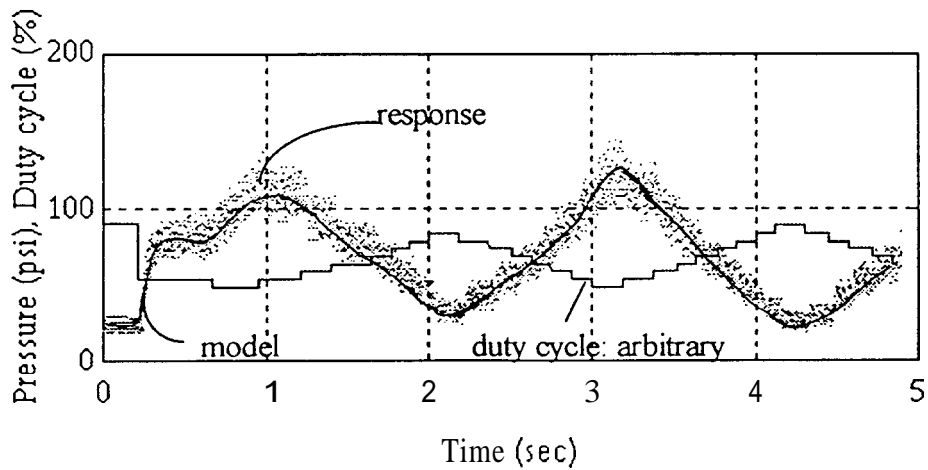
Fig.11 Model simulation result with arbitrary duty cycle input.

Appendix D: Modeling and Control Design for a Computer Controlled Brake System

(See the attached technical report.)

Modeling and Control Design for a Computer Controlled Brake System

by

H. Raza, Z. Xu, P. Ioannou and B. Yang

Modeling and Control Design for a Computer Controlled Brake System*

H. Raza, Z. Xu and P. Ioannou

Dept. of Electrical Engineering-Systems

University of Southern California

Los Angeles, CA 90089-2563

B. Yang

Dept. of Mechanical Engineering

University of Southern California

Los Angeles, CA 90089-1453

Abstract. The brake subsystem is one of the most significant part of a vehicle with respect to safety. The design of a computer controlled brake system has the capability of acting faster than the human driver during emergencies, and therefore has the potential of improving safety. In this paper we consider the problem of modeling and control design for a computer controlled brake system. The brake model is developed based on a series of experiments conducted on a test bench which contains the full scale brake subsystem of Lincoln town car* and a computer controlled actuator designed by Ford Motor Company. The developed model has the form of a first order nonlinear system with the system nonlinearities lumped in the model coefficients. The unknown model parameters are identified using curve fitting techniques on the experimental data. The major characteristics of the system input-output curves such as time delay, effect of static friction, transient and steady state parts, have been identified in terms of model parameters. The brake controller design makes use of a standard feedback linearization technique along with some modifications to meet the closed loop performance specifications. The simulation results show that the proposed controller guarantees no overshoot and zero steady state error for step inputs. Finally the controller is tested on the brake test bench and results indicate that the required performance is achieved.

1 Introduction

With an ever-increasing number of vehicles on the limited highways, it has become urgent to develop sophisticated technical solutions to today's surface transportation problems. It has been shown that Intelligent Vehicle/Highway Systems (IVHS) are promising solutions [1]-[5]. An Important part of IVHS is the Advanced Vehicle Control Systems (AVCS),

*Lincoln town car is the trade mark of Ford Motor Company

which has three essential parts: throttle control, steering control, and brake control. In autonomous driving, brake control is very important from safety point of view. To reduce the risk of human life, an extremely reliable brake system and its controller must be used. In order to design a reliable and fault tolerant brake controller the brake system should be accurately modeled.

During past few years, a sufficient interest has developed among different research groups to develop the models of brake system for AVCS application. One of the significant contribution is the work of Gerdes et al [6]. A bond graph method for modeling the components of manual brake system is considered in the paper by Khan, Kulkarni and Yocef-Toumi [7]. In those studies more emphasis is given to identify the dynamics associated with each component. A comprehensive dynamic model of brake system in **AVCS** environment, which identifies the mapping from input to output, is not emphasized. *The main purpose of this paper is to develop a model and a controller for brake system that can be used in AVCS application.*

The brake model is developed based on experiments with the brake test bench. The block diagram of the brake system under study is shown in Figure 1. The test bench has all the conventional brake components, in addition, it contains an auxiliary hydraulic module (**AHM**) which consists of a hydraulic pump, control valves and an actuator and is designed by Ford specifically for automatic brake application. This design allows the driver to override at any time. In this paper we will develop the model for the brake system which includes the **AHM.** The approach followed here is to propose a model motivated by the experimental results. The curve fitting techniqaes are then applied to data obtained from these experiments to identify the unknown model parameters. The resulting model is nonlinear but is suitable for control design.

The control design objective in this paper is to cancel the nonlinearities of the system and to make the brake system behave as uniformly as possible throughout the operating range of the system. The brake controller design proposed here makes use of standard feedback linearization from nonlinear control theory along with a PI compensator to achieve the performance requirements. To account for a limited control input authority, a suitable modification is introduced in the PI compensator design. This modification allows us to obtain the fastest possible response, restricted by system's physical constraints, with no overshoot. Although, this modification is developed specifically for the brake system under consideration, it can be easily adopted for different systems having saturation limits in the control authority. Some other brake control strategies which are introduced as a part of vehicle longitudinal control can be found in [10]-[11].

The following section describes the structure of the brake system components. Only brief introduction of the main components of brake system is given here. For a detailed discussion of the subject, suggested readings are [8], [6]. The proposed model and the motivation for

2

this selection is discussed in section three. In section four we consider the problem of identification of unknown model parameters. This is followed by simulation results and model validation. Section six covers some of the limitations **of** the proposed model. The control design with the modification logic for **PI** compensator is given in section seven. In section eight stability analysis of the controller and some robustness issues are discussed briefly. The controller implementation and simulation results are given in section nine. Key points are discussed again in conclusion section.

2 Brake System Components

The main components of the brake system shown in Figure 1 are discussed below.
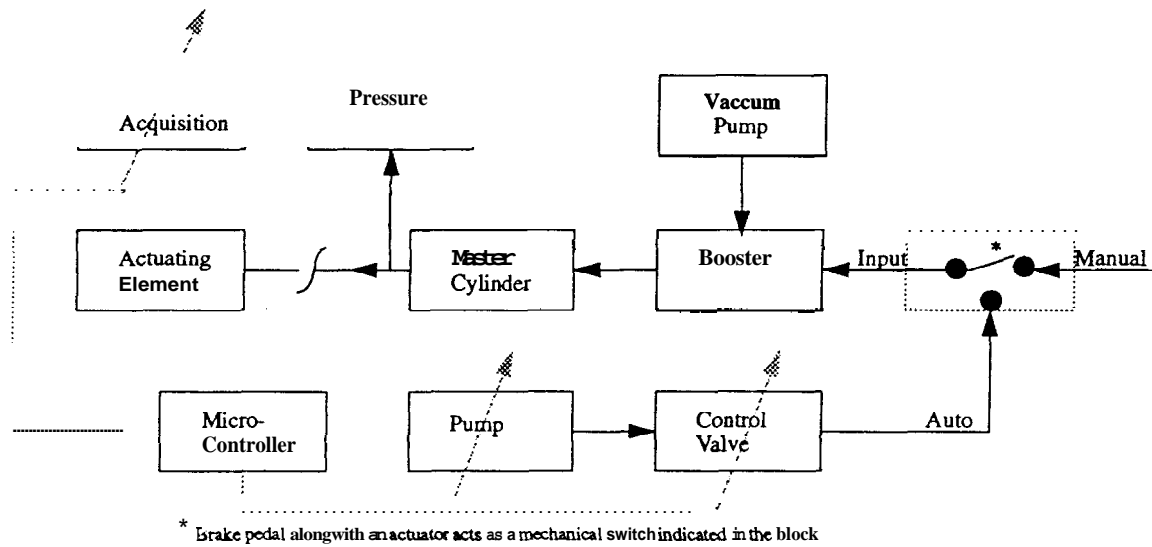
Figure 1: Block Diagram of the Brake System

2.1 Auxiliary Hydraulic Module

The function of AHM is to provide an input force to vacuum booster through an actuator and brake pedal. The AHM takes control input in the form of a pulse width modulated (PWM) signal and generates a pressure to be applied to the brake pedal through an actuator. The input (PWM) signal is in the form of a square wave of fixed frequency but varying duty cycle. The output pressure of the actuator and hence the brake line pressure can be controlled by changing the duty cycle of PWM signal.

As shown in Figure **2** AHM consists of **a** hydraulic pump, an arrangement of valves and an actuator. **As** a constant amount **of** fluid is pumped through the valves by the hydraulic pump, no pressure is developed inside the cylinder of the actuator if the valves are open. Whereas a sudden rise of pressure is obtained if the valves are closed completely. Hence
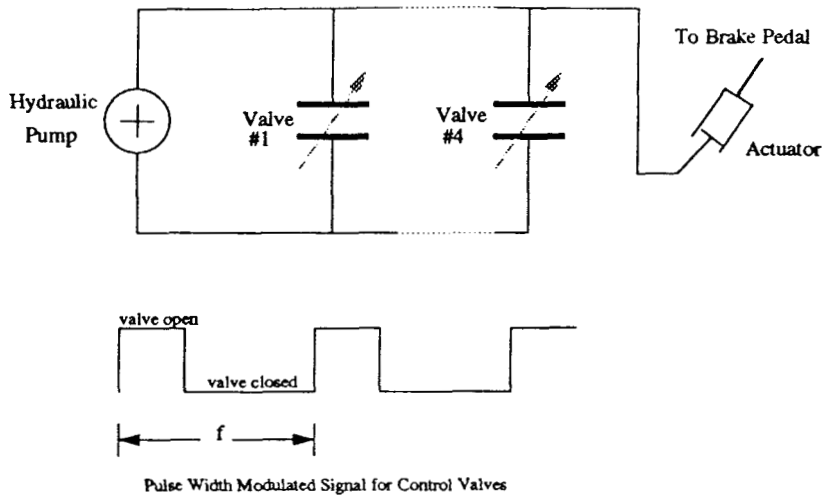
<center>3</center>

Figure **2:** Block Diagram of Auxiliary Hydraulic Module

an average amount of pressure can be maintained inside the cylinder of the actuator by switching the valves at high frequency (typically 100 Hz) with changeable duty cycle (percentage of valve open time in one switching period). This pressure will push the piston of the actuator and apply a force to the brake pedal.

When the duty cycle is changed, the pressure inside the cylinder of the actuator changes too. Hence the force applied to the brake pedal can be controlled by varying the duty cycle of the PWM signal. It should be noted that the maximum value of duty cycle corresponds to valves being open for most of the time and hence no force is applied to the brake pedal, which results in minimum brake line pressure at the output of master cylinder. From the overall system point of view any permissible pressure value at the output of master cylinder can be obtained by some particular value of duty cycle. *The model developed in this paper* **would** *identify the mapping* from *duty cycle to the line pressure.*

2.2   Vacuum Booster

The simplified construction of vacuum booster is shown in Figure **3.** The force amplification is caused by a pressure differential between the apply and vacuum chambers. Ideally, the amplification ratio between input and output force should be constant over the recommended range **of** operation. However, due to booster dynamics this ratio is not constant. According to operation of booster each brake application operation can be broken down into three basic stages: 1. apply stage **2.** hold or lap stage **3.** release stage. These steps are shown in Figure **4.**

• In the apply stage control valve moves forward, atmospheric valve is opened and vacuum valve is closed, hence a pressure differential is created, causing the diaphragm to move
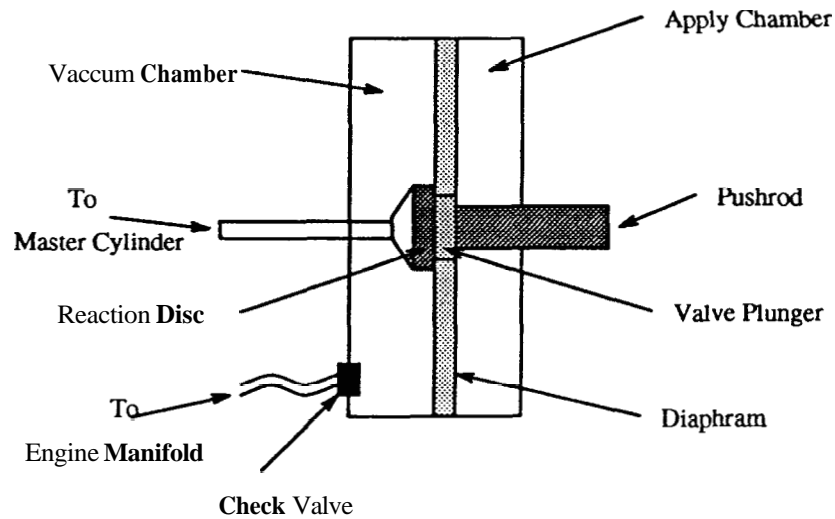
4

Figure **3:** Block Diagram of Vacuum Booster

forward.

o When the diaphragm travels further, valve housing catches up with the control valve. This movement also closes atmospheric valve. The diaphragm and valve body are now in hold position.

o When the brake pedal is released, the control valve moves back due to spring force, apply and vacuum chambers are connected and the pressure differential is reduced to zero.

Since the inertia of push rod and diaphragm is quite significant, the associated dynamics can not be neglected. Furthermore, the changes of pressure in apply and vacuum chambers also give rise to thermodynamics. For more detailed discussion **of** these effects, see [6].

2.3 Master Cylinder

The block diagram of a tandem master cylinder is shown in Figure 5. Input force, after being amplified by the vacuum booster, is applied through a push rod to the primary piston. The secondary piston, however, is pushed by hydraulic force built up by the primary piston.

Each portion of the master cylinder has its own separate reservoir, compensating port and outlet port. When an input force is large enough to move the primary piston to close the compensating port, pressure begins to build up between the primary and secondary piston. When the secondary compensating port is **closed,** pressure buildup occurs in the secondary portion too. At the same time hydraulic pressure developed during this operation is transferred through primary and secondary brake lines to brake pads.

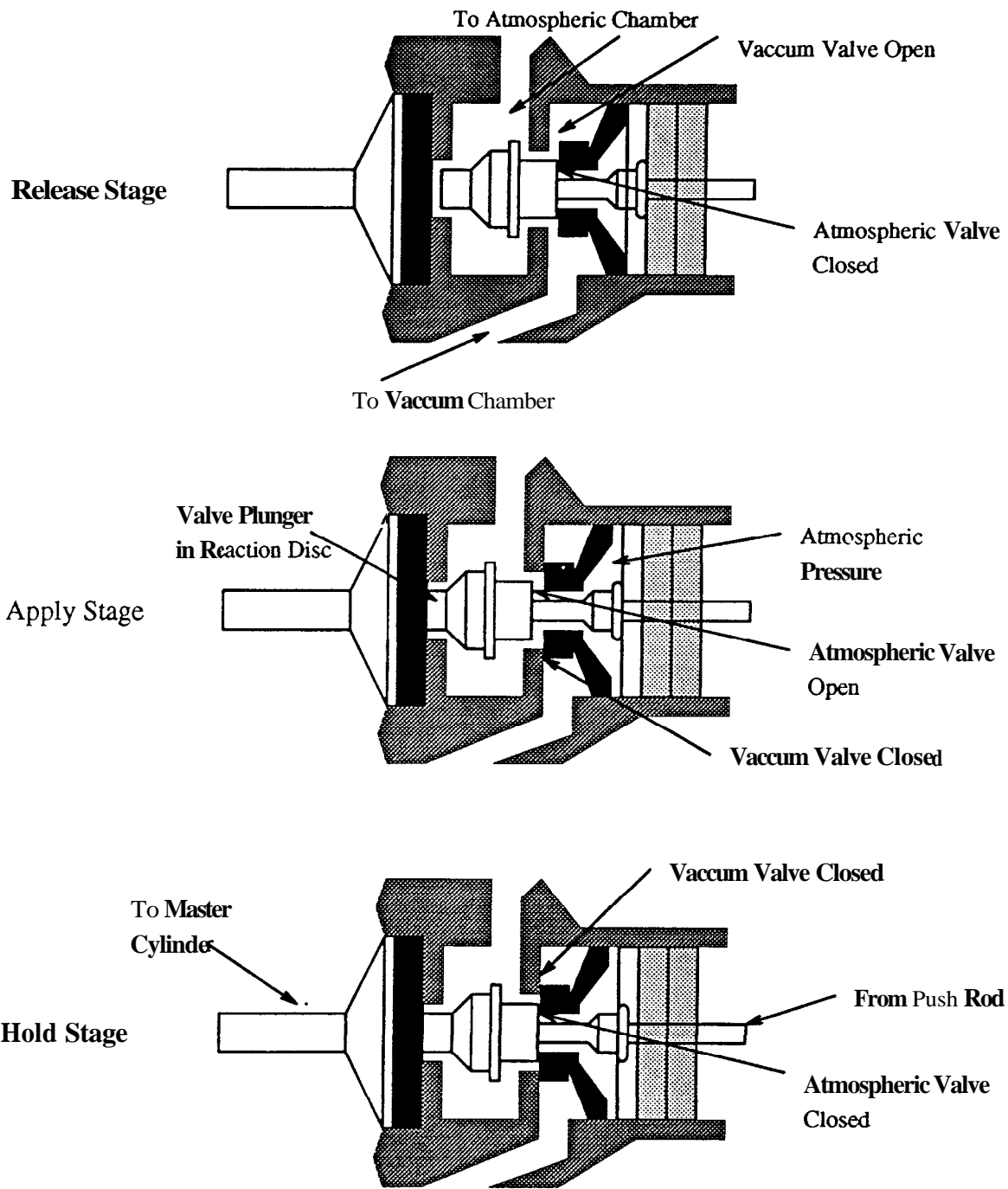**As** discussed in [6], since the masses of the pistons are negligible, the dynamics associated

Release Stage

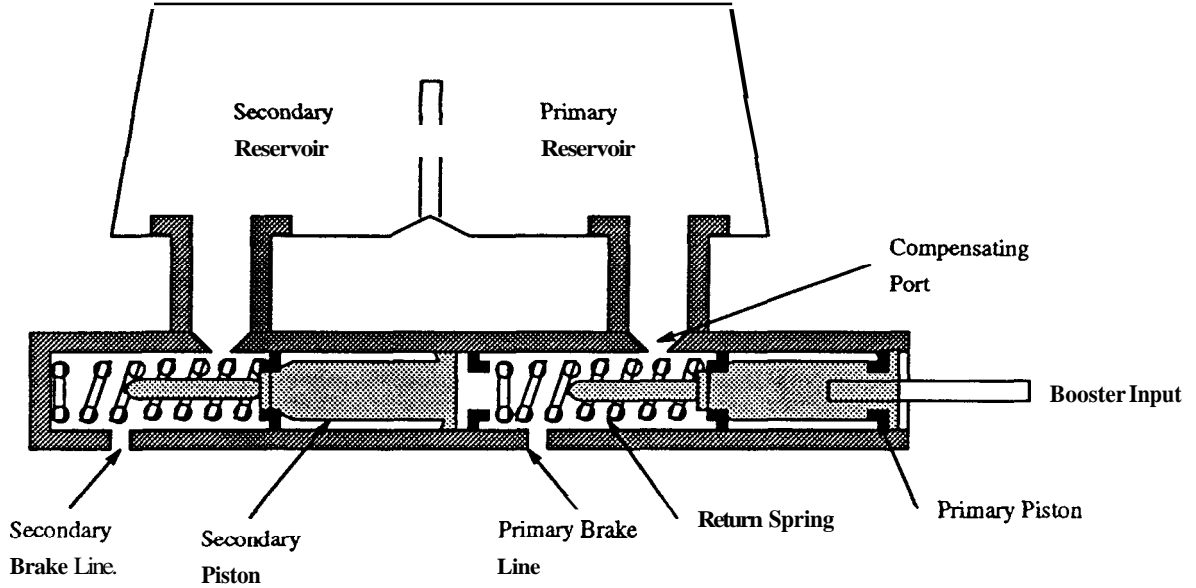To Atmospheric Chamber

Vaccum Valve Open

Atmospheric Valve Closed

To **Vaccum** Chamber

Apply Stage

Valve Plunger in Reaction Disc

Atmospheric **Pressure**

Atmospheric Valve Open

Vaccum Valve Closed

Hold Stage

To **Master Cylinder**

Vaccum Valve Closed

From Push **Rod**

Atmospheric Valve Closed

Figure **4:** Vacuum **Booster Operation**

Figure *5:* Block Diagram of Master Cylinder

with them can be neglected.

3 Proposed Brake Model

A series of experiments were conducted on the test bench of brake system. Some results of the experiments with step inputs of different magnitudes (corresponding to inputs of different duty cycle) are shown in Figures 6 and 7. These figures portray two basic modes of operation of the system: building and bleeding pressure modes. Another important system feature, which can be observed from these figures, is the variable time delay associated with different inputs and operating modes.

Since, time delay is an important factor in calculation of safety distance for normal vehicle following, hence was given special attention in this study. A large time delay of the order of **0.2** second is observed for relaxed system, i.e., when line pressure is zero. This time delay become negligibly small $(\approx 0.01 sec)$ for any line pressure other than zero. Hence this leads to the following relation, where t_d denotes delay time.

$$t_d = \begin{cases} \mathbf{0.2} & \text{if } x = 0 \\ 0.01 & \text{else} \end{cases} \tag{1}$$

The system response in Figure 8 shows time delays for the two cases discussed above.
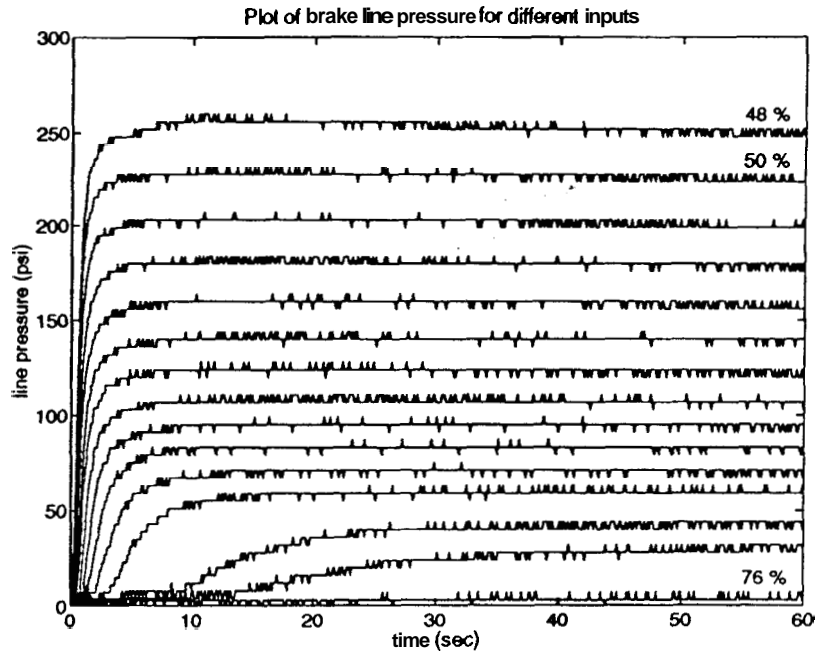
Figcre *6:* Brake line pressure for building mode. Inputs range from 76 to 48 %
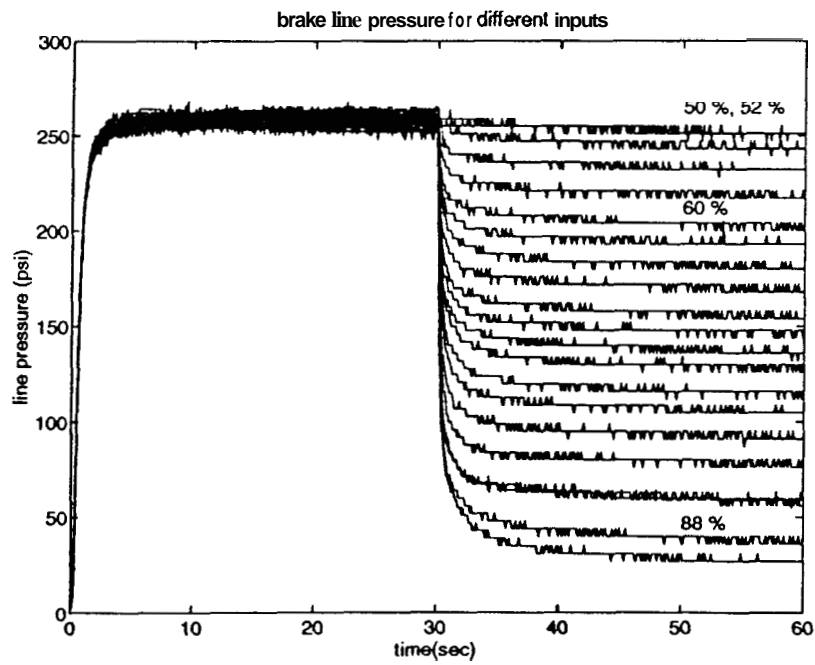
Figure 7: Brake line pressure for bleeding mode. Input **is** 48 % for $0 \leq t < 30sec$ and is changed at $t = 30sec$ to different values ranging from 50 to 90%.
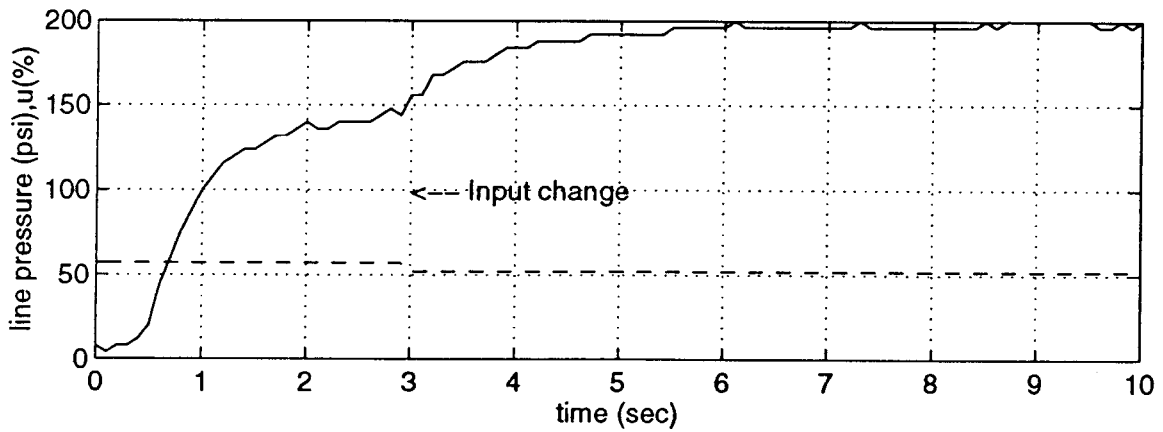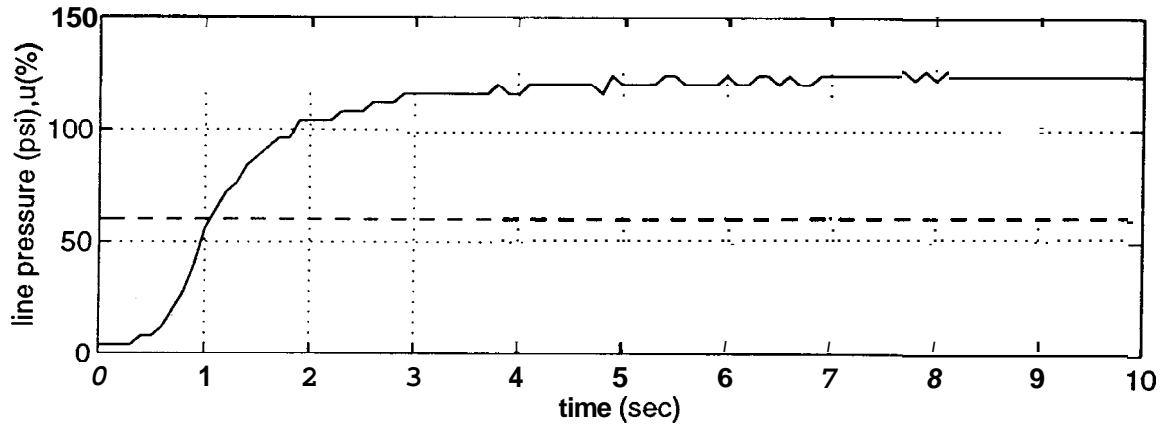
Figure 8: Top portion **of** the Figure shows that **for** relaxed system a large time delay, **0.2** sec, is observed. However, **for** any subsequent change in input(bottom portion), time delay is very small (≈ 0.01 sec).

The experimental results shown in Figure *6* and 7 suggest the presence of the dominant first order dynamics. Further analysis, to be explained later, exhibits nonlinear behavior of the system and motivates the following nonlinear dynamic model:

$$\dot{x}(t) = f_1(x(t), u(t^*), u(t^* - T)) \qquad (2)$$

The variables in (2) are:

x : system state (brake line pressure)

u : system input (duty cycle of the pwm signal)

f_1 : unknown function to be identified

where $x, u \in \mathcal{R}^1$, $t^* = t - t_d$, t_d is time delay defined in (1), T is some small number (taken to be equal to the sampling period) and $u(t^* - T)$ denotes the previous input. **As** given in (1), the value of t_d is negligibly small except when the system is relaxed. Hence t_d can be safely assumed to be zero in (2). Since, in this study of the brake system the modeling is done by using the input output data which is obtained at sampling instants only, hence instead of the continuous model in (2), we propose a discrete time model given **as:**

$$x(k + 1) = f(x(k), u(k), u(k - 1)) \qquad (3)$$

The shape of response for each fixed input, shown in Figures *6* and 7, can be approximated by a first order system given **as:**

$$x(k + 1) = x(k) + Tb(a - x(k)) \qquad (4)$$

where $a, b \in \mathcal{R}^+$. Parameters a and b in **(4)** characterize the steady state value and the speed of transient response respectively, for a given input $u(k)$. These parameters have similar meaning in linear systems, but have nonlinear relationship with respect to input u and state x of the system in this case. The experiments show that the steady state value of the pressure a can be modeled **as** given in (5).

$$a = g(x, u(k)) \qquad (5)$$

The **speed** of transient response (time constant) *6* vary significantly for different initial conditions and is sensitive to the previous history of the system, i.e., depends not only on the current input $u(k)$, but also on the previous input $u(k - 1)$. This phenomenon can be explained in terms of nonlinear fluid dynamics, the change in pressure is significantly slow if an input change occurs near a steady state pressure condition. Hence the system time constant represented by b depends on the current pressure relative to the steady state pressure for previous input. This suggests a functional form for the parameter b, which is given **as:**

$$b = h(x(k), u(k), u(k - 1)) \qquad (6)$$

In (5) and (6), g and h are unknown functions to be identified.

4 Parameter Identification

The parameter identification was done in two steps.
1) Fixed step inputs were used to identify the steady state value **a** and time constant $1/b$ for each input.
2) **A** series of staircase signals are used to modify the results of step **1.**

The motivation of breaking down the identification process into two steps follows from the fact that system response shown in Figures **6** and **7,** for a **fixed** input, can be approximated by response of a linear system to a step input. Hence standard results from linear system identification can be used to estimate the parameters. In the next step the nonlinear behavior of these parameters is explored by staircase signals. These signals cover the possible changes in input that excite building and bleeding modes of the system and enable us to study the switching process between these modes. The results from these experiments are used to modify the parameters a and b so that their values are valid for possible input variations applied to the system.

Finally it is shown that these parameters, identified by using step and staircase signals, give fairly accurate matching of the model and the actual system for continuously varying inputs. This is due to the fact that any continuous signal can be approximated by a staircase signal, where the accuracy of the approximation depends on the chosen step size. This approximation can be represented **as:**

$$u(t) = u(kT) \qquad kT \leq t < (k+1)T \tag{7}$$

Where T is sampling time and should be sufficiently small compared with bandwidth of the input signal $u(t)$ and system dynamics.

4.1 Step Inputs

The step response curves shown in Figures 6 and **7** for each fixed input u can be approximated **as** a solution to the first order linear differential equation, discretized at time step kT.

$$x(k) = x(0)(1 - Tb)^k + a(1 - (1 - Tb)^k) \tag{8}$$

where

$\quad a$: steady state value

$\quad 1/b$: time constant

$\quad x(0)$: initial condition

This simplification helps us to identify the parameters a and b for each input separately by using standard curve fitting techniques. It should be noted that the approximation given in (8) does not hold true for inputs with duty cycle greater than **68%**. However, line pressures below 70 psi, corresponding to the aforementioned inputs, have little or no significance in actual braking. Hence this approximation has no effect on model accuracy within range of interest.

The steady state value of the pressure, a, in the building mode is found to be relatively insensitive to the state x of the system. Furthermore, the two modes of operation shown in Figures **6** and 7 have different steady state values and slopes for the same inputs. The reason is the hysteresis produced due to friction, pre-loaded spring inside the vacuum booster and dead zone associated with the master cylinder and booster. Hence separate mappings for the two modes are required. The experimental results in Figure 6 suggest that for building case both a and b depend only on the current input, i.e.,

$$a = g(u(k)) \ ; b = h(u(k)) \qquad \text{(building)} \qquad (9)$$

On the other hand for bleeding mode a is a function of current input whereas b depends also on the current state x, i.e.,

$$a = g^*(u(k)) \ ; \ b = h^*(u(k), x(k)) \qquad \text{(bleeding)} \qquad (10)$$

These mappings g, h, g^* and h^* are given in Tables 1 and 2 respectively.

4.2 Staircase Inputs

Another series of experiment was conducted with inputs changing from one value to the different values and these changes were made to occur at different line pressures. Results show that the values of a calculated in these cases are consistent with those given by Table 1. Whereas the values of b vary significantly and was found to be a function of the current pressure, x, at which input was changed. Experiments show that the change in value of b is noticeable if the input is changed at a pressure which is more than 50% of the steady state value for the previous input. This change shows a monotonically decreasing behavior, with a maximum reduction of around **25%** at a pressure approximately equal to the steady state value. The change in value of b as a function of current pressure for two different **Au** is shown in Figure **9.** Guided by the experimental results, the following linear approximation was introduced to model this change:

$$b = h(u(k)) \left(\frac{5}{4} - \frac{x(k)}{2g(u(k-1))} \right) \text{ when } x(k) \geq \frac{g(u(k-1))}{2} \qquad (11)$$

Furthermore, the experimental results indicate that the change in b occurs only if the input changes, since b corresponds to the dynamics associated with the system which don't show any significant change for a constant input. Whereas, the relation given in (11) updates
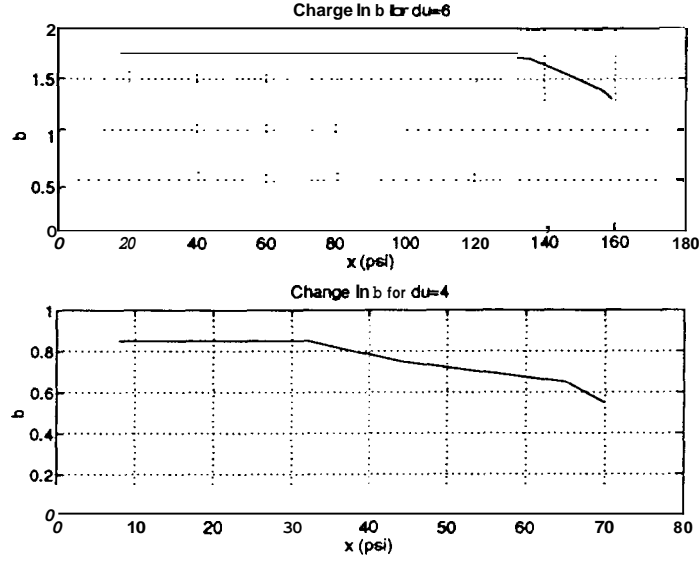
12

Figure 9: Change in b for change in input from 56% to **50%** ($\Delta u = 6$) and from *68%* to 64% ($\Delta u = 4$)

value of b at each sampling instant, which can be handled by introducing b as a state of the system, hence the updated value can be controlled through different conditions.

$$b(k+1) = \begin{cases} b(k) & \text{if } \Delta u = 0 \\ p_b b(k) + z_b \xi(k) & \text{else} \end{cases} \quad (12)$$

$$\xi(k) = \begin{cases} h(u(k)) & \text{if } x(k) < \frac{g(u(k-1))}{2} \\ h(u(k)) \left(\frac{5}{4} - \frac{x(k)}{2g(u(k-1))} \right) & \text{if } x(k) \geq \frac{g(u(k-1))}{2} \end{cases} \quad (13)$$

Where $\Delta u = u(k) - u(k-1)$, p_b and z_b are design parameters to smooth out the effects of switching while calculating the value of b using **(12)** and **(13)**, which is justifiable as the system dynamics don't show any sudden change. **As** explained later, this filtering would also help in control design.

From Table **1,** it is obvious that due to hysteresis, $g^*(u(k)) \geq g(u(k))$. From the experiments it was found that if a change in input causes the system state to be switched from building to bleeding mode with $g^*(u(k)) > g(u(k-1))$ then $a = x(k)$, and the line pressure x would maintain its previous value. Hence for bleeding mode, a, in **(10)** can be rewritten as:

$$a = min(x(k), g^*(u(k))) \quad (14)$$

The condition to determine the current mode of operation is:

$$x < g(u(k)) \Rightarrow \text{pressure is building} \quad (15)$$

13

This means that if current pressure is strictly less than the steady state value for the current input, then the system is in building mode and vice versa. Hence by using the condition (15) the results given in (10), (14), (12) and (13) can be combined to give the final form for model as:

$$x(k+1) = x(k) + Tb(k)(a - x(k)) \tag{16}$$

$$a = \begin{cases} g(u(k)) & \text{if } x(k) < g(u(k)) \\ min(x(k), g^*(u(k))) & \text{if } x(k) \geq g(u(k)) \end{cases} \tag{17}$$

$$b(k+1) = \begin{cases} b(k) & \text{if } \Delta u = 0 \\ p_b b(k) + z_b \xi(k) & \text{else} \end{cases} \tag{18}$$

$$\xi(k) = \begin{cases} h(u(k)) & \text{if } x(k) < \frac{g(u(k-1))}{2} \\ h(u(k)) \left(\frac{5}{4} - \frac{x(k)}{2g(u(k-1))} \right) & \text{if } x(k) \geq \frac{g(u(k-1))}{2} \\ h^*(u(k), x(k)) & \text{if } x(k) \geq g(u(k)) \end{cases} \tag{19}$$

5 Model Validation

The model described by (16)-(19) was simulated for different inputs, results are shown in Figures **14** and **15.** From Figure **15,** we see that the actual system and model output differ for low pressure values ($\leq$ **60** psi). However, as discussed before, due to less significance of these pressure values for actual braking purposes, this error is not severe.

It can also be seen form Figure **15** that for pressure values greater than **60** psi the error is within **f8** psi. This error figure is not too bad considering the fact that the pressure sensor used in the actual system has resolution of **4** psi. Furthermore, from Figure **15** it is obvious that the model output for staircase approximation of continuous signal is the same as that of the original signal. Hence, the estimates of parameters *a* and *b* which were calculated as though the input signal is made up of finite steps hold even when the step width T is reduced to zero.

6 Limitations

1. Model accuracy, for the representation given above, depends mainly on the accuracy of identification of parameters *a* and *b*.

2. The modification for *b* given by **(11)** holds only if $x < g(u(k-1))$, i.e., steady state is not attained. When steady state actually is achieved, then the value of *b* shows a further decrease as time increases. In other words, the longer the system stays at one steady state value, the harder it is for system to change the state. It was found by experiments that for a fixed input the steady state is not attained for a step width of less than 5 seconds, hence in this case the approximation given by **(11)** holds true. This is not a severe limitation considering the fact that actual braking commands do fall into this category.

7 Control Design

The nonlinearity **of** the brake system under consideration is in the form **of** hysteresis and variable time delay. The main objective **of** the controller design in this paper is to *make the performance of the brake system as uniform as possible throughout the range of operation.* One way to achieve this objective is to use *feedback linearization* to cancel the nonlinearities of the system.

The design of the brake controller in this paper follows the guidelines provided **by** the feedback linearization technique given in [12]. The brake model given in **(16)** has no explicit control input term. Since *a* in brake model is a nonlinear function **of** control input u and state x and the inverse mapping

$$u(k) = g^{-1}(a(k), x(k)) \tag{20}$$

is guaranteed to exist for all values of *a* and x within operating range **of** the system, i.e.,

$$\mathcal{S}_o = \{y \in \mathcal{R} : |y| \leq P_{max}\} \qquad \mathcal{U}_0 = \{u \in \mathcal{R} : u_{min} \leq u \leq u_{max}\} \tag{21}$$
$$\forall a, x \in \mathcal{S}_o \quad \Rightarrow \quad g^{-1} \text{ exists and } u \in \mathcal{U}_o$$

where P_{max} is the maximum allowable pressure, u_{min} and u_{max} represent minumum and maximum control input respectively. Hence with the condition given in (21), we can assume a as a control input. This assumption would help us to linearize the system by using standard input-output feedback linearization techniques. The controller design proceeds by first linearizing the brake model (16), with output $x(k)$ and input a, without changing the internal state dynamics $b(k)$ given in (18).

$$x(k+1) = x(k) + Tb(k)(a - x(k)) \tag{22}$$

We first let $x(k+1) = \nu$ by choosing **a** as:

$$a = \frac{1}{Tb}\nu + \left(1 - \frac{1}{Tb}\right)x(k) \tag{23}$$

then we let $\nu = \alpha x(k) + \omega$, where α is some design constant and w is the new input. The resulting system is:

$$z(k+1) = \nu = \alpha x(k) + w \tag{24}$$

for any w and *cr*, using the following equation

$$a = \frac{1}{Tb}(\alpha x(k) + w) + \left(1 - \frac{1}{Tb}\right)x(k) \tag{25}$$

we can compute **a.** The control input u is then found by using the inverse mapping **(20).** The linearized transfer function of the system becomes:

$$G'(z) = \frac{x(z)}{\omega(z)} = \frac{1}{z - \alpha} \tag{26}$$

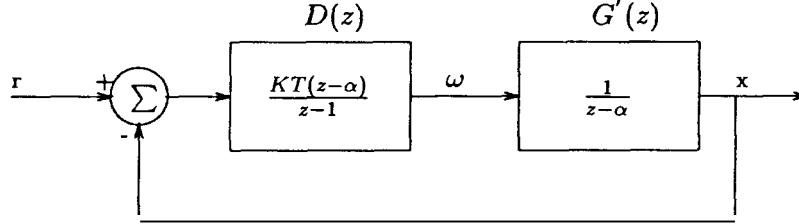**As** pointed out before any linear control law can be applied to obtain the control input

Figure 10: Block diagram of the closed loop system.

w. In this case a PI compensator is added in the loop to reduce the effects of modeling errors. In addition this compensation would help to meet the performance specification of zero steady state error for step inputs. The compensator is given **as:**

$$D(z) = K_P + \frac{K_I T}{z - 1} = \frac{K_P(z - 1) + K_I T}{z - 1} \tag{27}$$

The loop transfer function with the addition of compensator becomes:

$$L(z) = K_P \frac{(z - 1) + \frac{K_I T}{K_P}}{(z - 1)(z - a)} \tag{28}$$

Hence with the addition of a PI compensator the order of the closed loop system has increased. This, however, can be avoided by carefully selecting the gains K_P and K_I, one such combination is given **as:**

$$K_P = KT \qquad K_I = K(1 - \alpha)$$

where $K > 0$ is the design constant to place the closed loop pole at desired location. Hence the input *w* in (24) becomes:

$$\omega = \frac{KT(z - a)}{2 - 1}(r - x) \tag{29}$$

The closed loop transfer function $T(s)$ shown in Figure **10** is given **as:**

$$T(z) = \frac{x(z)}{r(z)} = \frac{KT}{z - 1 + KT} \tag{30}$$

The control law is summarized in Table (5) and an implementation block diagram is given in Figure *11.*

$$\omega = \frac{KT(z-\alpha)}{z-1}(r - x)$$

$$\nu = \alpha x + w$$

$$a = \frac{1}{Tb}\nu + \left(1 - \frac{1}{Tb}\right)x$$

$$u = g^{-1}(a, x)$$

Table 1: Summary of Control Law
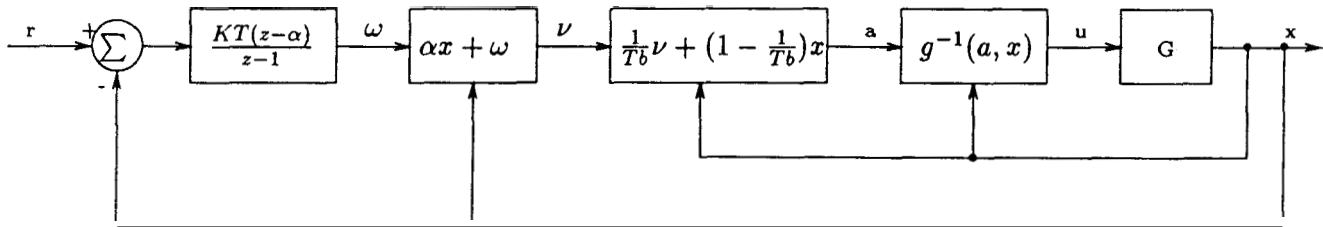
Figure 11: **Block** diagram for implementation of the **feedback** linearized control system.

7.1 Controller Modifications

The control input generated by feedback linearization in Table (**1**) is usually calculated based on the assumption that there is no saturation of the control input. However, from safety point of view a limited control authority is available in the given system. Hence to avoid performance deterioration, some additional logic is embedded within standard PI compensator. These modifications along with some justification are presented below:

   o In order to avoid the integration wind up problems a limited integrator is used in place of ideal integrator.

   o In order to avoid overshoot while maintaining swiftness of response, the logic added with PI compensator is shown in Figure **12.** Since brake system under consideration has a large delay, $\approx 0.2sec.$ at start up, hence the branch labeled ***delay kill*** in Figure 12 stops integrator accumulation during this interval. This reduces the saturation of control input during delay period and helps to avoid overshoot at low operating pressures.

   o To reduce overshoot at high pressure, the branch labeled *shoot **kill*** cuts off integrator when either:
- the nonlinear function *a,* used as linearization input, exceeds the maximum steady state pressure value and actual pressure x is less than the desired one
- or when *a* is negative and the brake pressure is greater than the desired.
This modification results in minimum possible overshoot for normal and high pressure regions. Hence during initial startup time and at the time when the controller output is saturated, this logic avoids excessive integrator accumulation, that may cause subsequent overshoot. The output of PI compensator is now given as:

$$
\omega = \begin{cases} KT(r - x) & \text{if } x < P_{min} \text{ or } ((r - x) < 0 \text{ and } a < 0) \\ & \text{or } (a > a_{max} \text{ and } (r - x) > 0) \\ \frac{KT(z-\alpha)}{z-1}(r - x) & \text{else} \end{cases} \tag{31}
$$

where P_{min} is the minimum line pressure in idle state, when time delay is large. Since the inverse mapping, $u = g^{-1}(a, z)$, is guaranteed to be invertible when the inputs a, x are within safety limits of equipment, hence a saturation function $p(.)$ is introduced at the output of *a.*

$$
p(a) = \begin{cases} a & \text{if } a_{min} < a < a_{max} \\ a_{min} & \text{if } a < a_{min} \\ a_{max} & \text{else} \end{cases} \tag{32}
$$

where $a_{min} = 0$ and $a_{max} = P_{max}$, P_{max} is the maximum allowable pressure. Some simulation results before and after addition of this logic are shown in Figure 16. **A** comparison
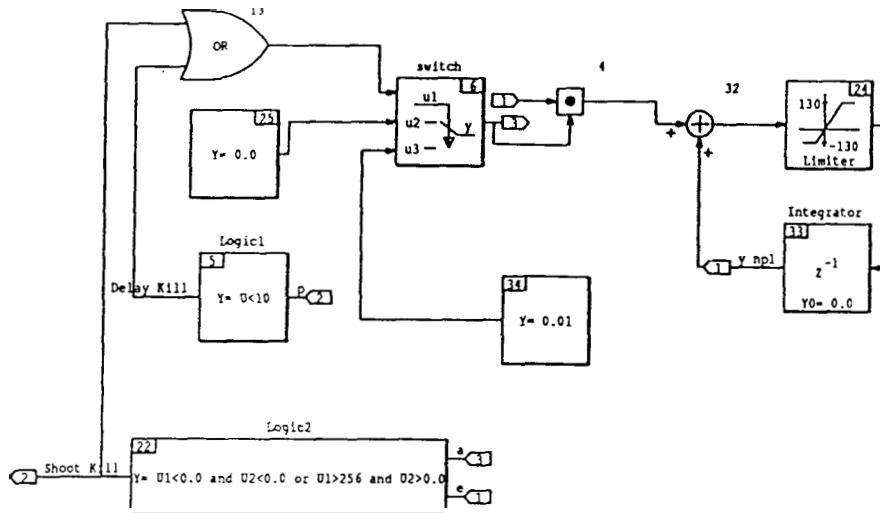
Figure 12: Block diagram for modified integrator.

of the attainable performance using this modification, with the standard PI compensator is given in Table (2).

controller	rise time	settling time	s.s. error	overshoot
Standard PI	1.0 sec	3.5 sec	≈ 0	10%
Modified PI	1.1 sec	2.5 sec	≈ 0	0

Table 2: Comparison of performance

With the proposed modification introduced, the main characteristics of the closed **loop** system are summarized **as:**

o step response is fast enough to meet the **AVCS** performance specifications

• There is no overshoot or undershoot, this would **help** to avoid the slinky type effects and to meet the strict spacing constraints

o zero steady state error for step inputs.

19

8 Stability Analysis

First of all we discuss the conditions **of** open loop stability **of** the system. Since the nonlinear functions $a = g(x, u)$ and $b = h(x, u)$ in (17) and (18) are guaranteed to be bounded, i.e.,

$$g(x, u) \in C_1 = \{y_1 \in \mathcal{R} : a_{min} \leq y_1 \leq a_{max}\} \tag{33}$$

$$h(x, u) \in C_2 = \{y_2 \in \mathcal{R} : b_{min} \leq y_1 \leq b_{max}\} \quad \forall u, x(0) \in \mathcal{L}_\infty \tag{34}$$

where $a_{min} \geq 0$ and $b_{min} > 0$. Hence for any bounded initial condition, any bounded input to the system would result in a bounded state.

$$u, x(0) \in \mathcal{L}_\infty \Rightarrow x \in \mathcal{L}_\infty \quad \forall t \geq 0$$

Furthermore, $u \in \mathcal{U}_o \Rightarrow x \in \mathcal{S}_o$, where $\mathcal{U}_o$ and $\mathcal{S}_o$ are as defined in (21). **As** discussed before, the nonlinear function a is used in place of control input u for linearization of open loop plant (22). **As** given by condition (21), if we guarantee that $a, x \in \mathcal{S}_o$ then it implies that u $\in \mathcal{L}_\infty$, rather $u \in \mathcal{U}_o$, where $\mathcal{U}_o$ forms the set of acceptable inputs to the system.

Theorem 1 *If the controller given in Table 1 with the modification (31) is initialized such that $u \in \mathcal{U}_o$, then the closed loop signals w, r, a, u and x are bounded $\forall t \geq k_0 T$.*

Proof: The assumption that at $t = k_0 T$, $u \in \mathcal{U}_o$ is not restrictive **as** the controller would be initialized with some acceptable input. To establish the boundedness of all the signals in closed **loop,** we begin **as:**

Since $u(k_0) \in \mathcal{U}_o \Rightarrow x(k_0) \in \mathcal{S}_o$. Considering PI compensator, we can write:

$$\omega(k) = W(k) * (r(k) - x(k)) \tag{35}$$

where $*$ represents the convolution operation and $r(k)$ is the desired output trajectory, obviously $r(k) \in \mathcal{S}_o$.

$$\Rightarrow |\omega(k_0)| \leq \|W(k)\|_\infty |r(k_0) - x(k_0)| \tag{36}$$

where $(r(k_0) - x(k_0)) \in \mathcal{S}_o$ and $W(z)$ is a stable proper transfer function, hence $\omega(k_0) \in \mathcal{L}_\infty$. In the case of modified **PI** compensator (31) not only $\omega(k_0) \in \mathcal{L}_\infty$ but $\omega(k_0) \in \mathcal{O}(\mathcal{S}_o)^\dagger$. From (24) we can write:

$$|\nu(k_0)| \perp \alpha |x(k_0)| + |\omega(k_0)| \tag{37}$$

$\dagger$ A function $f(x)$ is $\mathcal{O}(x)$ if there exists a finite constant c > 0, such that $|f(x)| \leq c|x| \ \forall x$.

Hence $\nu(k_0) \in \mathcal{L}_\infty$ and for any finite $\alpha > 0$, $\nu(k_0) \in \mathcal{O}(\mathcal{S}_o)$. From (23) we can write:

$$|a(k_0)| \leq |x(k_0)| + |\frac{1}{b(k_0)}||\nu(k_0)| \qquad (38)$$

since $b(k) \geq b_{min} > 0 \Rightarrow a(k_0)$ E $\mathcal{L}_\infty$. Also for arbitrarily small values of b, $a \in \mathcal{O}(\frac{1}{b})$, otherwise for normal operating range of equipment, when b is close to unity, $a(k_0)$ E $\mathcal{O}(\mathcal{S}_o)$. Finally the saturation function $p(.)$ defined in (32) ensures that $a(k_0)$ E $\mathcal{S}_o$.

Hence, from (21) we get $u(k_0 + 1)$ E $\mathcal{U}_o \Rightarrow x(k_0 + 1) \in \mathcal{S}_o$. Now by induction we can show that closed loop signals are bounded for all $k \geq k_0$. $\qquad \square$

9 Simulation and Implementation Results

The control law given in Table 1 along with modifications proposed in the section seven was simulated using Matrixx and nonlinear brake model. The block diagram of the closed loop system is shown in Figure 13. The simulation results for some of the typical braking
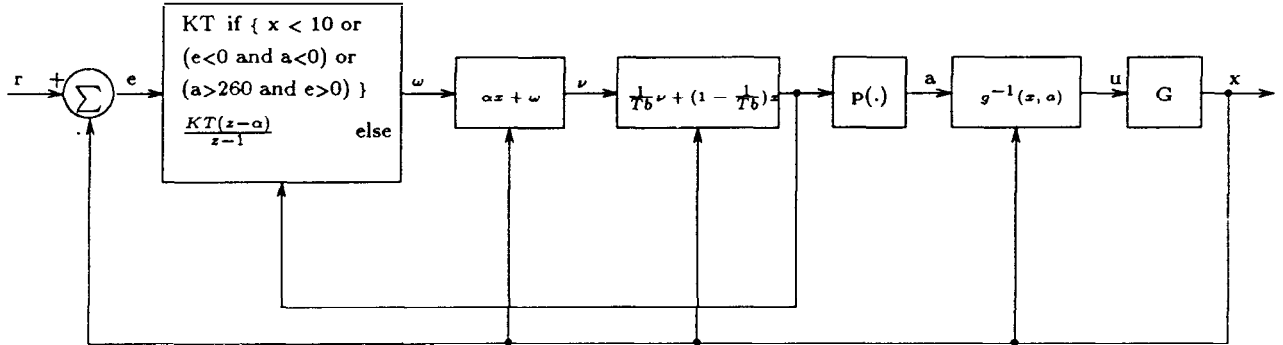
Figure 13: Block diagram of the feedback linearized control system.

scenarios are shown in Figures 17a-19a. The simulation results confirm the claims about the performance in terms of zero steady state error, no overshoot and sufficiently fast response (limited by the equipment constraints).

The controller given in Figure 13 was implemented on the actual brake system. The results obtained from the actual closed loop system are shown in Figures 17b-19b. The simulation results in Figures 17a-19a are almost identical to the actual closed loop system response shown in Figures 17b-19b. Furthermore, one of the design objectives to make the system behave linearly is proved by comparing the actual closed loop system response with that of the equivalent linear system $(\frac{KT}{z-1+KT})$. The comparison for the three inputs considered before is shown in Figure 21.

21

10   Conclusion

A nonlinear model for describing the input output behavior of the brake system was proposed. The model was simplified to make it resemble the first order linear system but with nonlinear coefficients and time delays. The unknown parameters were identified using standard curve fitting techniques on the data obtained by conducting experiments on the test bench with brake system of Lincoln Town Car and actuator for automatic brake control. Although the parameter identification was done using staircase inputs but was shown to be valid for continuous inputs. The hysteresis phenomenon was modeled by isolating the two operating modes and identifying separate sets of parameters for each case. The worst case modeling error was found to be less than 5% within range of interest of the system.

The brake controller makes use of the standard feedback linearization technique applied to the nonlinear model developed in first part. A PI compensator with some modifications was introduced in the closed loop to meet the performance specifications. Comparison of the simulation results and tests on actual system validate the claims made about the designed controller.

References

[1] Shladover, S., E., "Longitudinal Control of Automotive Vehicles in Close–Formation Platoons", ASME Journal on Dynamic Systems, Measurement and Control, vol. **113, 1991,** pp. **231-241.**

[2] Shladover, S., E., Desor, C., A., Hedrick, J., K., Tomizuka, M., Warland, J., Zhang, W., B., McMohan, D., Peng, H., Sheikholselam, S., McKeown, N., "Automatic Vehicle Control Developments in PATH Program, IEEE Trans. on Vehicular Technology", vol. **40, 1991,** pp. **114-130.**

[3] Sheikholelslam, S., Desoer, C., **A.,** "A System Level Study of the Longitudinal Control of a Platoon of Vehicles", ASME Journal of Dynamic Systems, Measurement, and Control, **1991.**

[4] Varaiya, P., "Smart Cars on Smart Roads: Problems of Control", PATH Technical Memorandum, **91-S,** December **1991.**

[5] Chien, C., C., Ioannou, **P.,** "Automatic Vehicle Following", Proc. American Control Conference, Chicago, Il., June **1992.**

[6] Gerdes, J., C., Maciuca, D., B., Devlin, P., E., Hedrick, J., K., "Brake Modeling for IVHS Longitudinal Control", ASME **1993.**

[7] Khan, Y., Kulkarni, P., and Youcef-Toumi, K., "Modeling, Experimentation and Simulation of a Brake Apply System", Proceedings of the **1992** American Control Conference, pp. **226-230.**

[8] Nunney, **M., J.**, "Light and Heavy Vehicle Technology", 2nd Edition, Newnes, Oxford OX2 8DP, 1992, pp 516-552.

[9] Hedrick **J. K.,** McMahon D., Narendran V., Swaroop D., "Longitudinal Vehicle Controller Design for IVHS System", Proceeding of American Control Conference", Vol. 3, pp. 3107-3112, June 1991.

[10] Xu Z., Ioannou P., "Throttle and Brake Control Systems for Automatic Vehicle Following", IVHS Journal, 1994, Vol. 1(4), pp.345-377.

[11] Hauksdottir A. *S.*, Fenton R. E., "On the Design of Vehicle Longitudinal Controller", IEEE Transaction on Vehicular Technology, Vol. VT-34, No. 4, pp. 182-187, Nov. 1985.

[12] Slotine J. E., Li W., "Applied Nonlinear Control", Prentice Hall, Englewood Cliffs, NJ, 1991.

A   Lookup Tables

u (%)	$a = g(u)$ (psi)	$b = h(u)$	$a = g^*(u)$ (psi)
48	253	1.8	253
50	226	1.7	253
52	202	1.6	252
54	181	1.4	251
56	159	1.2	245
58	140	1.0	233
60	124	0.9	219
62	108	0.75	194
64	94	0.65	182
66	83	0.50	170
68	70	0.35	157
70	60	0.20	148
72	48	0.10	138
74	30	0.07	129
76	5	0.02	116
78	0	0	107
80	0	0	94
82	0	0	79
84	0	0	65
86	0	0	57
88	0	0	40
90	0	0	29

Table **3:** Least square fit values of functions g, h and g^* for the curves in Figures 6 and **7**

u \ x	0	30	60	80	95	105	125	145	160	180	200	225	253
48	X	X	X	X	X	X	X	X	X	X	X	X	1.8
50	X	X	X	X	X	X	X	X	X	X	X	1.7	1.8
52	X	X	X	X	X	X	X	X	X	X	1.6	1.7	1.8
54	X	X	X	X	X	X	X	X	X	1.4	1.6	1.7	1.9
56	X	X	X	X	X	X	X	X	1.2	1.4	1.6	1.8	1.9
58	X	X	X	X	X	X	X	1.0	1.2	1.4	1.7	1.8	2.0
60	X	X	X	X	X	X	0.9	1.0	1.2	1.5	1.7	1.9	2.1
62	X	X	X	X	X	0.75	0.9	1.0	1.3	1.5	1.8	1.9	2.2
64	X	X	X	X	0.65	0.75	0.9	1.1	1.3	1.6	1.8	2.0	2.3
66	X	X	X	0.5	0.65	0.75	1.0	1.1	1.4	1.6	1.9	2.0	2.4
68	X	X	X	0.5	0.65	0.8	1.0	1.2	1.4	1.7	1.9	2.1	2.5
70	X	X	0.2	0.5	0.7	0.8	1.0	1.2	1.5	1.8	2.0	2.2	2.6
72	X	X	0.2	0.5	0.7	0.8	1.1	1.3	1.5	1.8	2.0	2.3	2.6
74	X	0.07	0.2	0.6	0.7	0.9	1.1	1.3	1.6	1.9	2.1	2.4	2.7
76	X	0.07	0.2	0.6	0.7	0.9	1.1	1.4	1.6	1.9	2.2	2.5	2.7
78	0	0.07	0.3	0.6	0.7	0.9	1.2	1.4	1.7	2.0	2.3	2.5	2.8
80	0	0.07	0.3	0.6	0.7	0.9	1.2	1.5	1.7	2.0	2.3	2.6	2.8
82	0	0.07	0.3	0.7	0.7	1.0	1.2	1.5	1.8	2.1	2.4	2.6	2.9
84	0	0.07	0.4	0.7	0.8	1.0	1.3	1.5	1.8	2.1	2.4	2.7	2.9
86	0	0.07	0.4	0.7	0.8	1.0	1.3	1.6	1.9	2.2	2.5	2.7	3.0
88	0	0.07	0.4	0.7	0.8	1.0	1.3	1.6	1.9	2.2	2.5	2.7	3.0
90	0	0.07	0.4	0.7	0.8	1.0	1.3	1.6	1.9	2.2	2.5	2.7	3.0

Table 4: Least square fit values of $b = h^*(u, x)$ for the curves in Figure 7. An X as a table entry indicates an invalid state for bleeding mode.
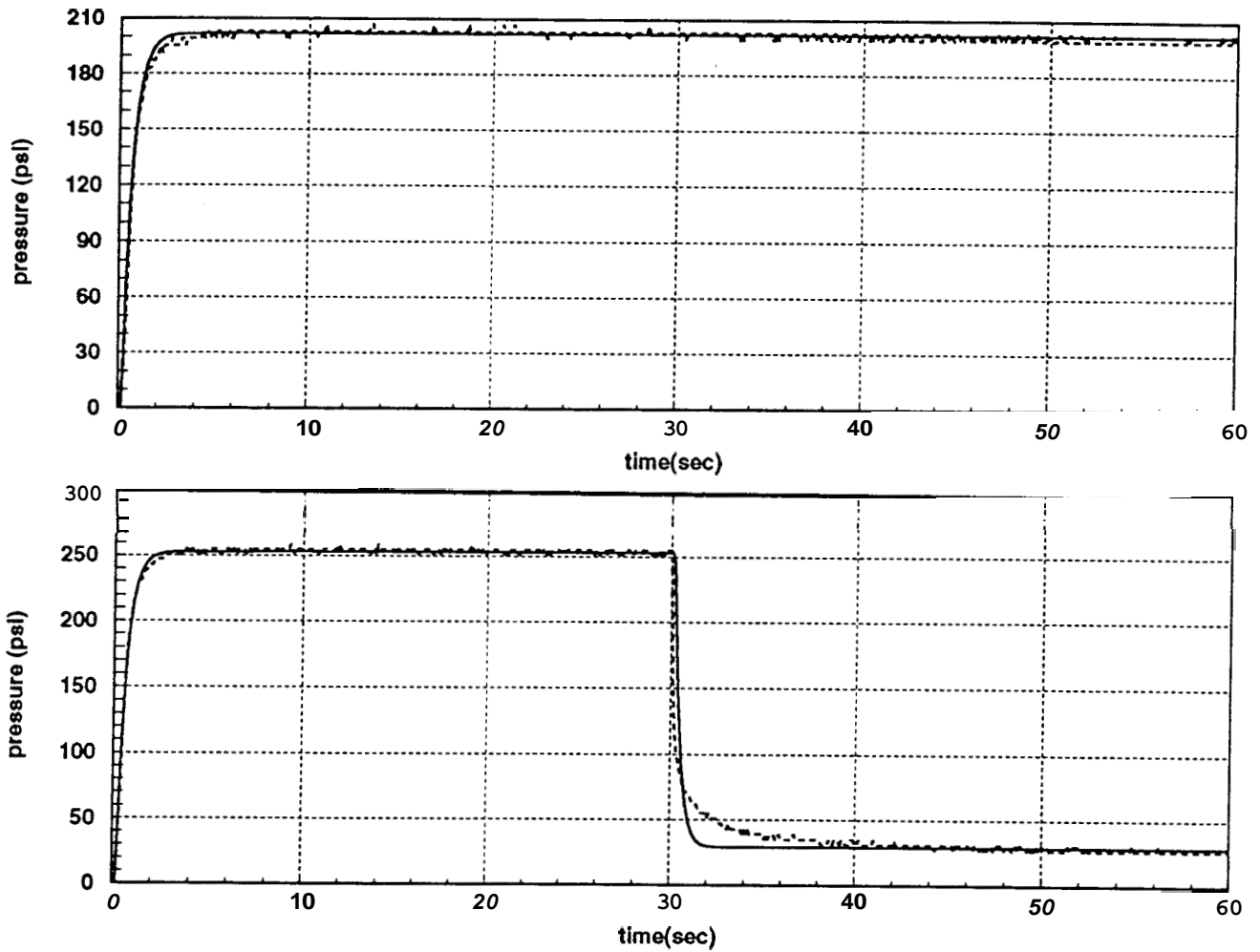
Figure **14: A** comparison of the actual and model output for a step input of 52% is shown in the top portion of the Figure. Whereas in the bottom one input changes from 48% to **90%** at t=30 sec.

26
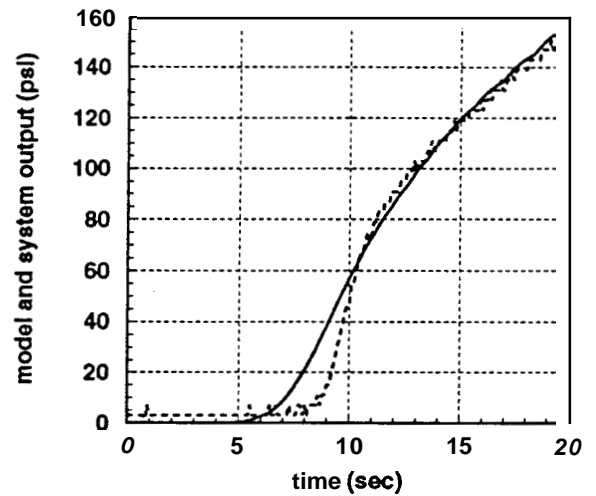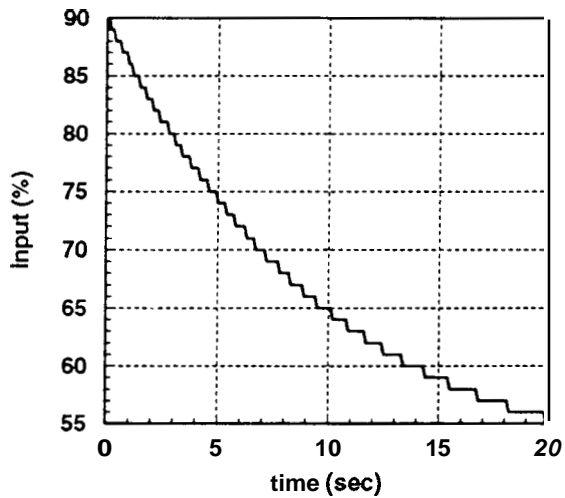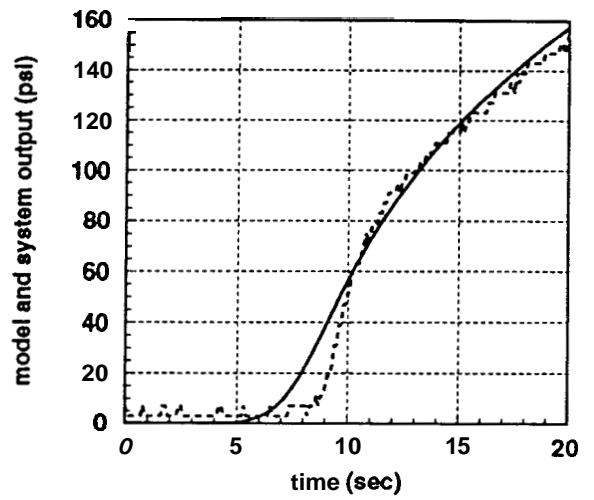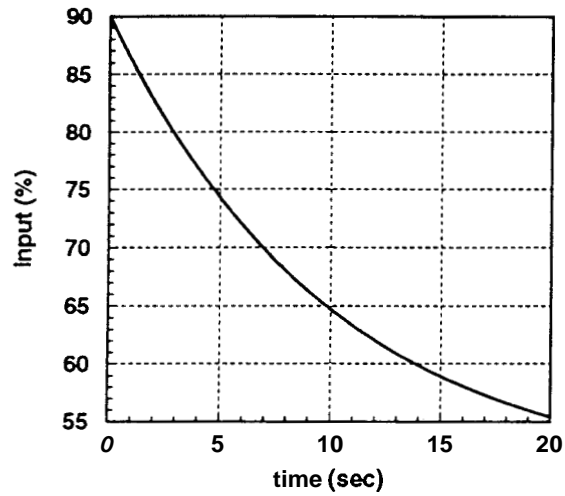
Figure 15: The top left portion of the Figure shows the input signal being applied to actual system and brake model for comparison. The system and model outputs are shown in top right position for given input signal. A staircase approximation of the same input signal is shown in bottom left graph. The comparison of outputs is shown in bottom right graph.
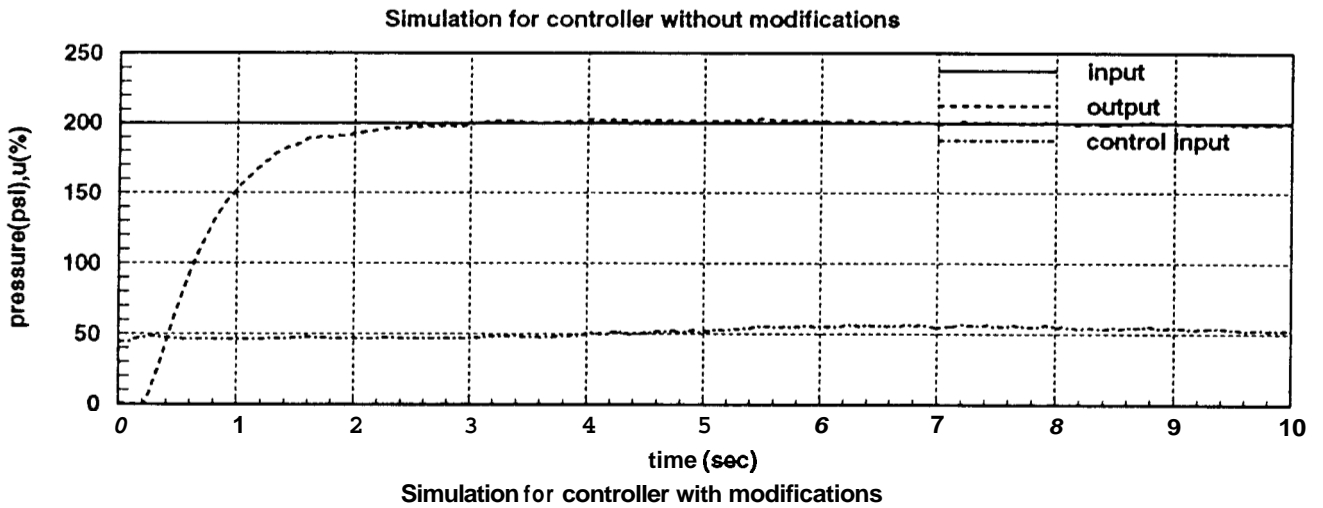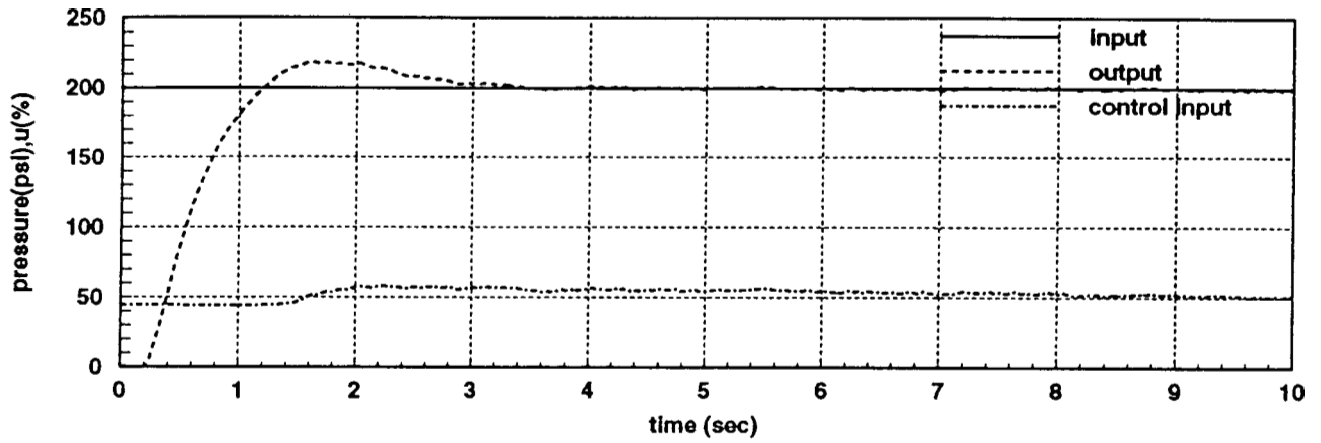
Figure **16:** Comparison of closed loop response for PI compensator with and without modifications.
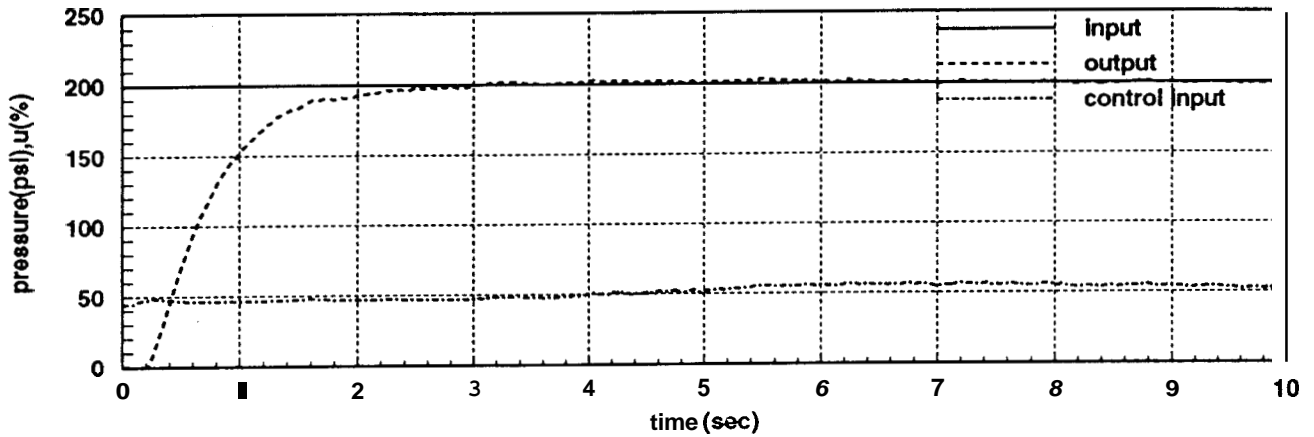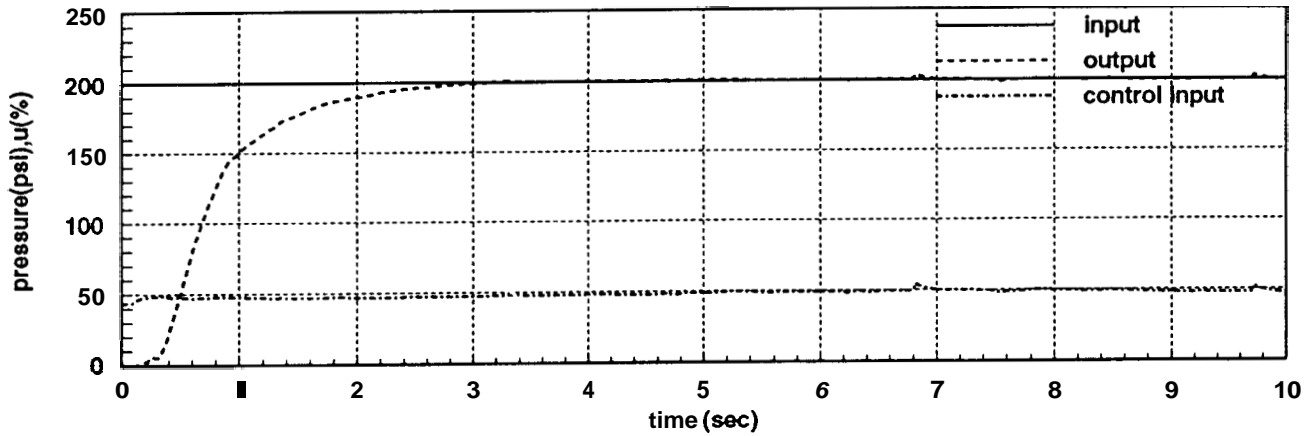
Figure 17: Simulation and actual system response for step input, corresponding to a desired pressure of 200 psi.
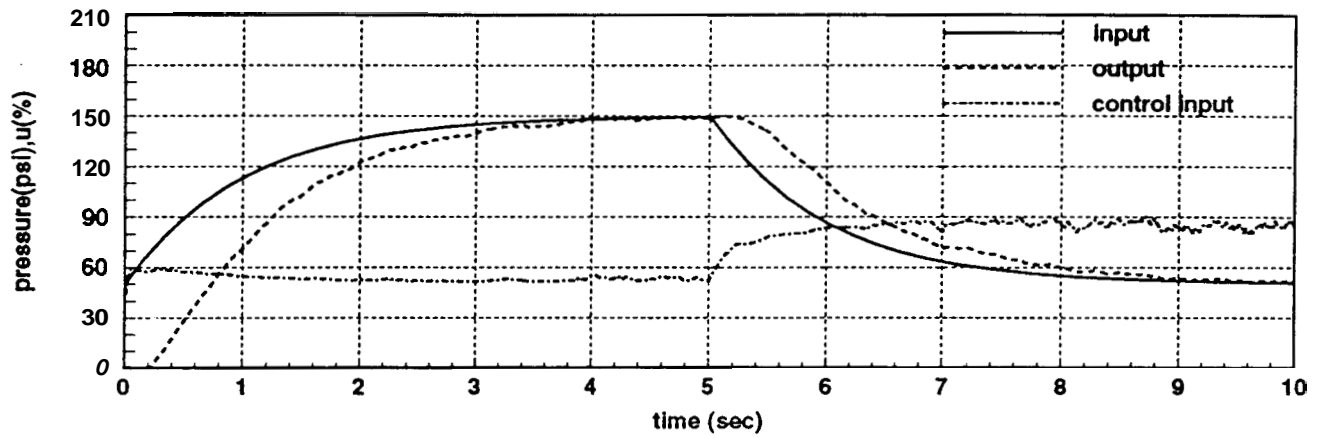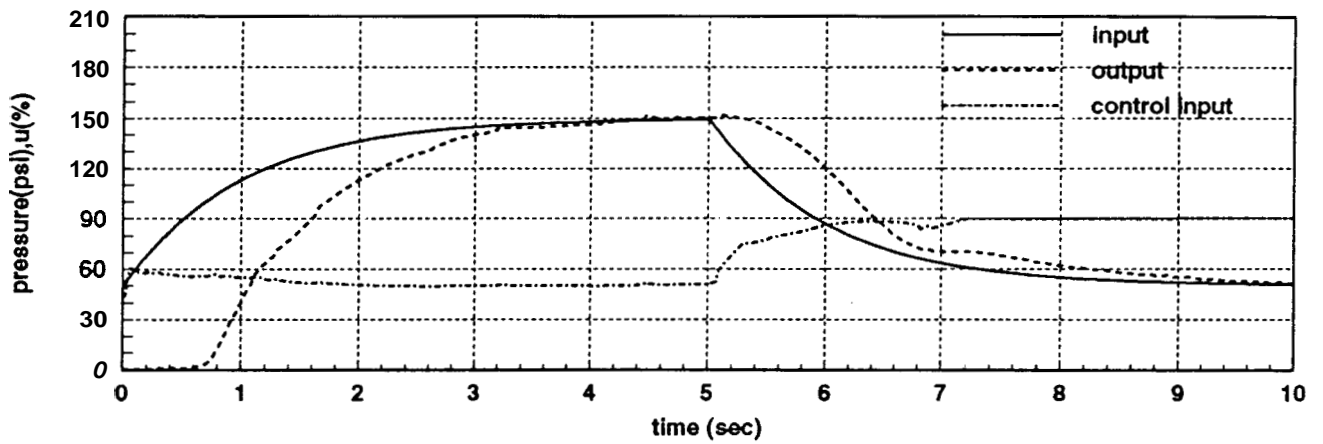
Figure 18: Simulation and actual system response for exponential input.
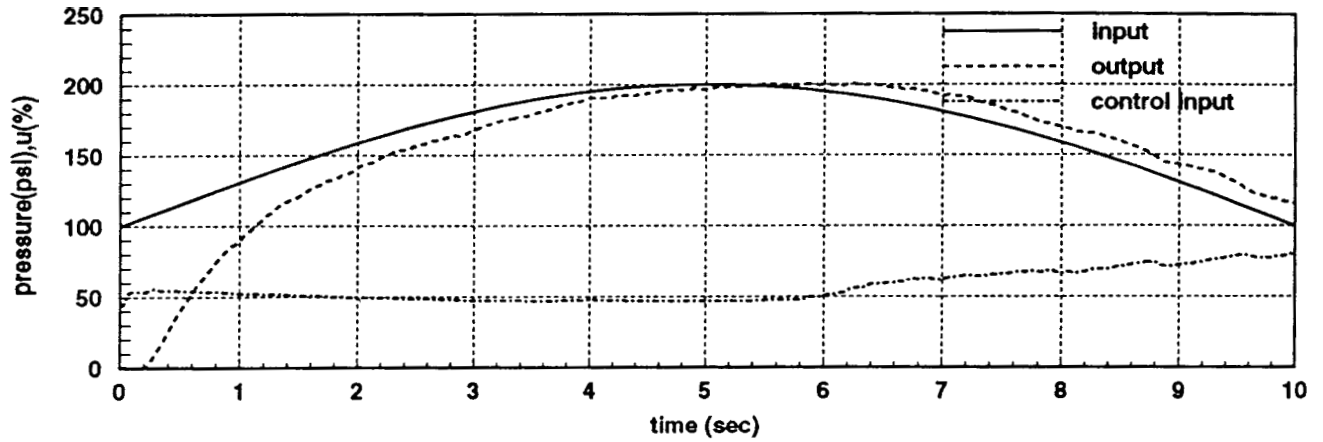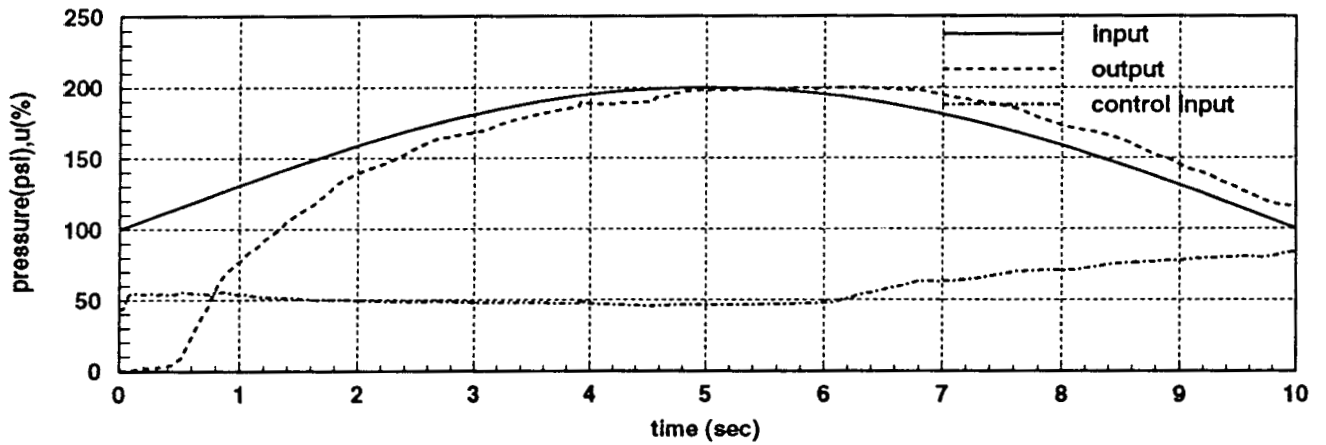
Figure 19: Simulation and actual system response for sinusoidal input.
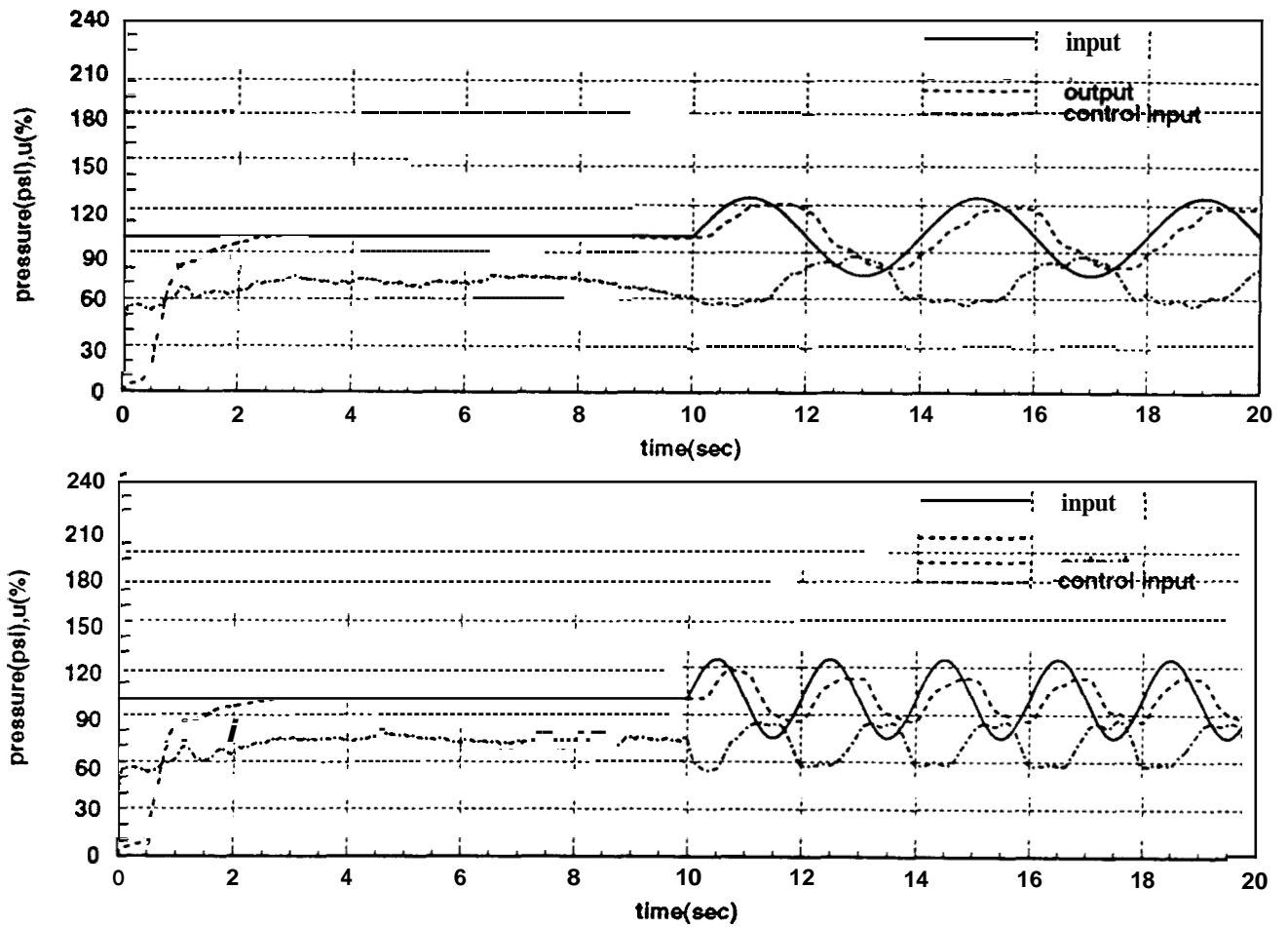
Figure 20: Closed loop system response for sinusoidal input of 0.25 **Hz.** (top) and 0.5 **Hz.** (bottom). The desired pressure is step input of 100 psi from 0 to 10 sec, from 10 sec to 20 sec a sinusoidal input with amplitude of 25 psi is superimposed on the step input. It should be noted that system bandwidth is around 0.5 **Hz.**

32
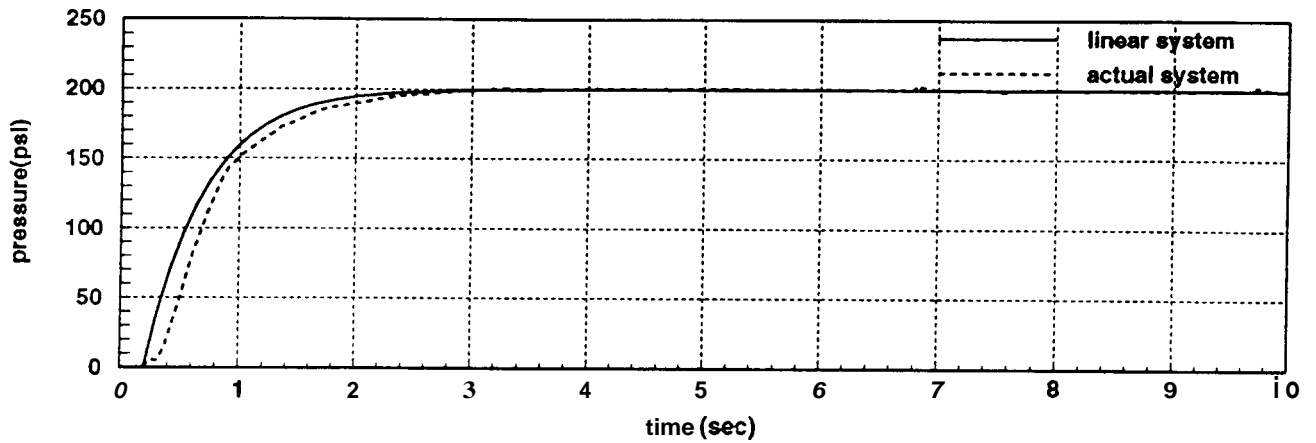
Figure 21: Comparison of the **feedback** linearized system response with the equivalent linear system response for two different inputs.

Failure Detection of a Computer Controlled Brake System

by

H. Raza, Z. Xu, P. Ioannou and B. Yang

Failure Detection of Computer Controlled Brake System*

H. Raza, Z. Xu and P. Ioannou

Dept. of Electrical Engineering-Systems

University of Southern California

Los Angeles, C A **90089-2563**

B. Yang

Dept. of Mechanical Engineering

University of Southern California

Los Angeles, C A **90089-1453**

Abstract. For the brake system under consideration, possible failure modes are identified using Fault Tree Analysis. For identification of these failure modes three different fault detection schemes are presented. These schemes fall under the category of residual error detection principle and differ on the basis of underlying assumptions and applicability. To counteract the effects of modeling inaccuracies and parameter drift the idea of closed loop detection is proposed. With successive modifications introduced in the detection algorithm a robust detection scheme with no false alarms is achieved.

1 Introduction

For vehicles operating on automated highways the reliability and safety of the overall system is a major design factor. As for any reliable/safe process design the procedure may be broadly categorized as:

1. Reliability/Safety Analysis

2. Detection/Diagnosis

The first part deals with the conceptual design process, whereas the second part is concerned with the implementation issues for reliability enhancement. In first part the system design can be checked against reliability and safety standards by using analysis techniques such as Failure Modes and Effect Analysis (FMEA) and Fault Tree Analysis (FTA). This analysis helps to identify the weak links in the system design. In addition this analysis identifies the potential failure modes associated with the system and a classification in terms of their occurrence probabilities and criticality. It helps to generate the failure modes data

base which is required for any knowledge based fault diagnosis scheme.

Second part of the reliable **process** design is the implementation of suitable detection and diagnosis schemes to identify the potential failure modes **of** the system. Like any other system operating in autonomous environment, the future vehicle must have the capability to effectively handle the potential failures without causing any life hazard to the passengers. In this way a robust detection/diagnosis scheme that can identify the root causes of failures in a system can increase the safety and reliability of the whole system.

In this paper we propose detection schemes that can be applied to the brake system in **AVCS** environment. This work augments the modeling and control part discussed in [1]. In section two, potential failure modes pertaining to the brake system under consideration are identified by using fault tree analysis. Three different schemes are discussed in section three, they all fall under the category of residual error detection theory. However, these schemes differ on the basis of underlying assumptions and hence the applicability and detection accuracy.

Scheme #1 assumes that the failures occur in such a way *so as* to affect the steady state value of the pressure only and hence relies on the steady state error measurements. Scheme #2 uses failure signature in terms of magnitude and direction associated with each fault. It follows the general theory of fault detection filters reviewed in [3]. For the brake system under consideration, a significant drift in the parameters was found to exist, hence the proposed model cannot accurately describe the system behavior. These modeling inaccuracies may result in high false alarm rate. **To** counteract these effects scheme #3 compares residual errors and states in closed loop configuration, in an effort to reduce the sensitivity of the detection algorithm to the system parameter variation.

In section four, simulation results are presented and discussed briefly and a comparison of these simulations with the results of implementation on the actual system is given. Major results are summarized again in conclusion section.

2   Fault Tree Analysis (FTA)

The Fault Tree diagrammatically shows euent combinations leading to a single top event which is generally an undesirable event for *the studied system.*

In this method deductive reasoning is applied to find basic events leading to some undesirable event in the system. The basic events are independent of one another and their occurrence probability is known. It should be noted that a fault tree is not a model of all the failures likely to occur in the system. In fact, it is a model of the interaction logic between events leading to the top event [5].

The advantages obtained from this analysis are:

1. It gives an easy-to-follow pictorial representation of cause and effects of undesirable events in the system.

2. It gives a complete hierarchal structure, which indicates the dependence of the major failure modes on the basic module level events, and is required for any knowledge based fault diagnosis scheme operating on line.

3. In addition to identifying the logical connection between failure events in relation to defined top events, **FTA** can be used to quantify the top event probabilities in terms of the predicted basic event probabilities using cut set and tie set methods [6].

For brake system the undesirable event is the complete or partial loss of braking capability. Fault trees for these two separate cases are shown in Figures **7-13.** The symbols used to identify the logical connection between the events are adopted from [6]. In the following we list some of the most common failures, derived from this analysis, which can cause a complete or partial loss of braking.

- *o* Cut in brake line, leading to complete loss of fluid and hence the braking power

- *o* Complete or partial loss of fluid in master cylinder

- *o* Mechanical damage of master cylinder, such as ring or seal wear

- *o* Mechanical failure in actuator valve

- *o* Electrica! failure in actuator valve, such as valve plunger operating circuitry failure which require high power and is susceptible to failure

- *o* Stuck mechanical linkage in actuator, such as brake pedal

- *o* Mechanical or power failure in hydraulic pump for actuator

- *o* Software failure due to wrong inputs leading to controller failure

- *o* Reduction in effective vacuum available at the brake power booster

Some of these faults would be used to check the accuracy of detection schemes to be developed in subsequent sections.

3 Detection/Diagnosis

As pointed out in the introduction, the second part of a reliable process design deals with the implementation of a suitable detection/diagnosis scheme to identify the failure modes of the system. However, in this paper we restrict our attention to the development of different fault detection schemes and comparison of their applicability and performance only. The development of a comprehensive fault diagnosis scheme which exploits the complete information provided by the fault tree analysis needs addition of more sensors to the existing system, which are not available to us at this moment, hence would be considered in the follow up studies.

In this paper, we **use** the model developed for the brake system under consideration and propose three different fault detection schemes. The basic events identified in fault tree analysis are used to simulate some of the failure modes which are required to test the accuracy of the detection schemes.

3.1 Detection Techniques

Before the discussion of detection schemes a brief introduction of the brake model developed in [1] is given in this section. The block diagram of the brake system under consideration is given in Figure 1. The form of the brake system model motivated by the experimental

* Brake pedal along with an actuator acts as a mechanical switch indicated in the block
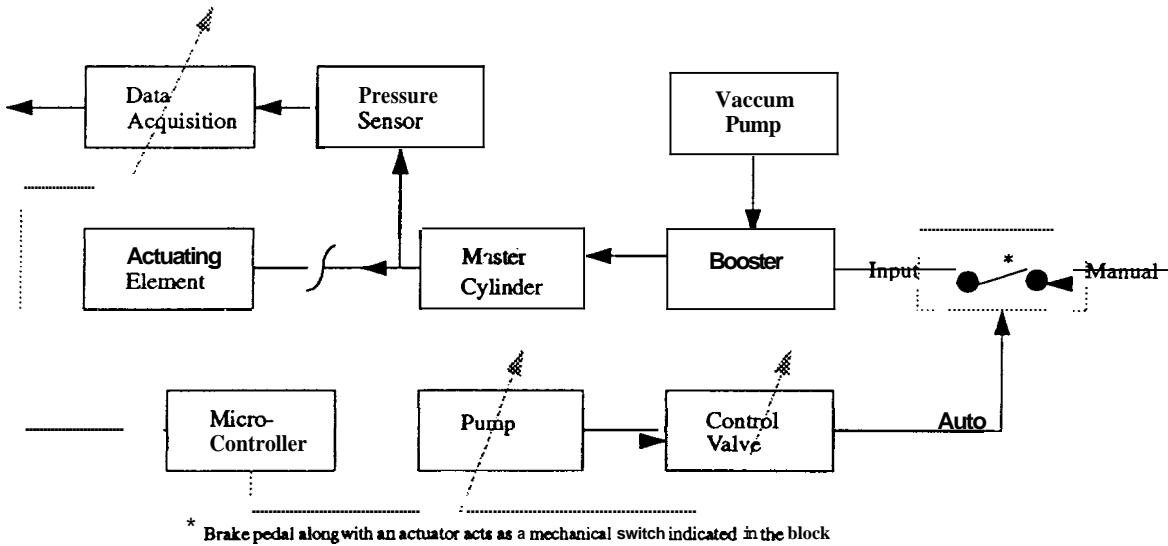
Figure 1: Block diagram of the brake system.

results is given as:

$$x(k+1) = f(x(k), u(k), u(k-1)) \qquad (1)$$

where,

4

x : system state (brake line pressure)

u : system input (duty cycle of the pwm signal)

f : unknown function to be identified

The brake system response for each fixed input is approximated by that of a first order system given **as:**

$$x(k+1) = x(k) + Tb(a - x(k)) \qquad (2)$$

where a, b E $\mathcal{R}^+$. Parameters a and b in (2) characterize the pseudo steady state value and the speed of transient response respectively. These parameters have similar meaning in linear systems, but have nonlinear relationship with respect to input u and state x of the system in this case. Analysis of experimental data is used to derive a functional form for the parameters a and b, a summary of the results presented in [1] is given below.

$$x(k+1) = x(k) + Tb(k)(a - x(k)) \qquad (3)$$

$$a = \begin{cases} g(u(k)) & \text{if } x(k) < g(u(k)) \\ min(x(k), g^*(u(k))) & \text{if } x(k) \geq g(u(k)) \end{cases} \qquad (4)$$

$$b(k+1) = \begin{cases} b(k) & \text{if } \Delta u = 0 \\ p_b b(k) + z_b \xi(k) & \text{else} \end{cases} \qquad (5)$$

$$\xi(k) = \begin{cases} h(u(k)) & \text{if } x(k) < \frac{g(u(k-1))}{2} \\ h(u(k)) \left(\frac{5}{4} - \frac{x(k)}{2g(u(k-1))} \right) & \text{if } x(k) \geq \frac{g(u(k-1))}{2} \\ h^*(u(k), x(k)) & \text{if } x(k) \geq g(u(k)) \end{cases} \qquad (6)$$

Where, p_b and z_b are design constants and are used to filter out the effects of switching while calculating the value of b using (5) and (6). It should be noted that the model given
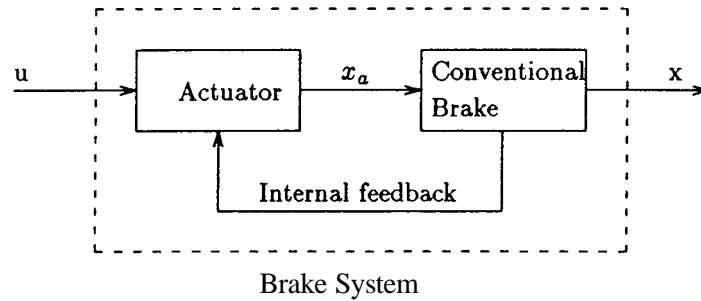
Brake System

Figure 2: Brake system viewed **as** interconnection of actuator with conventional brake system through internal feedback.

by (3)-(6) identifies the mapping from input u to the brake line pressure x. However, in a

separate study [2], the mapping from input u to the actuator output x_a is identified. Due to presence of internal feedback from brake system to the actuator, it is hard to represent the system as cascaded blocks without precise knowledge of the feedback. The feedback is predominantly in the form of reaction from the booster and induction of extra tluid in actuator cylinder due to brake pedal movement and is hard to model with the measurements available on the test bench.
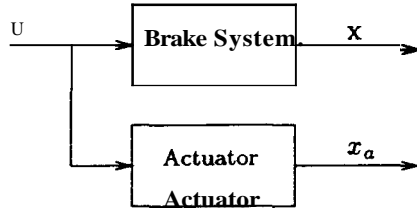

Figure **3:** An alternative representation of brake system in Figure **2.**

The system, however, can be viewed as shown in Figure **3,** where the additional measurement x_a can be used to increase the accuracy of detection and in some cases can even help to isolate the faults associated with actuator only. Since the dynamics associated with the actuator are much faster than the overall system [2], these faults can be identified using the measurement of x_a without excessive delay.

In the following three different fault detection schemes for the brake system are discussed. In all of these schemes, we use the validated brake model given in **(3)-(6)** and some additional measurements. In order to avoid repetition, we use the followin sign convention:
- a subscript p with a variable indicates brake system (plant)
- a subscript m with a variable indicates brake model

3.1.1   Scheme #1 : Constant Input

This scheme makes use of residual **error** to detect the presence of any fault. The residual error is generated by comparing the brake system output (line pressure) with that of the validated model **(3)-(6)** in parallel configuration, shown in Figure **4.** In this scheme no additional measurement is used, we begin with the following assumptions:

Assumptions:

A–I Only one sensor is available, which measures the brake line pressure y_p.

A–II The sensor noise $n(k)$ is wide sense stationary, zero mean with known finite variance, i.e., $m_n = 0$, $\sigma_n = K < \infty$.

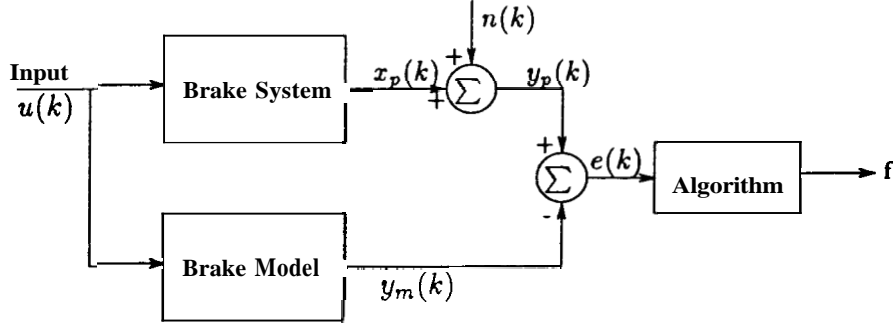A–I1 After fault occurance, input $u(k)$ to the system is constant.

6

Figure **4:** Block diagram of the fault detection scheme.

The assumption A-III may appear to be restrictive, but it is justifiable when the failure magnitude is large enough to cause saturation of the control input.

Proposition 1 *With the assumptions A-I - A-III, fault can be detected by steady state tmcking error measurement. Furthermore, the threshold for detection d_o is bounded only by the noise variance $\sigma_n = K$.*

Proof: From the model given in (3)-(6), plant output $y_p(k)$ can be written **as:**

$$x_p(k+1) = x_p(k) + Tb_p(a_p - x_p(k)) \tag{7}$$
$$y_p(k) = x_p(k) + n(k) \qquad \forall k > k_1$$

where k_1 is the instant fault occurs or input becomes constant, $b_p = b_p(k_1)$ is the value of parameter $b(k)$ in *(5)* at instant k_1, a_p is given in **(4)** with $x(k)$ replaced by $x_p(k)$, noise $n(k)$ follows assumption A-II. Similarly model output $y_m(k)$ can be written **as:**

$$x_m(k+1) = x_m(k) + Tb_m(a_m - x_m(k)) \tag{8}$$
$$y_m(k) = x_m(k) \qquad \forall k > k_1$$

where a, is as given in **(4)** with $x(k)$ replaced by $x_m(k)$, $b_m = b(k_1)$, since same input is applied to plant and model and before occurance of fault $x_p = x_m$, hence from *(5)-(6)* we have $b_p = b$, $= b$.

By defining the output tracking error *e* **as:**

$$e \stackrel{\triangle}{=} y_p - y_m \tag{9}$$

we obtain the following error model

$$e(k+1) = (1 - Tb)e(k) + Tb(a_p - a_m) + n(k+1) \tag{10}$$

7

If mean of the tracking error is denoted by m_e, then m_e is obtained by solving the following difference equation.

$$m_e(k+1) = (1 - Tb)m_e(k) + Tb(a_p - a,)$$ (11)

In (11), we have used the fact that $m, = 0$. Hence the pseudo steady state value of m_e can be calculated as:

$$\lim_{k \to \infty} m_e(k) = \lim_{z \to 1}(z-1)m_e(z)$$
$$= a_p - a,,,$$ (12)

Denoting $\lim_{k \to \infty} m_e(k)$ as $\bar{m}_e$, we get:

$$\bar{m}_e = a_p - a_m$$ (13)

The threshold for detection is calculated by finding the variance of tracking error e as follows.

$$\sigma_e(k+1) = (1 - Tb)^2\sigma_e(k) + \sigma_n(k+1)$$
$$\lim_{k \to \infty} \sigma_e(k) = K$$ (14)

where, in (14) we have used the fact that $\sigma_n(k) = K$ *Vk*. Hence, threshold for failure detection is bounded only by the noise variance $\sigma_n = K$. □

Practical Considerations:

1. Effect of averaging over finite samples:

The assumption of the zero mean noise require that to cancel the effect of noise in the detection model (10), an average over a reasonably large number of samples is required. However, this introduces intolerable amount of delay in fault detection. Hence, a trade off exists in terms of detection time and false alarm rate. The detection algorithm becomes:

$$\bar{m}_e > d_o \Rightarrow fault$$
$$d_o = K + Am$$ (15)

Hence, the effect of non-zero mean can be counteracted by raising the threshold given in (14) to that given in (15), where **Am** given in (15) represents the offset introduced by noise.

2. Effect of modeling uncertainty:

In the development of the detection scheme above a perfect knowledge of the system parameters is assumed, i.e.

$$\text{no fault} \Rightarrow a_m = a_p$$
$$\Rightarrow e = y_p - y_m = 0$$

However, in actual practice a perfect knowledge of the system parameters is not possible even if the system is precisely modeled, because parameters show drift with aging and changes in operating conditions. Hence some compensation for incorrect modeling should be introduced in the threshold d_o given in (15). With a known bound on system parameter variation the threshold can be written as:

$$d_1 = d_o + AT \tag{16}$$
$$AT = \sup_w |a_p - a_{po}|$$

where a_{po} is the nominal value of the parameter a_p.

Limitations:

1. Applicable only when a saturation in control input occurs due to large magnitude of fault.

2. Almost linear dependence of threshold d_1 on system parameter variation. This defect is removed in scheme #3, which exploits the robustness against parameter variation introduced by feedback present in the closed loop system.

3. From the brake model given in (3), we *see* that if the input $u(k)$ is constant then the nonlinear parameter $b(k)$ becomes a constant value. Hence with the given assumption we cover the cases in which the failure occurs in such a way that the effect on transient response, characterized by b_p and b_m in (7) and (8) respectively, is negligible, i.e., $b_p = b, = b$. The steady state value of pressure is, however, modified from $a,$ (desired value) to a_p (observed value).

4. A trade off is involved in selecting the value of the threshold, d_o or d_1, as a lower value would increase the speed of detection at the cost of increased false alarms.

It should be noted that the assumption A-III is necessary to build a linear detection model even though the actual system is nonlinear. It can be shown that the nonlinear relationship of error on the two unknown modified parameters b_p and a_p can be estimated by applying a correction factor obtained by adaptive estimation of b_p. The simulation results are shown in Figure **14.** For this simulation the value of threshold is chosen to be ± 10 psi, which gives a detection time of 0.15 seconds with no false alarms.

3.1.2 Scheme #2

In this scheme we make use of the brake line pressure as well as actuator pressure measurement, as shown in Figure **3,** to improve the accuracy and range of detection. Furthermore, the detection scheme discussed below **is** a generalization of scheme #1 as it do not require any assumption on the input. Since the input is not assumed to be constant, hence the scheme compares the instantaneous residual error against some threshold.

*Case 1: **No** sensor faults (only component and actuator faults):*

We start with the brake system equation, where a particular fault indicated by f_i is assumed to be present. In this case we only need the direction associated with each fault, hence time history of the fault is not important.

$$x_p(k+1) = x_p(k) + T\hat{b}(k)(\hat{a} - x_p(k)) + f_i\phi(k) + d_u \qquad (17)$$
$$y_p(k) = x_p(k)$$

By comparing the faulty system output (17) with that of the nominal system model (19), we can generate tracking error for detection and isolation of a particular fault.

$$x_m(k+1) = x_m(k) + T\hat{b}(k)(\hat{a} - x_m(k)) \qquad (18)$$
$$y_m(k) = x_m(k)$$

Here, $x_p = [x_p^b, x_p^a]^\top$, $x_m = [x_m^b, x_m^a]^\top$, $\hat{a} = [a, a_1]^\top$, $\hat{b} = [b, b_1]^\top$,

x_p^b, x_m^b : line pressure (system, model respectively)

x_p^a, x_m^a : actuator pressure (system, model respectively)

a : system parameter for steady state value

a_1 : actuator model parameter for steady state value [2]

b : system parameter for transient response

b_1 : actuator model parameter for transient response **[2]**

f_i : fault signature for *ith* fault, indicating direction of a particular fault

ϕ : an arbitrary bounded function of time

$d,$: unknown disturbance due to noise and modeling errors

It should be noted from the form of equations (17) and (19) that presence of fault is indicated in terms of extraneous signal $f_i \phi(k)$, which is sufficient to charectarize the offset created by each fault. Hence a change in plant parameters a and $b(k)$, as in scheme #1, is not necessary.

Defining the output tracking error to be:

$$e_1 = y_p - y_m \qquad (19)$$

we can write the detection model as follows:

$$e_1(k+1) = (1 - T\hat{b}(k))e_1(k) + f_i \phi(k) + d_u \qquad (20)$$

From the detection model given in (20) we can write the magnitude of instantaneous tracking error as:

$$\|e_1\|_1 \leq c\hat{b}^{-1}(\|f_i\|_1 \|\phi\|_\infty + d_2) \qquad (21)$$

where $d_2 = \|d_u\|_\infty$, and $c = \frac{1}{T}$ is a finite constant. In (21) we have assumed that $e_1(0) = 0$. If we denote $d_3 = c\hat{b}^{-1}d_2$, then d_3 is the threshold for assertion of any fault. This threshold can be selected based on the noise present in the system as well as model uncertainties, as given in scheme #1. Hence the detection algorithm can be written as:

$$
\begin{aligned}
&fault && if \ \|e_1\|_1 \geq d_3 \\
&ith \ fault && \text{given by direction of tracking error in (20)}
\end{aligned}
$$

Case 2: Sensor faults only:

In a similar way we can write system equation with the assumption that a particular sensor failure has occured and represent the direction associated with jth fault by k_j.

$$x_p(k+1) = x_p(k) + T\hat{b}(k)(\hat{a} - x_p(k)) + d_u \qquad (22)$$
$$y_p(k) = x_p(k) + k_j \psi(k)$$

The nominal model of system is same as described in (19). Some of the additional terms defined in (22) are:

k_j: jth sensor fault signature

ψ: an arbitrary bounded function of time

Defining the state and output tracking errors to be:

$$e_o = y_p - y_m; \qquad \xi = x_p - x_m \tag{23}$$

we get the following detection model:

$$\begin{aligned} \xi(k+1) &= (1 - T\hat{b}(k))\xi(k) + d_u \\ e_o(k) &= \xi(k) + k_j\psi(k) \end{aligned} \tag{24}$$

The magnitude of instantaneous output tracking error can be written as:

$$\|e_o\|_1 \le c\hat{b}^{-1}\|d\|_\infty + \|k_j\|_1 \|\psi\|_\infty \tag{25}$$

From (25) the detection algorithm can be written as:

$$\begin{aligned} fault & \qquad if \; \|e_o\|_1 \ge d_3 \\ jth\,fault & \qquad \text{given by direction of tracking error in (24)} \end{aligned}$$

From (20) and (24) it is obvious that the component and actuator faults as well as sensor faults can be detected by comparing the output tracking error against some threshold. However, the isolation of a particular fault require the knowledge of fault signatures f_i and k_j, which are developed by understanding system behavior at the occurrence of each particular fault and require further study. The value of threshold d_3 is a design factor and is carefully selected to give reasonably fast detection with no false alarms.

3.1.3   scheme # 3

Both of the schemes discussed above compare output of the model with that of the actual system. Since the comparison is done in an open loop configuration, hence is greatly affected by modeling errors and parameter drift. These modeling errors and parameter variations can be handled by increasing the threshold in (15) and (21). This, however, reduces the resolution and speed of detection, rendering the schemes useless in extreme situations.

These defects are removed in the scheme presented below, where the accuracy of detection is improved at the cost of decreased sensitivity. The block diagram for this detection scheme is shown in Figure 5. The scheme consists of actual brake system and model connected in closed **loop** configuration. The motivation behind this scheme is that the actual system is used in closed loop, and addition of controller provides extra variables for comparison.
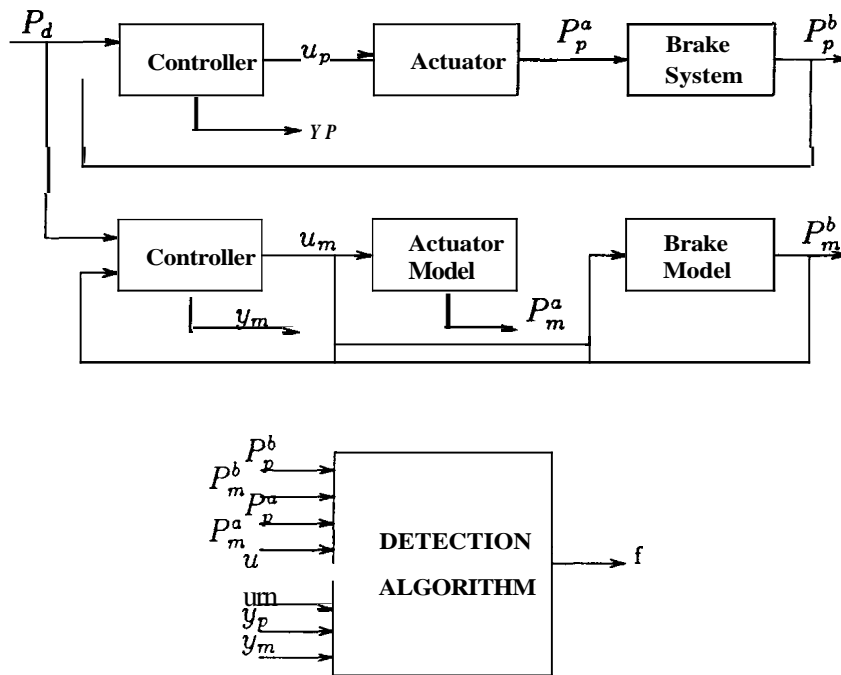

Figure 5: **Block** diagram of the fault detection scheme.

The advantages associated with closed **loop** configuration are:

1) The closed loop feedback systems are less sensitive to plant parameter variations, hence provide more robust detection of faults.

2) The modeling errors cause difference between actual and model closed loop. This difference is used **as** a threshold for detection schemes and due to reduced sensitivity these thresholds are much smaller than the open loop configurations and hence reduce the detection time.

The variables used in the detection scheme are:

1) Brake line pressures, P_p^b, P_m^b
2) Actuator pressures P_p^a, P_m^a
3) Controller outputs u_p, u_m
4) Integrator state of controllers y_p, y_m.

Detection Algorithm

The algorithm is based on the residual error comparison and is shown in Figure 6.
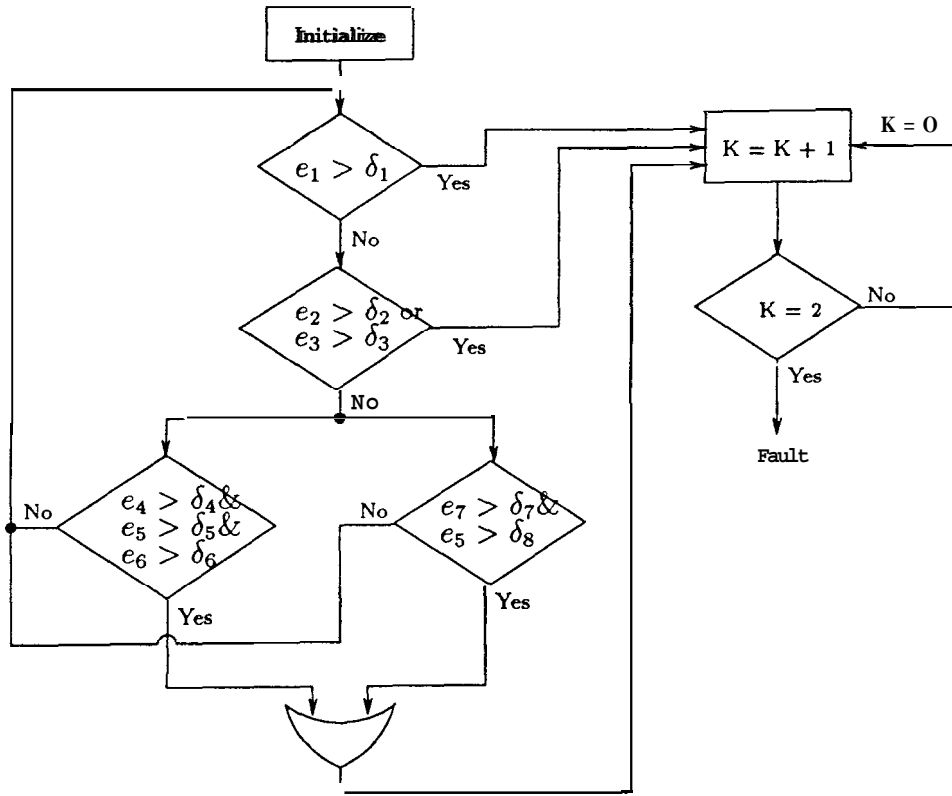
Figure 6: Detection algorithm **for** scheme **#3.**

Where $e_1 = |P_p^b - P_m^b|$, $e_2 = |\Delta P_p^b - \Delta P_m^b|$, $e_3 = |P_p^a - P_m^a|$, $e_4 = |p_t^b - p_m^b|$, e5 $= |u_p - u_m|$, $e_6 = |y_p - y_m|$ and $e_7 = |p_b^\beta - p_m^a|$. Here δ_i, $i = 1,\ldots,8$ are design constants and are selected as a compromise between speed of detection and false alarm rate. In the Figure 6, P_p^b and P_p^a denote sensor readings, whereas p_p^b and p_p^a are corresponding filtered values. Similarly $\Delta P_p^b = P_p^b(k) - P_p^b(k-1)$, $\Delta P_m^b = P_m^b(k) - P_m^b(k-1)$ denotes rate of change of line pressure for brake system and model respectively.

A separate check for unfiltered sensor readings and rate of change of pressure is included in the algorithm to detect the drastic failures without significant delay caused by the filtering action. Whereas a comparison of filtered values give more accurate detection for slow moving **or** partial failures. Hence the threshold used for un-filtered values, $\delta_1, \delta_2, \delta_3$, are much larger than that for the filtered ones. To counteract the effect of occasional noise glitch in the sensor readings a persistency check is also included, this helps to reduce the false alarm rate without significant change in the detection time.

4 Simulation and Implementation Results

The simulation of schemes #1 and #2 using faulty and nominal model of the system show accurate detection for different situations, with reasonably small detection time. However, as discussed before these schemes severely suffer from modeling errors and parameter variations. Small threshold values for residual errors increase false alarm rate, on the other hand large values increase the detection time considerably and reduce the resolution of fault detection.

Scheme #3 implemented on the actual brake test bench give satisfactory results as shown in Figures 15-20. From the fault tree diagrams in Figures 7-13, it is obvious that a complete or partial loss of braking capability can be caused by a variety of causes. Some of these failures were induced on the test bench to check the accuracy of the detection algorithm in real time. Due to their ease of implementation on the test bench, the failure modes selected for the simulation are:
1) Vacuum pump failure'
a) complete loss of vacuum b) partial loss
2) Auxiliary hydraulic module failure
3) Stuck brake pedal[†]
a) completely stuck b) partially stuck
4) Brake fluid leakage
a) in master cylinder b) in brake lines

The design constants selected for this test are:
$\delta_1 = 40psi$, $\delta_2 = 10psi$, $\delta_3 = 20psi$, $\delta_4 = 10psi$, $\delta_5 = 4\%$, $\delta_6 = 6$, $\delta_7 = 10psi$, $\delta_8 = 4\%$. The simulation results given in Figures 15-20, show that the faults were detected without any false alarms. Detection time ranges between 0.1-0.25 sec, which is comparable to the system time constant. The resolution of detection is about ten percent of the full scale pressure value, mainly due to the values of threshold used for

---

'In actual vehicle this corresponds to absence of engine manifold vacuum due to various reasons.
'In this configuration the actuator pressure is applied to brake pedal, hence this corresponds to absence of input force at the push rod.

simulation.

It should be noted that the actuator dynamics are much faster than the whole system dynamics [2], hence inclusion of the actuator model in the detection algorithm helps to identify the failures associated with Auxilliay Hydraulic Module [1] without excessive time delay caused by the slower overall system dynamics.

Scheme #3 which operates in closed loop, is relatively insensitive to small errors due to the robustness of the designed controller, which tries to track the desired pressure even under moderate parameter shift caused by a failure. Hence it identifies failures that cause parameter variations beyond the tracking range of controller. If desirable a separate comparison of control effort for the system and model can identify the failures within robustness range of controller.

5   Conclusion

Potential failure modes associated with the complete or partial loss of braking capability of a computer controlled brake system were identified using fault tree analysis. Three different fault detection schemes based on the residual error detection theory were proposed. Idea of closed loop system detection was introduced to increase the robustness of detection against parameter shifts and modeling inaccuracies. Finally, implementation of the detection algorithm on the brake system test bench proves the effectiveness of the proposed scheme.

References

[1] Raza, H., Xu, Z., Yang, B., Ioannou, P., "Modeling and Control design for Brake System", USC-CATT Report # .

[2] Du, L., Xu, Z., Yang, B., "Experimental Model of Control Valve Unit in the Auxiliary Hydraulic Circuit of a Vehicle Brake System", USC-CATT Report # .

[3] Frank, P. M., "Fault Diagnosis in Dynamic Systems Using Analytic and Knowledge-based Redundancy- A Survey and Some New Results", Automatica, Vol. 26, No. 3, pp. 459-474, 1990.

[4] Iserman, R., "Fault Diagnosis of Machines via Parameter Estimation and Knowledge Processing- Tutorial Paper", Automatica, Vol. 29, No. 4, pp. 815-835, 1993.

[5] Villemeur, A, "Reliability, Availability, Maintainability and Safety Assessment", Vol. 1, John Wiley and Sons Ltd., West Sussex PO19 1UD, England, pp. 149-195, 1992.

[6] O'Connor, P., "Practical Reliability Engineering", 3rd Edition, John Wiley and Sons Ltd., West Sussex PO19 IUD, England, **pp.** 152-156, 1991.
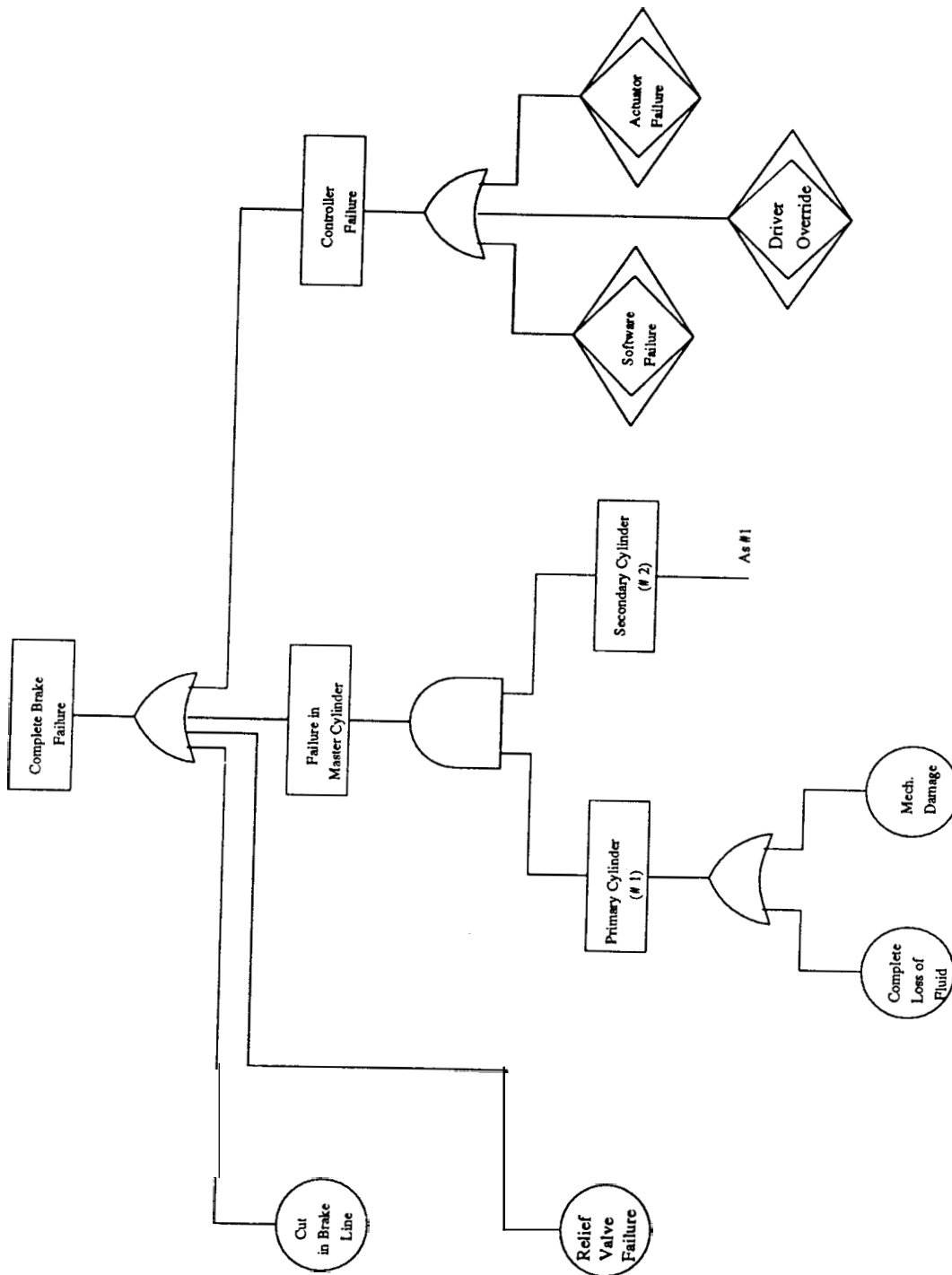
Figure 7: Fault Tree Analysis for the case of complete loss of braking power (main tree). Subtrees for controller and actuator failure, in general, depend on the equipment structure used in a particular implementation scheme. "Driver Override" represents the switching from automatic to the manual mode, initiated by the driver in case of emergency.
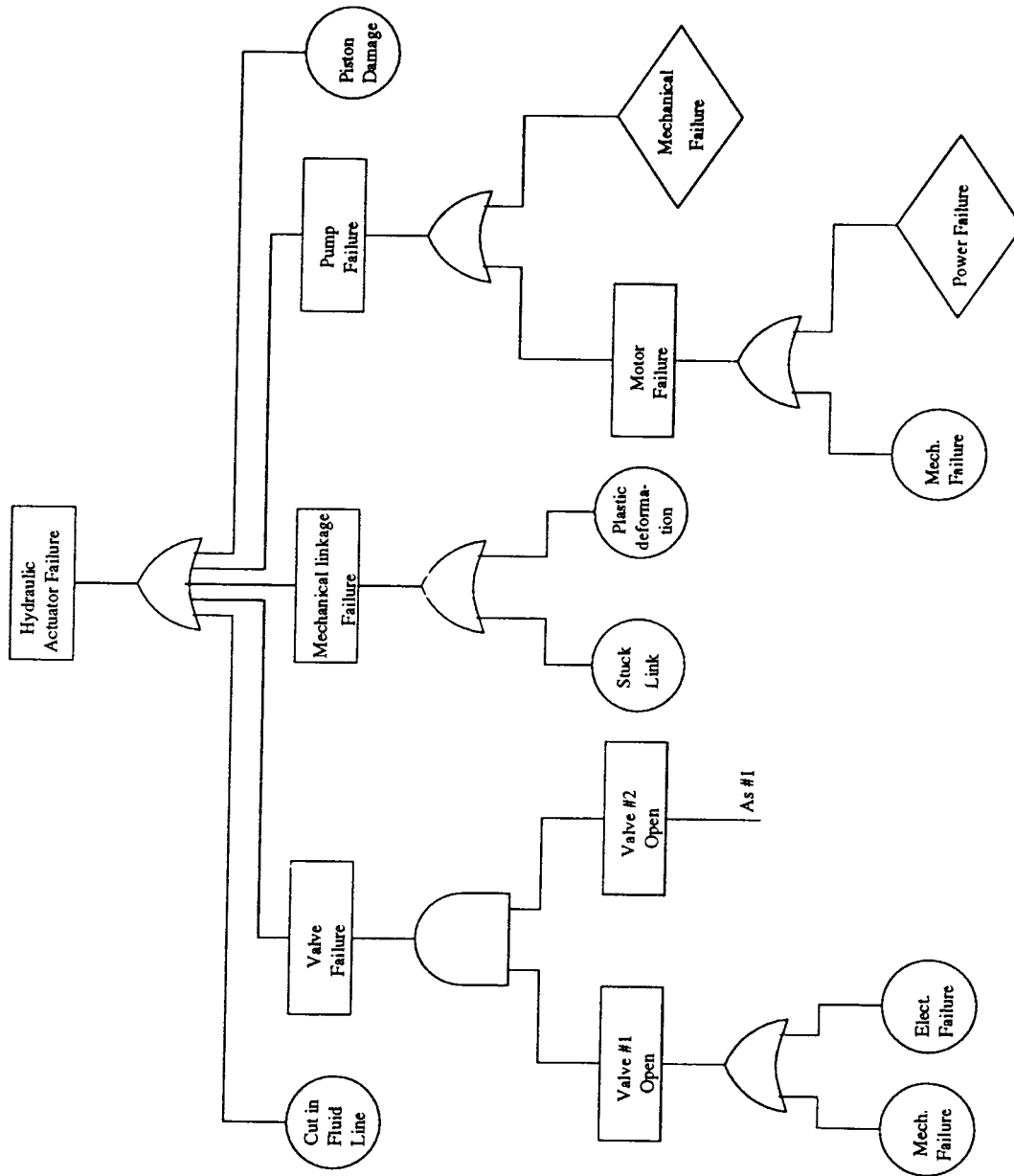
18

Figure 8: Fault Tree Analysis for the case of complete loss of braking power (actuator failure subtree).

19
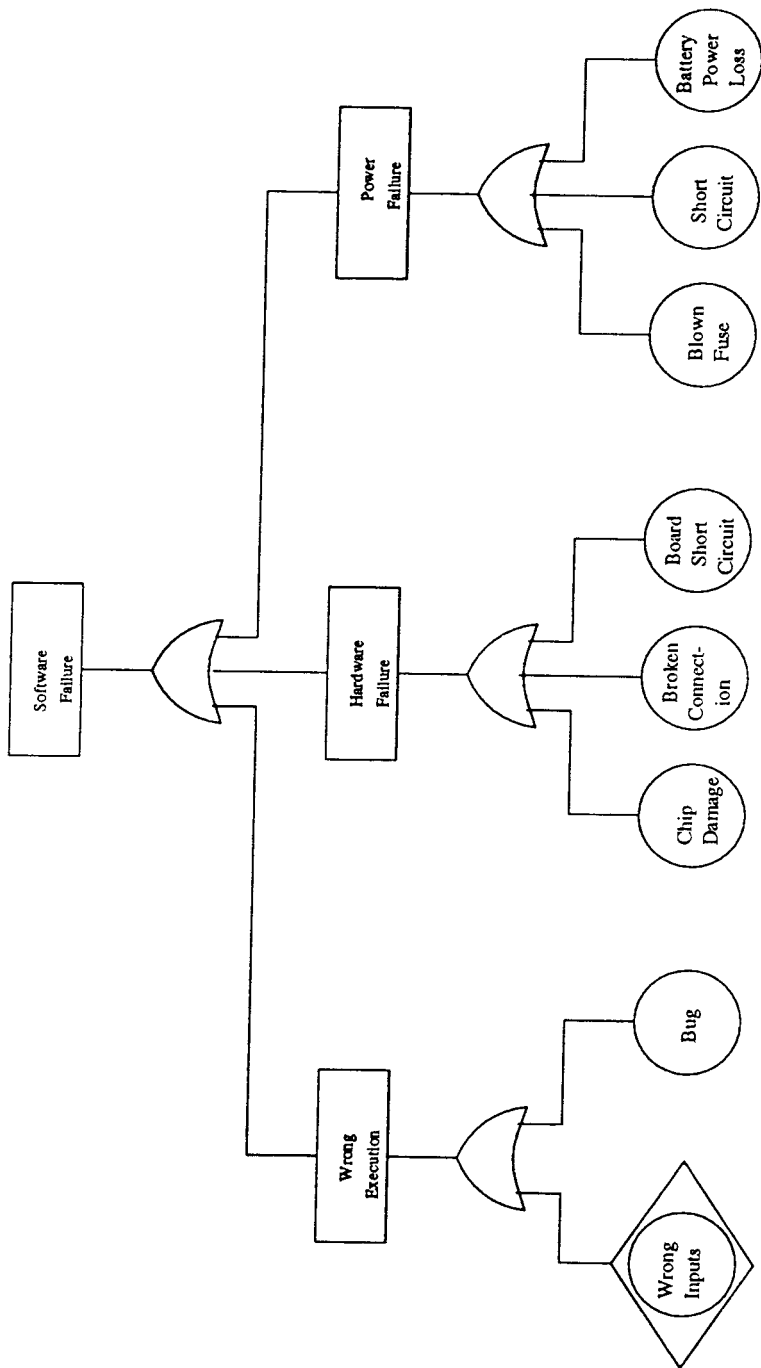
Figure 9: Fault Tree Analysis for the case of complete loss of braking power (software failure subtree).
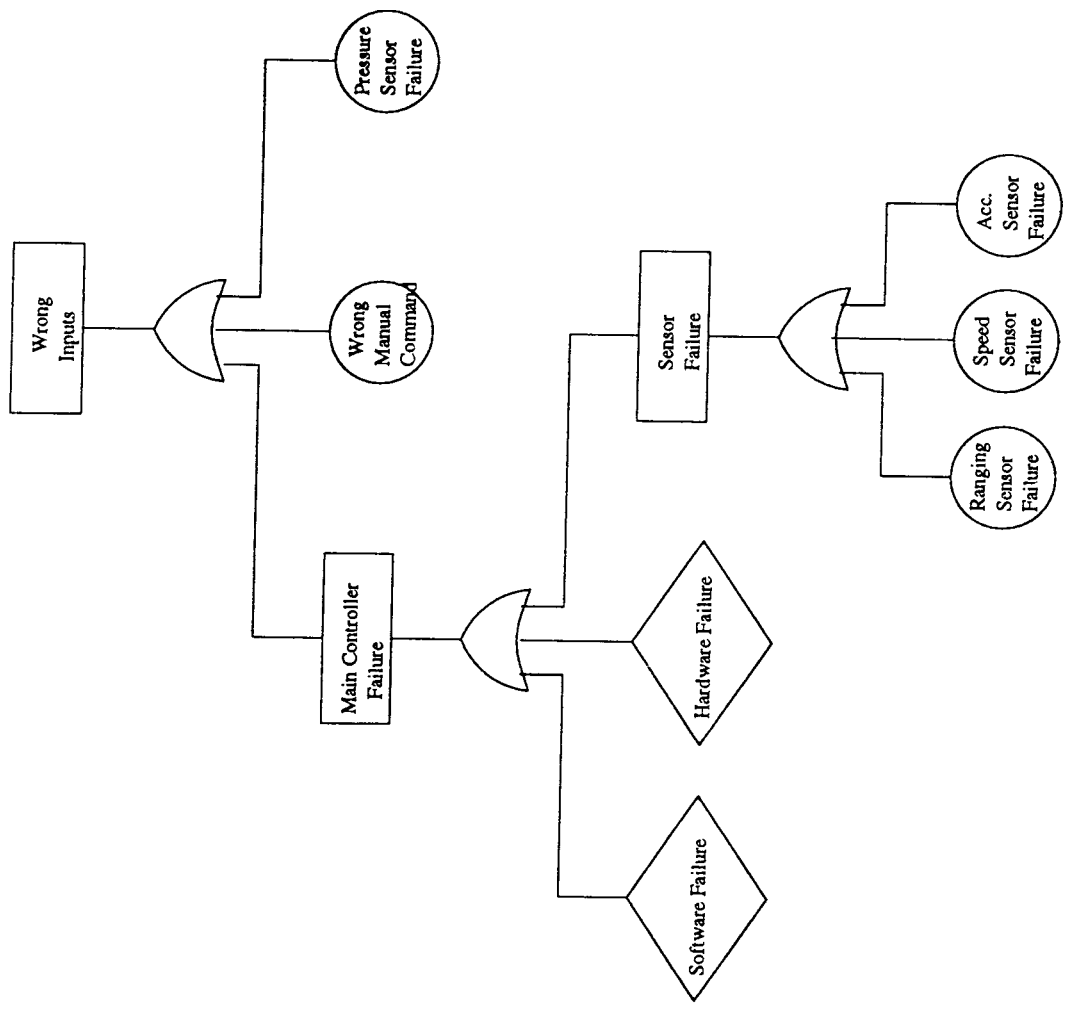
Figure 10: Fault Tree Analysis for the case of complete loss of braking power (wrong input subtree).
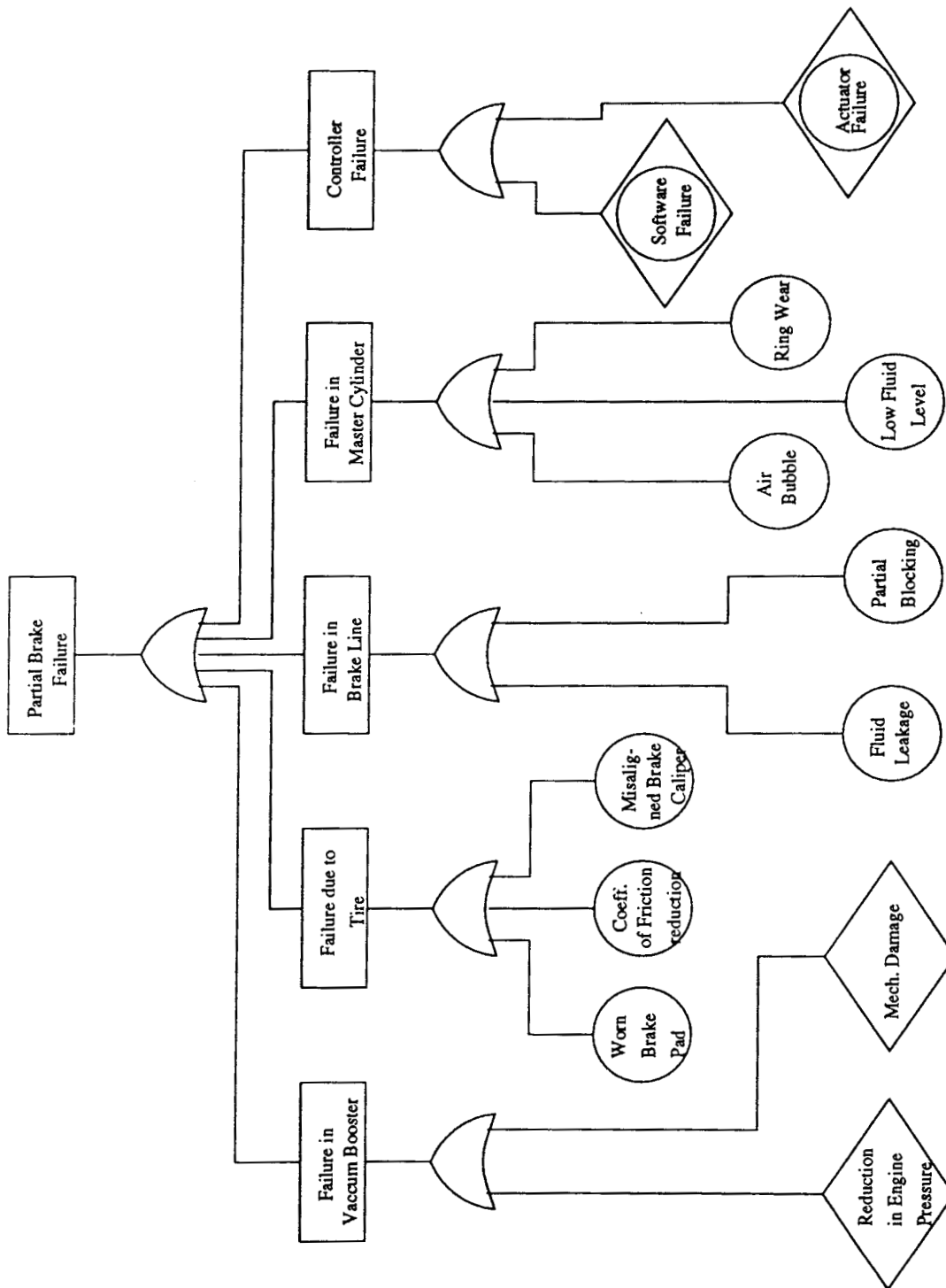
Figure 11: Fault Tree Analysis for the **case** of partial loss of braking power (maintree).
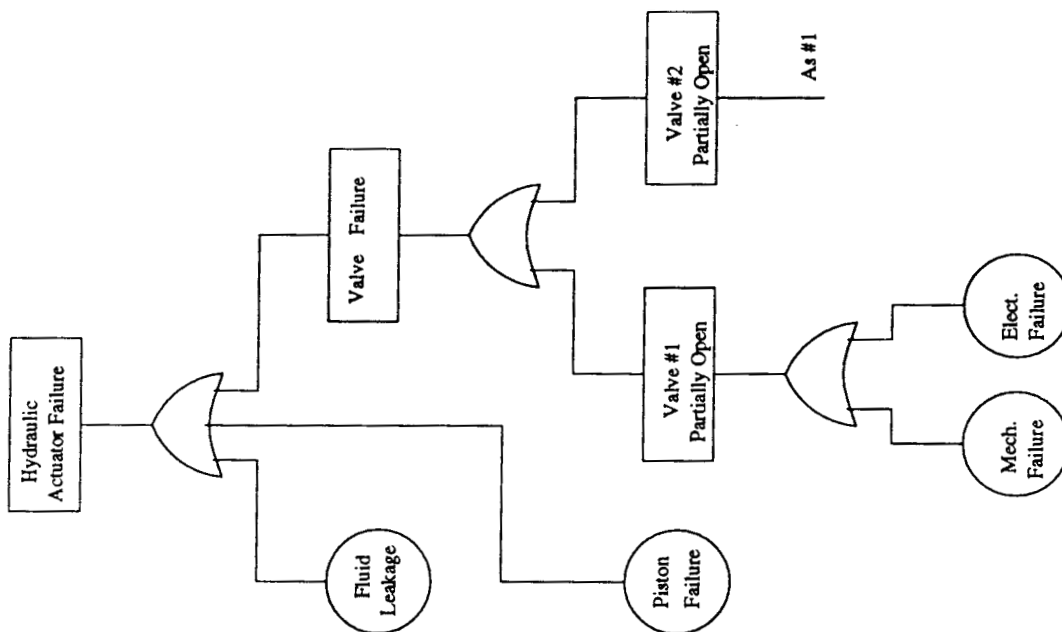
Figure 12: Fault Tree Analysis for the case of partial loss of braking power (actuator failure subtree).
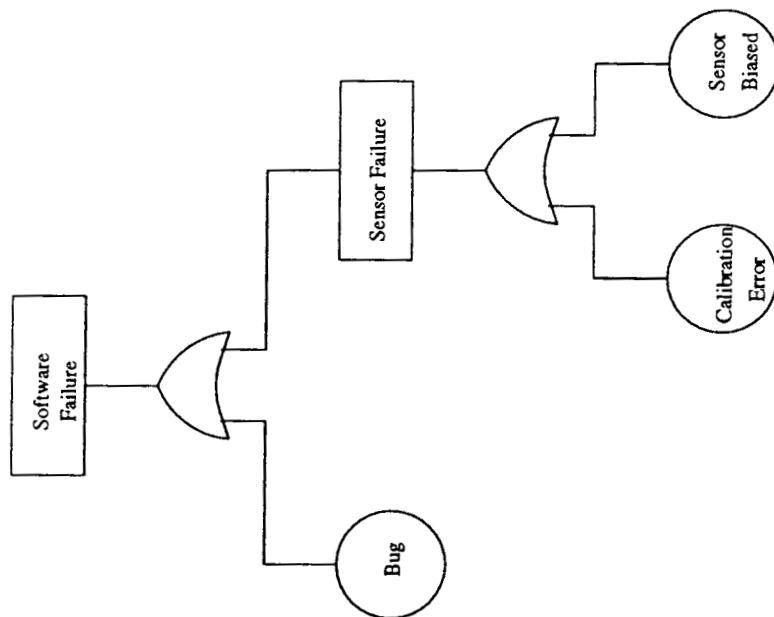
Figure 13: Fault Tree Analysis for the case of partial loss of braking power (software failure subtree).
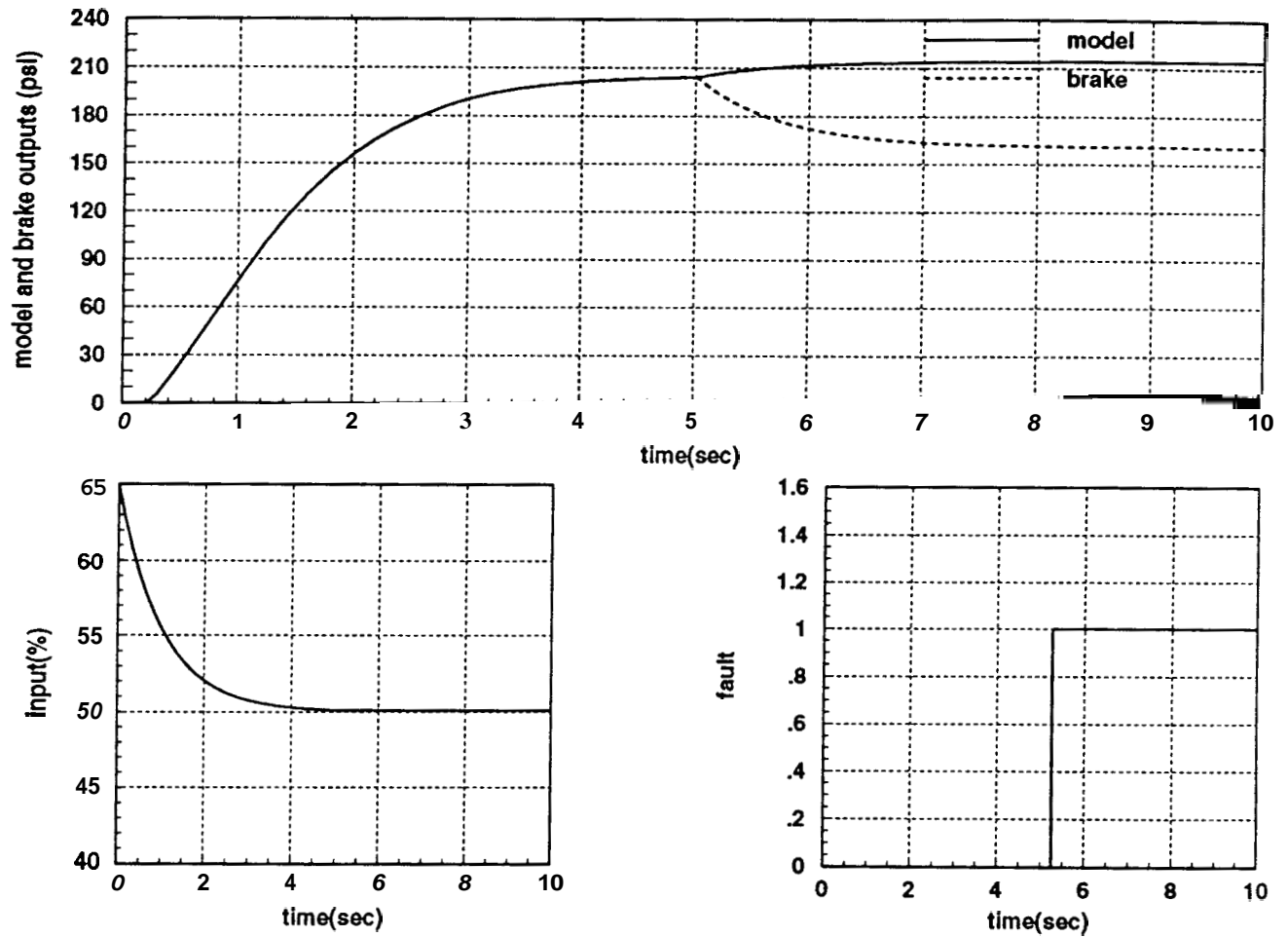
Figure **14:** Simulation result for scheme **# 1. A** fault **occurs** at t $= 5\ sec$, detection time is $\approx 0.15sec$.
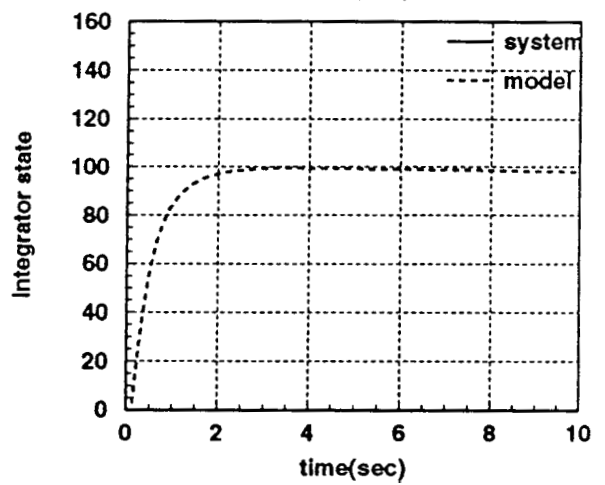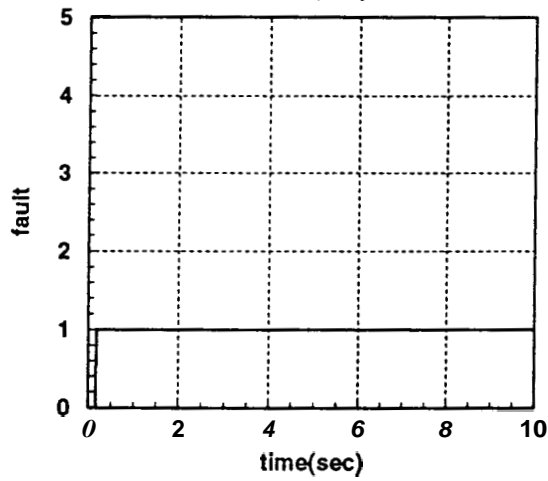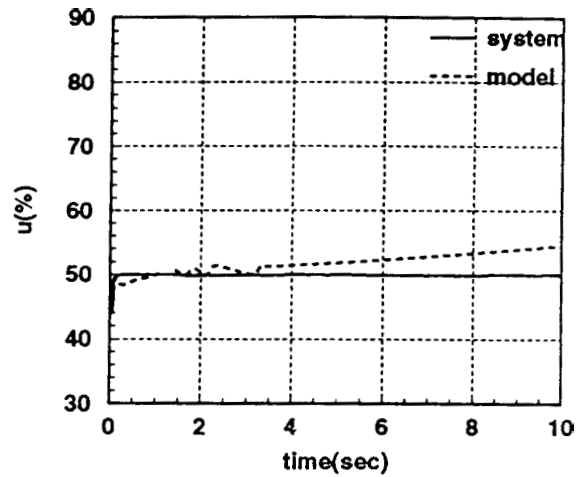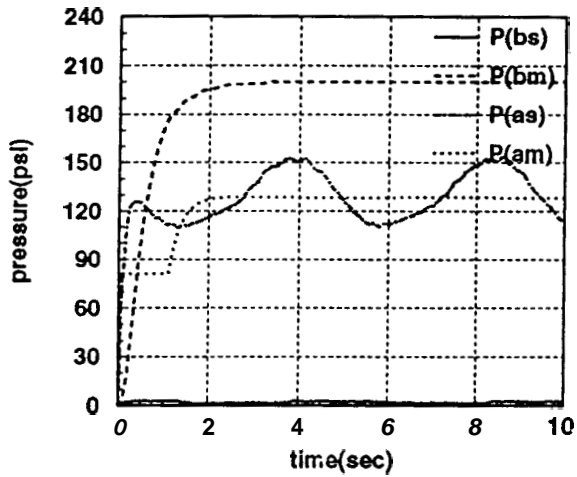
Figure 15: Simulation result for the case of complete loss of vacuum pressure.
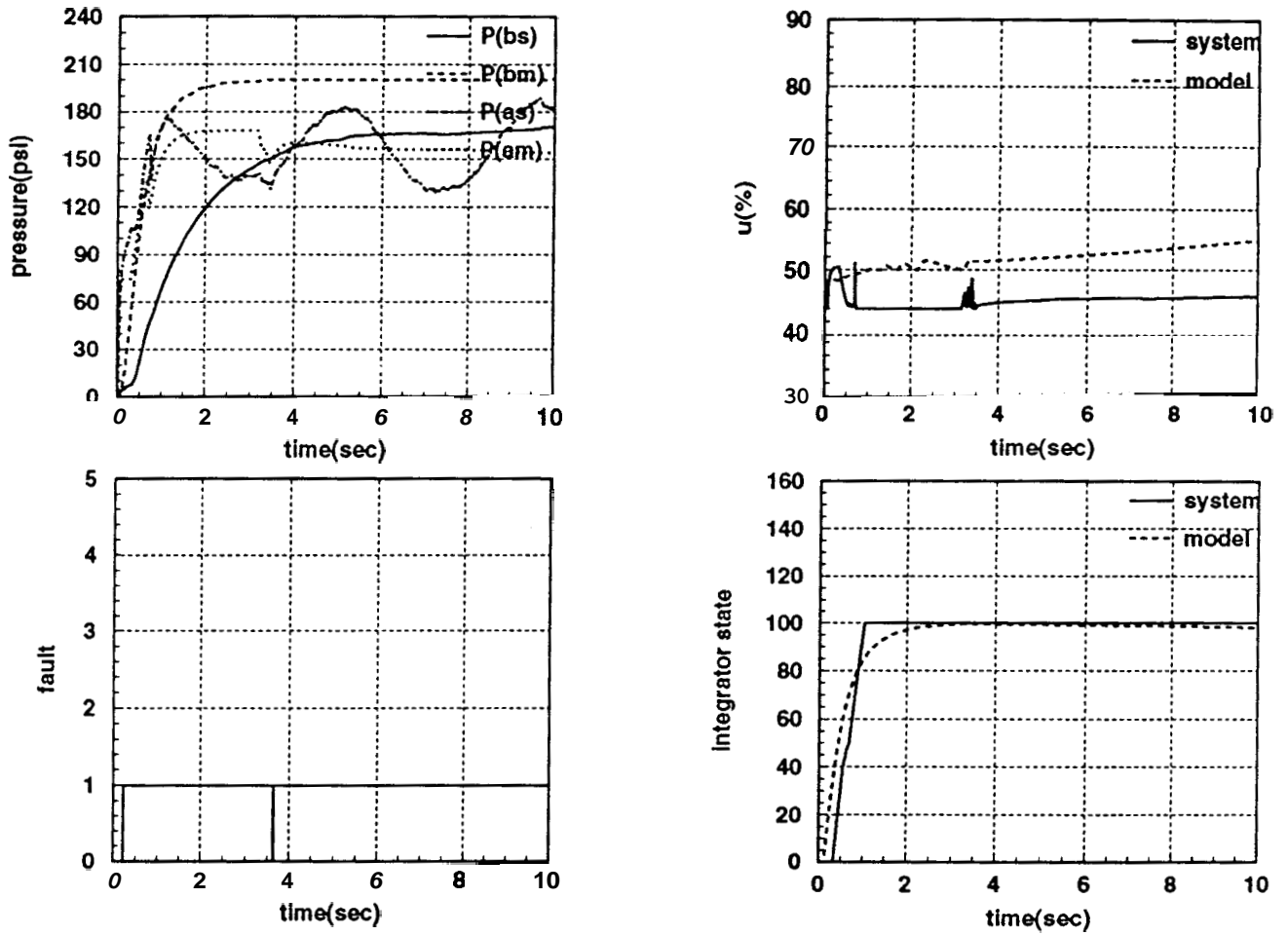
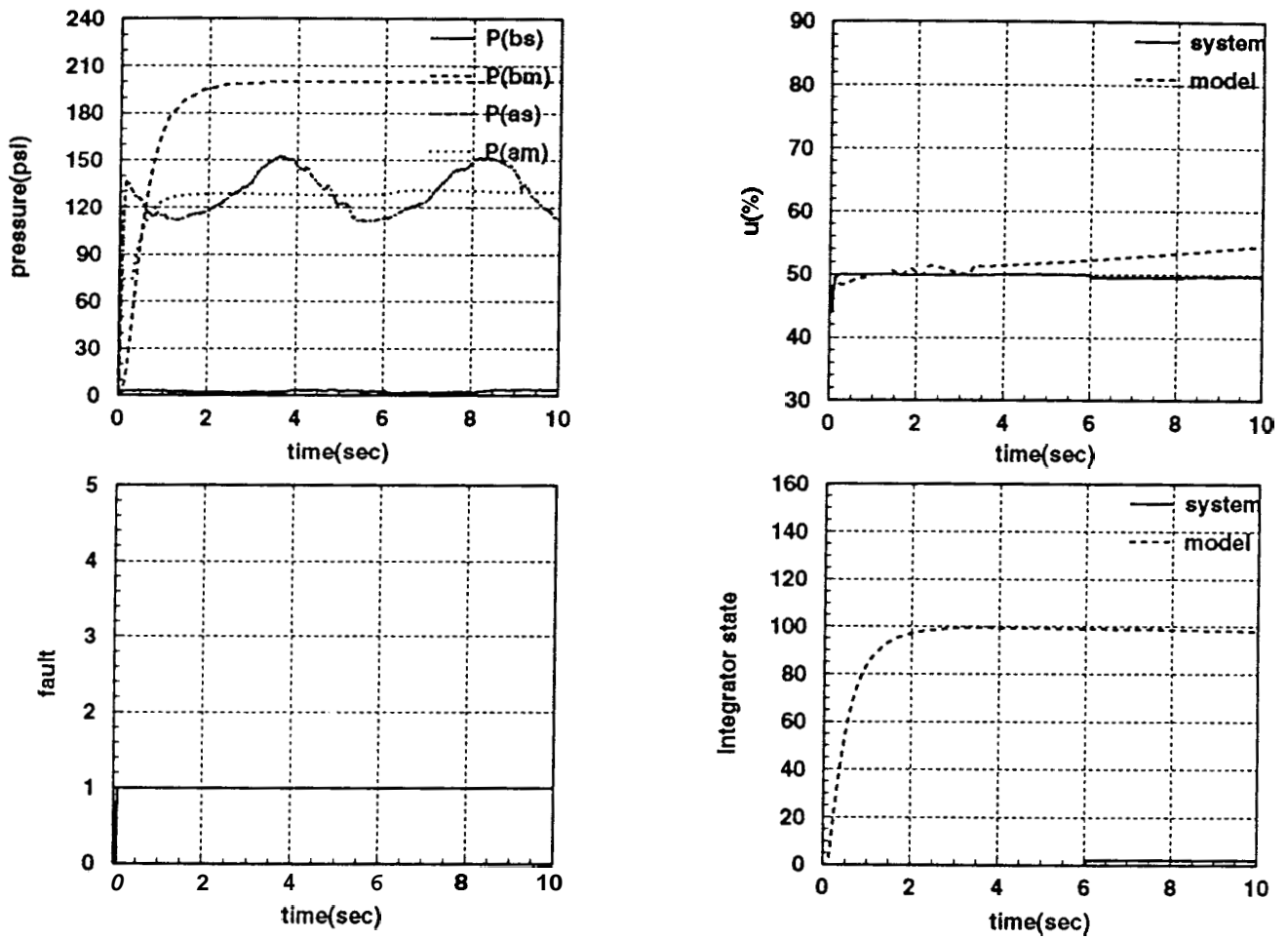Figure 16: Simulation result for the case of partial loss of vacuum pressure.

Figure 17: Simulation result for the case of completely stuck brake pedal, which corresponds to absence of input to the vacuum booster.
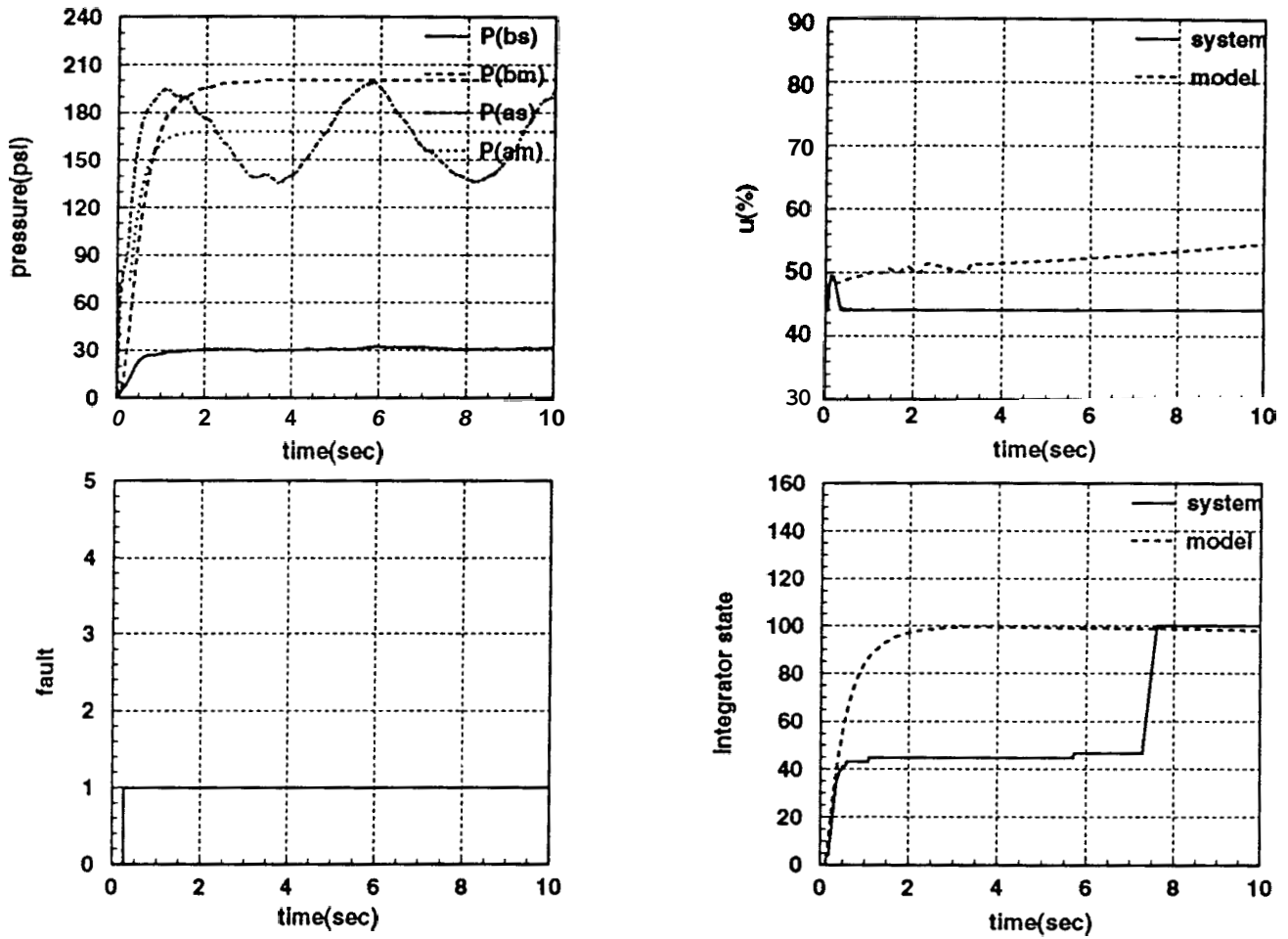
Figure 18: Simulation result for the case of partially stuck brake pedal, which corresponds to reduction of input to the vacuum booster.
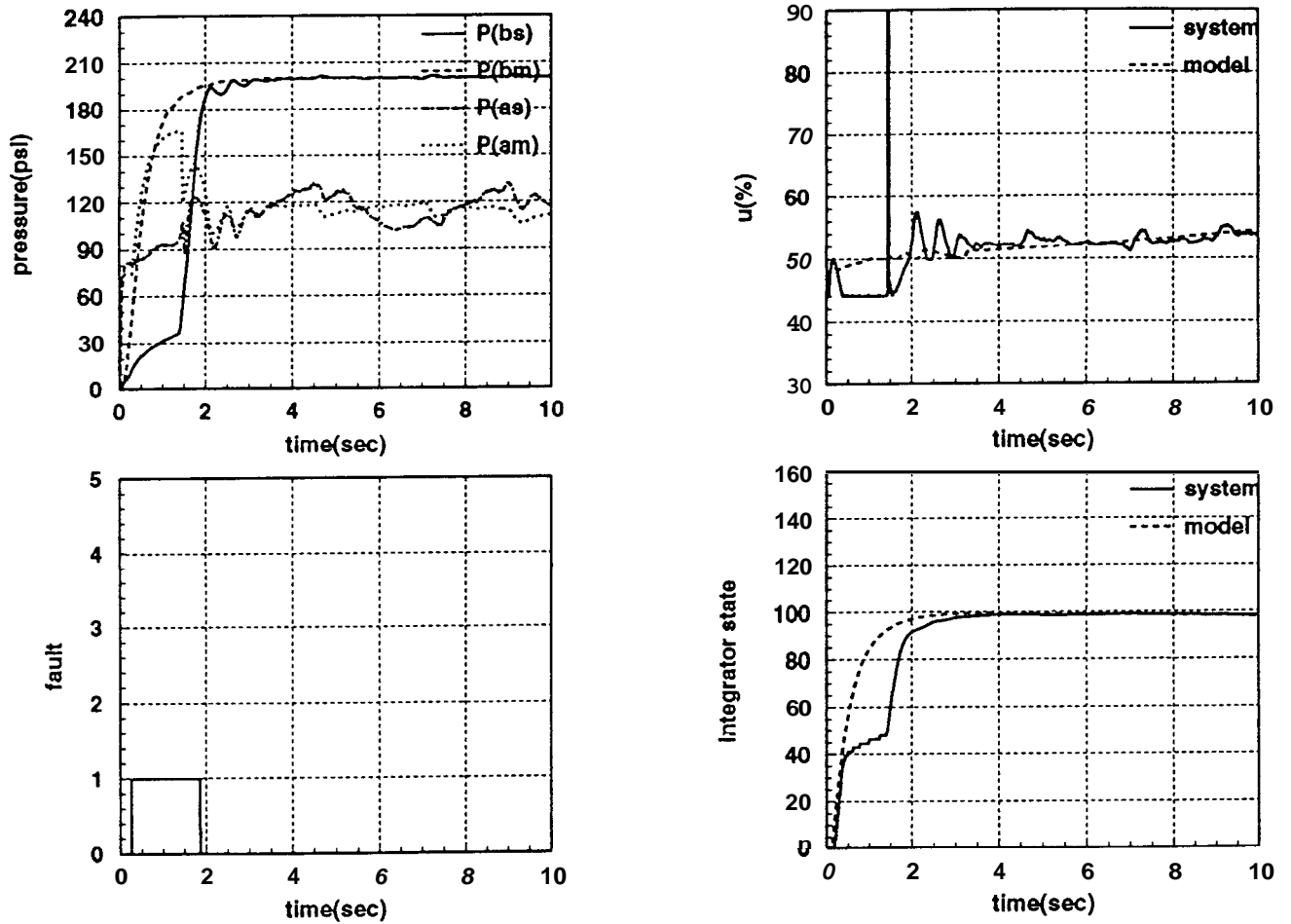
Figure 19: Simulation result for the case of fluid leakage in master cylinder. It can be seen that after loss of pressure at initial stage, system was able to attain the desired pressure with the help of larger movement of brake pedal at the input. Hence an accurate detection of this fault require additional sensor such as displacement sensor at the brake pedal.